REGULATION OF RAS AND RHO GTPASES BY POST-TRANSLATIONAL MODIFICATION: CYSTEINE OXIDATION AND UBIQUITINATION

Guy Aaron Hobbs

A dissertation submitted to the faculty of the University of North Carolina at Chapel Hill in partial fulfillment of the requirements for the degree of Doctor of Philosophy in the Department of Biochemistry and Biophysics.

Chapel Hill
2013

Approved by:

Sharon Campbell

Henrik Dohlman

Brian Kuhlman

Keith Burridge

Andrew Lee

ABSTRACT

Guy Aaron Hobbs: Regulation of Ras and Rho GTPases by Post-Translational Modification: Cysteine Oxidation and Ubiquitination
(Under the direction of Sharon L. Campbell)

Ras superfamily GTPases cycle between active GTP-bound and inactive GDP-bound forms to regulate a multitude of cellular processes, including cell growth, differentiation, and apoptosis. The activation state of Ras superfamily GTPases is regulated by protein modulatory agents that accelerate the slow intrinsic rates of GDP dissociation and GTP hydrolysis. In addition, evidence for the redox regulation of Ras superfamily GTPases is growing, and current data supports regulation by the generation of a thiyl radical. Oxidation and reduction events are critical to physiological and pathological processes and are highly regulated. In Ras GTPases, the redox-sensitive cysteine is in the NKCD motif, which is a motif that is critical for nucleotide binding. However, we show that oxidation that occurs absent of the generation of a thiyl radical does not result in Ras activation.

In the Rho subfamily of GTPases, there is increasing in vitro and cell-based data supporting the oxidant-mediated regulation of Rho GTPases that contain a redox-sensitive cysteine at the end of the conserved phosphoryl-binding loop motif (GXXXXG[S/T]C). While this motif is distinct from Ras, our data suggest that Rho GTPases are regulated by free radical-generation as well as oxidation of the thiol. Specifically for RhoA and other Rho GTPases that have two cysteine residues within the phosphoryl-binding loop motif (GXXCXG[S/T]C), oxidation can result in internal disulfide bond formation that can inactivate these GTPases. In addition, we characterized relevant cellular oxidation states of RhoA and show that oxidation can result in the activation and deactivation of RhoA.

Thus, from data presented herein, it is evident that Ras and Rho family GTPases are uniquely regulated by free radical and non-radical oxidants, and the modulation of activity of the GTPase due to oxidation is dependent on the position(s) of the redox-sensitive thiol. While Ras GTPases are only activated by free radicals because the redox-sensitive thiol does not make interactions with the bound nucleotide, in Rho GTPases, the redox-sensitive thiol makes direct interactions with the bound nucleotide, which results in activation upon modification of the redox-sensitive thiol in RhoA and related GTPases.

ACKNOWLEDGEMENTS

Foremost, I would like to acknowledge the individuals that have encouraged me always question the world around me. I would specifically like to acknowledge Dr. Gloria Lee for giving me a chance to work in her lab as an undergraduate. At the bench, Dr. Kiran Bhaskar and Dr. Daniel Ferraro were my first mentors in research while an undergraduate student at the University of Iowa. In addition, I would like to acknowledge Dr. Ramaswamy Subramanian and Dr. Bryce Plapp for their guidance and mentorship. I do not think I would be in the place I am today without the care and patience of these individuals.

I would also like to acknowledge my mentor, Dr. Sharon Campbell, for always being there to listen to my wild ideas and provide feedback on new data. Her willingness to discuss anything will be greatly missed. While others got me excited to perform research, Sharon taught me how to think like a scientist.

To specifically acknowledge every person that helped along the way would result in an acknowledgements section as long as the dissertation itself. Thus, I say thank you to current and previous lab members, classmates, and friends for asking questions, challenging my thoughts, and providing support when needed. Minh Huynh, who was an undergraduate student under my direction, served with me for two years and deserves a special acknowledgement. He ran every project during the last two years of my thesis by preparing proteins, buffers, and reagents, often with minimal direction, which allowed me the time to perform the most critical experiments as well as analyze and present the data. Without his help, the amount that I was able to accomplish would be significantly less.

Lastly, I want to thank my parents and family for encouraging and fostering a desire to read, learn, and take my education seriously. Their unwavering support and

encouragement to achieve good grades, instill a solid work ethic, and do what I loved has led me to be who I am today. There are no words to describe the level of gratitude I have for my parents for teaching me right from wrong as well as the importance of never quitting and doing your best.

I also wish the thank Heather. Although she joined me in my last two years of my journey at UNC, they were the most productive two years as well as the most exciting years. She taught me what school could never teach a person, led me out of the lab on some amazing adventures, and let me back into the lab to complete my work. While she has captured my heart, I will never be able to thank her enough for her help and support through some of the most demanding years in graduate school.

Lastly, I must thank Josh Gough for providing me with one of my favorite sayings, “It sucks to suck.” It truly does suck to suck, and this saying has repeatedly served as motivation and as words of encouragement.

Thank you.

TABLE OF CONTENTS

LIST OF FIGURES x

LIST OF TABLES xii

LIST OF ABBREVIATIONS AND SYMBOLS xiii

Chapter 1: Introduction and Background 1

Introduction 1

Generation of ROS and RNS in cells and antioxidant defense 4

Reactive oxygen and nitrogen species as second messengers 9

Free radicals modify and activate Ras through a reactive cysteine in the NKCD motif 11

Redox regulation of Rho GTPases by $1e^-$ and $2e^-$ mechanisms through a redox-active cysteine in the phosphoryl-binding loop 14

Chapter 2: Glutathiolated Ras: Characterization and Implications for Ras Activation 17

Introduction 17

Materials and Methods 20

Results 24

Discussion 32

Conclusions 37

Chapter 3: Characterization and Nitrosation of Oncogenic K-Ras^{G12C} 40

Introduction 40

Methods 42

Results 44

Discussion 52

Chapter 4: Oxidation of RhoA at Cys[20] regulates nucleotide binding 56

Introduction 56

Methods 60

Results 64

Discussion 82

Chapter 5: Site-specific monoubiquitination activates Ras by impeding GTPase-activating protein function 88

Introduction 88

Commentary 88

Chapter 6: Biophysical and Proteomic Characterization Strategies for Cysteine Modifications in Ras GTPases 101

Introduction 101

Materials 104

Methods 106

3.1: Cysteine pK_a determination using 4-fluoro-7-aminosulfonylbenzofurazan (ABD-F) 106

3.2: Generation of cysteine-modifying redox-active compounds (CysNO/GSNO generation) 109

3.3 $NO_2^{\cdot}$ generation and NONOates 110

3.4 Quantitative mass spectrometry 112

Notes 122

Chapter 7: Magnesium coordination of RhoG 127

Introduction 127

Methods 129
Results 130
Discussion 132
Chapter 8: Conclusions and future directions 136
Concluding thoughts 138
REFERENCES 140

LIST OF FIGURES

Figure 1. The GTPase cycle of Ras family GTPases 2

Figure 2. Generation and interconversion of ROS and RNS in cells 5

Figure 3. Mass spectrometry of glutathiolated Ras. 25

Figure 4. Biochemical characterization of glutathione-modified Ras. 27

Figure 5. 2D NMR ^{1}H-^{15}N HSQC comparison of Ras^{WT} and Ras^{SSG}. 29

Figure 6. ^{MANT}GDP nucleotide dissociation assays in the presence of the NO-generating agent DEANO. 31

Figure 7. Effect of oxidized glutathione on nucleotide binding in Ras. 33

Figure 8. Modification of Ras by glutathione can proceed by three different mechanisms. 36

Figure 9. CD spectroscopy of K-Ras^{WT} and K-Ras^{G12C}. 46

Figure 11. Nitrosylated K-Ras and nucleotide binding. 49

Figure 12. Nucleotide exchange and hydrolysis kinetics of Ras^{G12C} and Ras^{G12S}. 50

Figure 13. NMR analysis of Ras position 12 mutants. 51

Figure 14. Reaction of RhoA and RhoA variants with ABD-F. 68

Figure 15. Nucleotide binding assays of oxidized RhoA. 70

Figure 16. Oxidation mimetic $RhoA^{C20D}$ shows the critical role of Cys^{20} in nucleotide binding. 71

Figure 17. Biochemical characterization of RhoA redox-insensitive mutants. 73

Figure 18. GTP hydrolysis of RhoA and RhoA redox-insensitive mutants. 75

Figure 19. Thermal denaturation of RhoA and RhoA variants. 76

Figure 20. 2D NMR analyses of RhoA and RhoA variants. 79

Figure 21. Residues with chemical shifts plotted on pymol-generated structures. 80

Figure 22. SDS-PAGE of RhoA variants. 81

Figure 23. RhoA regulation by peroxide and activation state of redox variants. 83

Figure 25. Characterization of GTP hydrolysis of oxidized Ras^{CSKC}. 94

Figure 26. Depiction of the protein:protein ligations in this study. 96

Figure 27. Pymol-generated images of the small molecule modifications as well as PDZ2 and mUb. 97

Figure 28. ABD-F modification of H-Ras^{WT} over a selected pH range. 108

Figure 29. The reaction profile of $NO^{\cdot}$ generated from NONOates. 114

Figure 30. Generalized ICAT-based relative quantification schematic for measuring cysteine peptides. 116

Figure 31. The oxICAT schematic for measuring cysteine oxidation. 118

Figure 32. Nucleotide dissociation of RhoG and Rac1. 131

Figure 33. A model of the RhoG lysine switch hypothesis. 134

LIST OF TABLES

Table 1. T_m of K-Ras determined by CD spectroscopy 47

Table 2. Thiol accessibility in RhoA crystal structures 66

Table 3. Nucleotide dissociation and hydrolysis rates in the presence and absence of GEFs and GAPs 77

Table 4. Specifications and use of NONOate compounds 113

LIST OF ABBREVIATIONS AND SYMBOLS

ABD-F	4-fluoro-7-aminosulfonylbenzofurazan
BAECs	bovine aortic endothelial cells
BCA	bicinchoninic acid
BIAM	biotinylated iodoactamide
β-ME	Mercaptoethanol
CD	circular dichroism
CFC	Cardio-facio-cutaneous syndrome
$CO_3^{\bullet-}$	carbonate radicals
DAB	denaturing alkylation buffer
DAF	diaminofluorescein
DEANO NONOate	diethylammonium (Z)-1-(N,N-diethylamino)diazen-1-ium-1,2-diolate
DETANO-NONOate	(Z)-1-[N-(2-aminoethyl)-N-(2-ammonioethyl)amino]diazen-1-ium-1,2-diolate
DMPO	5,5-dimethyl-1-pyrroline N-oxide
DTBA	dithiobutylamine
DTT	dithiothreitol
DTPA	diethylenetriaminepentaacetic dianhydride
DUBs	deubiquitinating enzymes
EDTA	Ethylenediaminetetraacetic acid
eNOS	endothelial NOS
FASP	Filter-aided sample preparation
FTIR	Fourier-transformed infrared spectroscopy

GAPs	GTPase activating proteins
GDIs	guanine dissociation inhibitors
GEFs	guanine exchange factors
GRX-1	glutaredoxin-1
GSSG	oxidized glutathione
H_2O_2	peroxide
HCD-MS/MS	higher energy collisional dissociation
Hepes	4-(2-hydroxyethyl)-1-piperazineethanesulfonic acid
HSQC	heteronuclear single quantum coherence spectroscopy
IAA	iodoacetamide
ICAT	Isotope-coded affinity tag
iNOS	inducible NOS
IST	immuno-spin trapping
LC-MS	liquid chromatography-mass spectrometry
MALDI-MS	matrix-assisted laser desorption/ionization-MS
^{mant}GDP	2'-/3'-O-(N'-methylanthraniloyl)guanosine-5'-O-diphosphate
MES	2-(N-morpholino)ethanesulfonic acid
MS	mass spectrometry
mUb	monoubiquitination
mUbRas	mUb of KRas
NEM	n-ethyldmaleimide
N_2O_3	dintrogen trioxide
NO^+	nitrosonium ion
$NO^{\cdot}$	nitric oxide

$NO_2^{\bullet}$	nitrogen dioxide
NIm-DP	5-guanidino-4-nitroimidazole diphosphate
nNOS	neuronal NOS
NOS	nitric oxide synthase
NOX	NADPH oxidase
O_2	molecular oxygen
$O_2^{\bullet-}$	superoxide
$ONOO^-$	peroxynitrite
PAO	phenylarsine oxide
PAPA-NONOate	(Z)-1-[N-(3-aminopropyl)-N-(n-propyl)amino]diazen-1-ium-1,2-diolate
PKC	Protein Kinase C
p-loop	phosphoryl binding loop
PI3K	phosphoinositide 3-kinase
PTIO	2-Phenyl-4,4,5,5-tetramethylimidazoline-1-oxyl 3-oxide
PTMs	post-translational modifications
RBD	Ras-binding domain
REF52	Rat embryonic fibroblasts
ROS	reactive oxygen species
RNS	reactive nitrogen species
RSNO	nitrosothiols
RS^-	thiolate form
$RS^{\bullet}$	thiyl radical
RSH	thiol form
RSO^-	sulfenic acid

RSO_2^-	sulfinic acid
SCX	strong cation-exchange
SDS	sodium dodecyl sulfate
SIM	selected-ion monitoring
SIN-1	5-amino-3-(4-morpholinyl)-1,2,3-oxadiazolium chloride
SOD	superoxide dismutase
SOS	Son of Sevenless
TCEP	Tris(2-carboxyethyl)phosphine
TEV	tobacco etch virus
VSMCs	vascular smooth muscle cells

Chapter 1: Introduction and Background

Introduction

Ras and Rho GTPases are involved in many fundamental signaling pathways that affect cell cycle, growth, apoptosis, motility, and morphology (*4*). Dysregulation of these proteins can lead to numerous disease states, including cancer, cardiovascular disease, and neurological disorders. Ras and Rho GTPases are molecular "switches." GTP binding alters their conformation, which promotes effector binding and turns downstream signaling "on" (guanine exchange factors [GEFs]), whereas the GDP-bound form reduces effector binding, turning signaling "off" (GTPase activating proteins [GAPs]). In general, three distinct classes of proteins regulate the level of activated GTPases in the cell (**Figure 1**).

Ras superfamily GTPases can be modified by a variety of post-translational modifications (PTMs) that drive differences in localization and activity (*5*). Ras and Rho GTPases associate with the membrane upon lipid modification at the carboxyl-terminus (*6, 7*). Rac1, RhoA, and Cdc42 are geranylgeranylated and associate with the inner leaflet of the plasma membrane (*8*). Rho guanine dissociation inhibitors (GDIs) recognize the lipid moiety and prevent the GTPase from re-associating with the lipid membrane after dissociation (*9*).

Rac1 has also been shown to be palmitoylated at Cys^{178} (*10*). Palmitoylation has been shown to be critical for Rac1-mediated actin cytoskeleton remodeling in Cos-7 cells. Further, mutation of Cys^{178} to Ser resulted in decreased partitioning to the plasma membrane and reduced Rac1 activation. Another PTM observed in a subset of Rho GTPases is phosphorylation. RhoA, RhoG, and Cdc42 have been shown to be phosphorylated at Ser^{188} (RhoA numbering) (*11, 12*). For RhoA, phosphorylation increases association with GDIs,

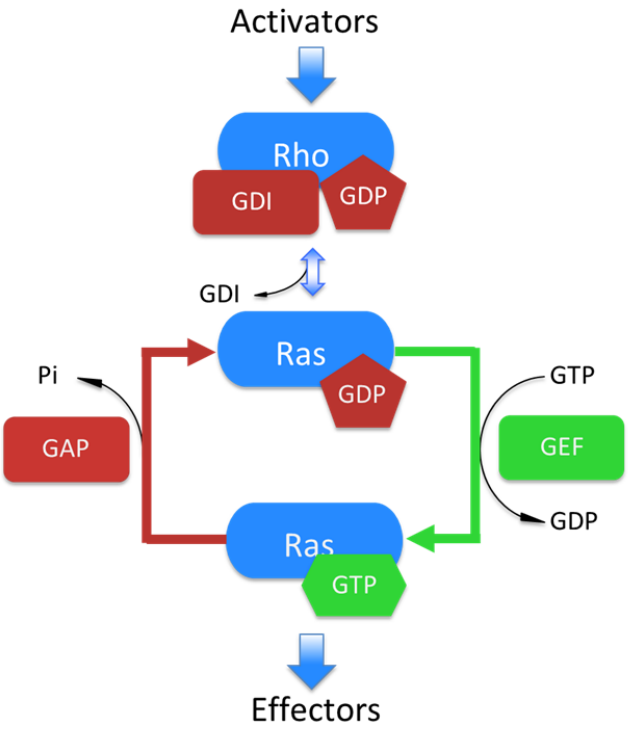

Figure 1. The GTPase cycle of Ras family GTPases

Ras GTPases cycle between GTP-bound active states and GDP-bound inactive states. Guanine nucleotide dissociation inhibitors (RhoGDIs), which are specific to the Rho subclass of GTPases, extract lipid-modified Rho GTPases from membrane to cytosol and prevent GDP dissociation until released upon stimulus. Following signal input, the exchange of the bound GDP is facilitated by the guanine nucleotide exchange factor (GEF) that dramatically increases the dissociation rate of nucleotides. This promotes GTP binding due to the 10-fold higher *in cell* concentration of GTP compared to GDP. Once GTP-bound, the active GTPase is capable of binding downstream effectors and executing its biological functions. The GTPase remains active until GTP is converted to GDP due to its intrinsic hydrolytic capacity, or through catalysis by GTPase activating factors (GAPs).

which causes release from the membrane and inactivation. The biological effect of Ser^{188} phosphorylation in RhoG and Cdc42, as well as in other Rho family GTPases, is currently unclear.

Ubiquitination, including mono,- di-, and polyubiquitination, is another PTM that has been recently discovered for Rho GTPases (*13*). These modifications result in the addition of single or multiple ubiquitin moieties (76-residue protein) that affects protein localization, stability, and trafficking (*14*). Recently, the reversible monoubiquitination of select lysine residues in Ras has been observed, which directly regulates its activity (*15, 16*). Recent evidence indicates that a subset of Rho GTPases can be ubiquitinated (*17*); however, Rac1 is the only Rho family GTPases that has been shown to be monoubiquitinated (*18*), whereas RhoA and Cdc42 have only been observed to be polyubiquitinated, which results in deactivation and degradation (*17, 19, 20*). Further, monoubiquitin can be removed by deubiquitinating enzymes (DUBs); however, Ras- and Rho-specific DUBs have yet to be discovered.

Another type of PTM in Ras superfamily GTPases is cysteine oxidation. Cysteine oxidation is a form of redox regulation and is a field that is often described of as an 'emerging' and 'novel' mechanism of GTPase regulation; however, cysteine oxidation was originally identified in Ras over 15 years ago (*21*). What makes cysteine oxidation a unique PTM is that these modifications are not directly catalyzed by an enzyme, which is the case for phosphorylation, lipid modification, and ubiquitination, but rather are modified by ROS and RNS. While enzymes produce redox agents capable of oxidizing proteins, such as nitric oxide synthase (NOS), NADPH oxidase (NOX), and superoxide dismutase (SOD), the oxidants themselves have long been viewed as hallmarks of oxidative stress and nonspecific. However, it has become increasingly apparent that RNS and ROS, including nitrogen dioxide ($NO_2^{\cdot}$), nitric oxide ($NO^{\cdot}$), superoxide ($O_2^{\cdot -}$), and peroxide (H_2O_2), target specific proteins containing redox-sensitive cysteine residues under physiological conditions (*22-*

24). A cysteine residue within a protein is generally considered 'redox-sensitive' if it is solvent accessible and contains a depressed pK_a, which has been shown to increase the reactivity of the thiol to oxidants (*25*). If a cysteine forms interactions within the protein that stabilize the thiolate (S^-) form, then the residue will have a lower pK_a relative to free cysteine (*26*). In general, a free cysteine has a pK_a of approximately 8.5, which leaves it in the thiol (SH) form at physiological pH. The rate of thiol reactivity depends on the thiol ionization state and the oxidant, with the thiolate state being more sensitive to oxidation than the thiol state (*27*). Furthermore, there is no known consensus sequence that can be used to predict redox-sensitive cysteines (*28*). While peroxynitrite has been shown to be able to oxidize the thiol form, it is more reactive with the thiolate form, although the radical-mediated breakdown products are more likely to oxidize cellular thiols (**Figure 2**) (*29*). In addition, peroxide will only react with the thiolate (S^-) form of cysteines (*30*), whereas, nitric oxide has been shown to react too slowly with thiols to be physiologically relevant (*31*). However, an altered pK_a is not always a prerequisite for redox sensitivity as Ras Cys^{118}, a known redox-sensitive cysteine, does not have an altered pK_a; however, Ras is only regulated through Cys^{118} by free radical-mediated oxidants.

Thus, as the Ras field is still largely unfamiliar with the redox regulation of GTPases and the redox field as a whole, in this review, we will present some basic information on redox signaling in cells and describe the current understanding of the redox regulation of Rho GTPases.

Generation of ROS and RNS in cells and antioxidant defense

Deregulation of the cellular redox potential is often correlated with various levels of oxidative stress and elevated levels of reactive oxygen (ROS) and nitrogen species (RNS) and contributes to and promotes a variety of diseases (*32*), including cancer, neurodegeneration (*33*), atherosclerosis, diabetes, and aging (*34*). As such, ROS and RNS are often considered damaging to cellular tissue, including proteins, lipids, and DNA. Thus, before we can fully

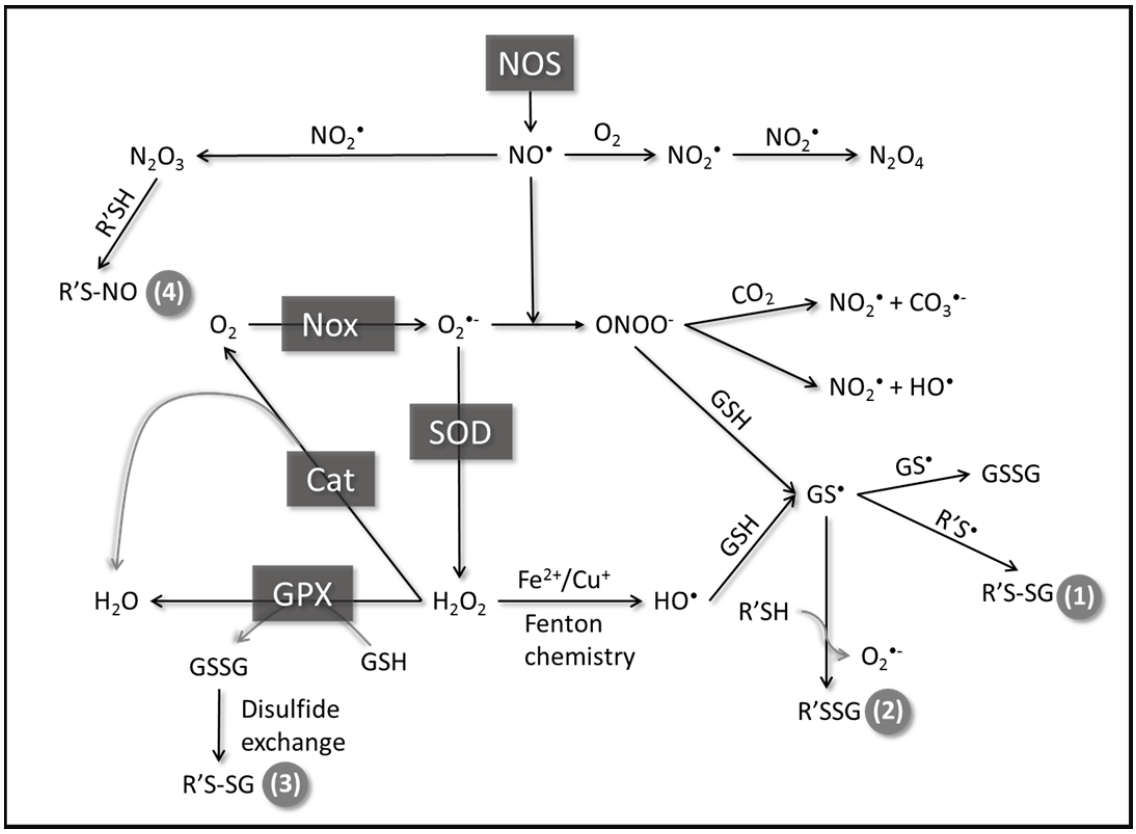

Figure 2. Generation and interconversion of ROS and RNS in cells

Select oxidation end products are presented, including radical-mediated glutathiolation (1), glutathiolation with $O_2^{\bullet-}$ production (2), disulfide exchange-mediated glutathiolation (3), and nitrosation by a non-radical pathway (4). Not all reactions shown are chemically balanced. Key: Cat, catalase; GPX, glutathione peroxidase; NOS, nitric oxide synthase; Nox, NADPH oxidase; SOD1, superoxide dismutase 1.

detail the role of ROS and RNS in the regulation of Rho GTPases, we will give a brief overview of the production of ROS and RNS in cells, antioxidant defense, and interconversion of cellular ROS and RNS (outlined in **Figure 2**).

While ROS and RNS are generally grouped into a category of reactive intermediates, it is important to understand that there are two classes of oxidants, one-electron and two-electron oxidants. Two electron oxidants have been shown to oxidize thiols to generate sulfenic acid and a predominant cellular two-electron oxidant is hydrogen peroxide (*26*). One-electron oxidants, such as nitrogen dioxide, generates a thiol radical, which will predominantly react with other thiols, including cellular glutathione, to form disulfide bonds and produces superoxide (**Figure 2**) (*35, 36*). Under normal cellular signaling, only the most reactive thiols will be subject to oxidation and signaling through ROS and RNS, and ROS and RNS have been observed to function as second messengers (*23*). However, it is important to note that oxidation observed *in vitro* does not always correlate with oxidation *in vivo*. This is because *in vitro* experiments tend to have few substrates in solution, which leaves the oxidant little competition. Therefore, for a protein to function in oxidative signaling, it needs to be readily oxidized *in vivo* under normal cellular conditions (*27*).

A primary source of cellular ROS exists within the mitochondria (*37*). As all aerobic organisms require oxygen for oxidative phosphorylation, the mitochondria is a central organelle that generates a number of cellular oxidants. One of the most common ROS generated by the mitochondria is superoxide ($O_2^{\bullet-}$) due to incomplete reduction of molecular oxygen (O_2). Superoxide does not readily diffuse across membranes, which limits the molecule to the compartment where it was generated. Furthermore, in aqueous solution, $O_2^{\bullet-}$ undergoes a fast dismutation reaction (rate constant of 5×10^5 $M^{-1}s^{-1}$ at pH 7.0) to H_2O_2. Superoxide Dismutase, an enzyme capable of reducing $O_2^{\bullet-}$ to H_2O_2, speeds up this reaction nearly 10^4-fold. In the mitochondria, SOD is maintained at a high concentration such that it

is unlikely that any mitochondria-derived $O_2^{\bullet-}$ escapes to the cytoplasm. However, H_2O_2 can easily cross the membrane and move into the cytoplasm (*38*).

Phagocytes are another common source of cellular ROS and can produce superoxide in 'bursts' due to the action of Nox enzymes. There are currently 7 known Nox enzymes (Nox1/2/3/4/5, Duox1, and Duox2). Nox1, Nox2, and Nox3 all require Rac1 for activation (*39*). Nox isoforms are highly regulated and tissue specific. In phagocytes, cytochrome b559 (a heterodimer consisting of Nox2 (formerly $gp91^{phox}$) and $p22^{phox}$) combines with p47phox, p67phox, and Rac1 to form the membrane-associated NADPH oxidase complex, which catalyzes the one-electron reduction of oxygen to superoxide ($O_2^{\bullet-}$) to eliminate invading pathogens by oxidation (*40*). In addition, superoxide ($O_2^{\bullet-}$) generated in the arteries by Nox2 and Nox4 compete with antihypertensive effects of nitric oxide ($NO^{\bullet}$) by reacting with nitric oxide to form peroxynitrite ($ONOO^-$; **Figure 2**) (*41*). In lung fibroblasts, the presence of different Nox isoforms promotes superoxide ($O_2^{\bullet-}$) production in the cytosol and extracellular space.

Another source of cellular ROS is in liver and kidney cells. These cells use cellular substructures called peroxisomes, which contain a variety of ROS and RNS generating enzymes and peroxisomal catalase that function in metabolic pathways and have been shown to produce as much as 35% of cellular peroxide (*42*).

Nitric oxide is perhaps the best known cellular RNS and is produced by a class of enzymes called NOSs. There are three isoforms of NOS, endothelial NOS (eNOS), inducible NOS (iNOS), and neuronal NOS (nNOS), all of which function as homodimers and generate nitric oxide from L-arginine (*43*). Some functions of nitric oxide ($NO^{\bullet}$) produced by NOS include the regulation of erectile function, blood pressure, vasodilation, and inflammation. Neuronal NOS is a cytosolic protein that is found primarily in the central nervous system and is activated by phosphorylation, calcium, and interactions with proteins with PDZ domains (*44*). Endothelial NOS is constitutively expressed and localized to the membranes

in cells and when activated, can produce low levels of nitric oxide ($NO^{\bullet}$). Activation of eNOS, like nNOS, is regulated by calcium-bound calmodulin (*45*), interactions with various effector proteins (*46*), and phosphorylation (*47*). Lastly, iNOS expression is induced in macrophages and other cell types and is constitutively active once expressed (*48*). The function of iNOS is to produce nitric oxide ($NO^{\bullet}$) to inhibit iron-sulfur proteins, damage tumor cells, and oxidize the DNA of invading parasites.

Discussion regarding the generation of endogenous oxidants would not be complete without considering the lungs. The lungs are constantly exposed to pollutants, cigarette smoke, ozone, and other industrial oxidants. This extra exposure to exogenous ROS and RNS makes the lungs more susceptible to oxidative stress, which can have different effects on protein function than oxidative signaling, which are beyond the scope of this introduction.

The cell has also evolved a network of antioxidant enzymes and small molecules to protect the cell from oxidative damage. An abundant antioxidant enzyme that deserves consideration is SOD. Three distinct isoforms of SOD: SOD1, a dimeric protein that binds copper and zinc and is localized in the cytosol; SOD2, a homotetrameric protein that binds one manganese ion per subunit and is localized in the mitochondria; and SOD3, a homotetrameric protein anchored to the extracellular matrix. SODs reduce $O_2^{\bullet-}$ to H_2O_2. Peroxide, in turn, can be reduced to H_2O by catalase and glutathione peroxidase (**Figure 2**). In addition, GSH-Pxs can reduce lipid peroxidases to their respective lipid alcohols. Other antioxidant enzymes include thioredoxin reductases, peroxiredoxins, and glutaredoxins, which all function in the removal of peroxide (*49*).

In addition to enzymatic antioxidants, the cell has evolved a host of small molecule antioxidants as well. Common cellular antioxidants include glutathione, ascorbic acid, tocopherol, and β-carotene. Glutathione is a tripeptide that contains cysteine thiol group and is the major cellular antioxidant. The cellular regulation of the GSH:GSSG ratio is critical for

managing oxidative stress (*50*). GSH functions with GSH-Pxs to reduce peroxides in the cell and can reduce other oxidized species (**Figure 2**). Ascorbic acid, more commonly known as Vitamin C, scavenges free radicals in the cytosol, whereas tocopherol (vitamin E) protects cellular membranes from oxidative damage (*51*). B-carotene serves to scavenge radicals as well, including peroxyl, hydroxyl, and superoxide radicals (*52*).

Reactive oxygen and nitrogen species as second messengers

Some examples of ROS are peroxide (H_2O_2), superoxide ($O_2^{\bullet-}$), and hydroxyl radical ($HO^{\bullet}$), and examples of RNS are nitric oxide ($NO^{\bullet}$), nitrogen dioxide ($NO_2^{\bullet}$), peroxynitrite ($ONOO^-$), and dintrogen trioxide (N_2O_3). However, for these molecules to function in cellular signaling, they must meet the definition of second messengers. As second messengers, RNS and ROS are generated in response to a specific stimulus, short lived, specifically target effectors, and transiently and reversible effect signaling. Superoxide ($O_2^{\bullet-}$) and peroxide (H_2O_2) are considered second messengers as these reactive species are less reactive than other ROS, such as $HO^{\bullet}$, which lacks specificity as it reacts at the rate of diffusion with any molecule it contacts. For RNS, nitrogen dioxide ($NO_2^{\bullet}$), not nitric oxide ($NO^{\bullet}$), is thought to be the major source of free radical-mediated oxidation of thiols. Peroxynitrite undergoes homolytic cleavage to generate nitrogen dioxide and carbonate radicals ($CO_3^{\bullet-}$) in the presence of CO_2, which can directly oxidize thiols; however, dinitrogen trioxide, and the nitrosonium ion (NO^+) are capable of nitrosating thiols through two-electron mechanisms (*53*) to generate nitrosothiols (RSNO).

Protein thiols in cysteine residues are amongst the most common sites of protein oxidation. However, for ROS and RNS to be considered as a second messenger, these PTMs should be reversible. Reversible oxidation states of protein thiols *in vivo* include sulfenic acid (RSO^-), nitrosation (RSNO), glutathiolation (RSSG; mixed disulfide bonds), and disulfide bonds (RSSR'; intramolecular disulfide bonds) (*54*). There is some evidence that sulfiredoxins can reduce sulfinic acid (RSO_2^-); however, sulfiredoxins have only been shown

Glossary 1

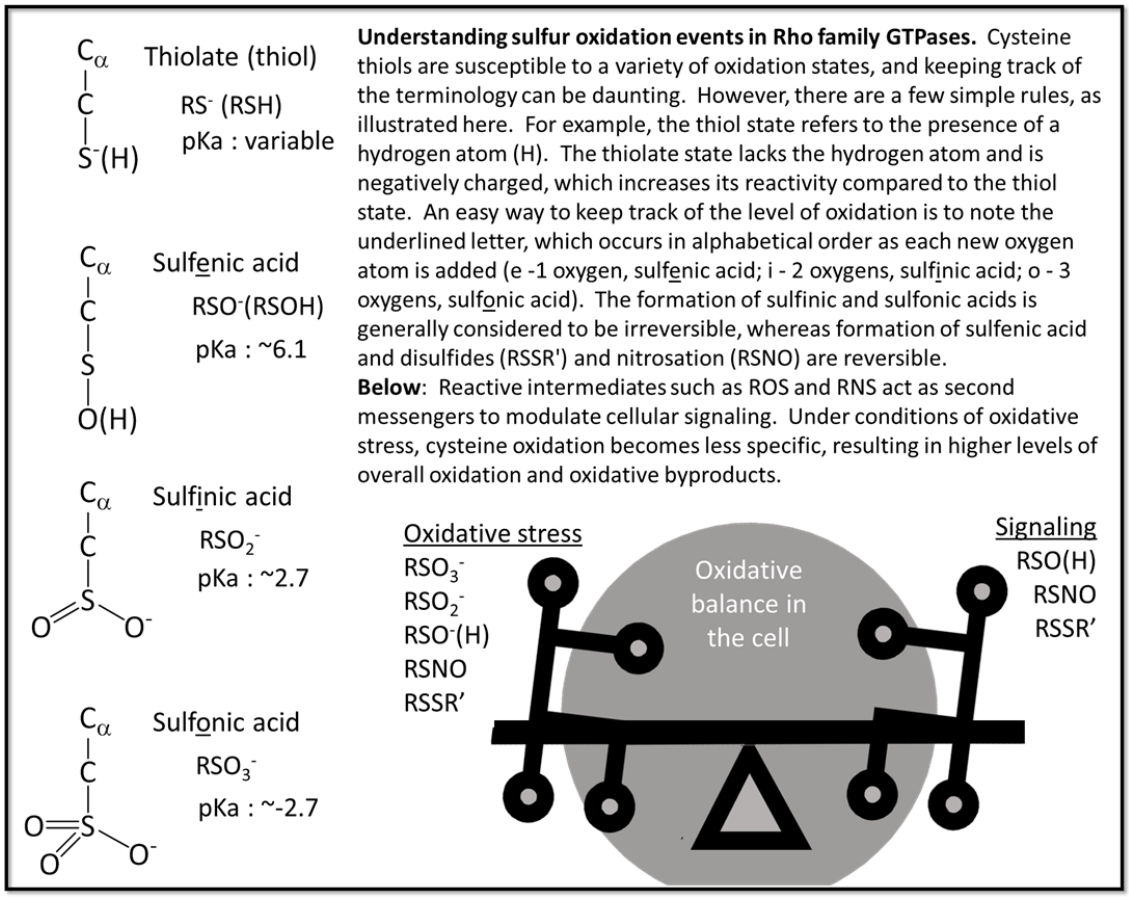
Cα
C
S-(H)
Thiolate (thiol)
RS- (RSH)
pKa : variable
Cα
C
S
O(H)
Sulfenic acid
RSO-(RSOH)
pKa : ~6.1
Cα
C
S
O
O-
Sulfinic acid
RSO2-
pKa : ~2.7
Cα
C
S
O
O
O-
Sulfonic acid
RSO3-
pKa : ~-2.7
Understanding sulfur oxidation events in Rho family GTPases. Cysteine thiols are susceptible to a variety of oxidation states, and keeping track of the terminology can be daunting. However, there are a few simple rules, as illustrated here. For example, the thiol state refers to the presence of a hydrogen atom (H). The thiolate state lacks the hydrogen atom and is negatively charged, which increases its reactivity compared to the thiol state. An easy way to keep track of the level of oxidation is to note the underlined letter, which occurs in alphabetical order as each new oxygen atom is added (e -1 oxygen, sulfenic acid; i - 2 oxygens, sulfinic acid; o - 3 oxygens, sulfonic acid). The formation of sulfinic and sulfonic acids is generally considered to be irreversible, whereas formation of sulfenic acid and disulfides (RSSR') and nitrosation (RSNO) are reversible.
Below: Reactive intermediates such as ROS and RNS act as second messengers to modulate cellular signaling. Under conditions of oxidative stress, cysteine oxidation becomes less specific, resulting in higher levels of overall oxidation and oxidative byproducts.
Oxidative stress
RSO3-
RSO2-
RSO-(H)
RSNO
RSSR'
Oxidative balance in the cell
Signaling
RSO(H)
RSNO
RSSR'

to function on specific peroxiredoxin enzymes (*55*). Sulfonic acid (RSO_3^-) is another form of thiol oxidation; however, this oxidation state is irreversible and generally results in proteasome-mediated degradation (*56*).

Free radicals modify and activate Ras through a reactive cysteine in the NKCD motif

As we have recently published a detailed review on RNS regulation of Ras activity and biology (*57*), we will only highlight the most recent and salient data herein. Lander et al first observed NO-mediated Ras activation in T cells (*58*), which was transient and concentration-dependent. Later, it was shown that treatment with sodium nitroprusside, a nitric oxide-generating compound, increased Ras downstream signaling through the mitogen-activated kinase pathway (*59*). An important tool in such studies, Ras^{C118S} is a variant that aids in determining the direct and indirect effects of RIs on Ras because it is RI-insensitive and does not alter Ras structure and activity (*60*). A recent study on macrophages demonstrated that Ras S-nitrosation was required for Erk1/2-mediated apoptosis using the NO· donor S-nitrosoglutathione (*61*). The Ras^{C118S} variant reversed the pro-apoptotic effects, indicating that the effects on cell survival were mediated by direct reaction with Ras. In this study, Tsujita et al suggested that the process of nitrosation, rather than covalent modification, activated Ras (*61*). Our lab extended these observations and showed that Ras activation depends on $1e^-$ (radical)-mediated oxidation, which induces nucleotide dissociation (*62*). As most of these earlier studies used exogenous NO· and/or were conducted in cells that overexpressed Ras, it was unclear whether NO· regulated Ras activity under physiological conditions.

However, recent evidence has linked eNOS to Ras nitrosation and activation in Ras-mediated tumorigenesis initiation and maintenance in mice. In the proposed activation pathway, oncogenic Ras activates the phosphoinositide 3-kinases (PI3K) pathway, which results in Akt-mediated (also protein kinase B) eNOS phosphorylation. Through a feedback

mechanism, eNOS-generated NO· activates Ras^{WT} and stimulates Ras downstream pathways (*63*). Further, Lim et al showed that, for H- and N-Ras, introducing the Ras^{C118S} mutation circumvented PI3K pathway activation and reduced tumor growth. In a separate cell-based study, eNOS-derived NO· activated N-Ras in T cells engaged with antigen presenting cells; Cys^{118} was required for activation (*64*). These data suggest that NO· mediates Ras activation directly through Cys^{118}.

Ras superfamily GTPases have four conserved nucleotide-binding motifs (*65*). While the X residue in the NKXD motif is not well-conserved, several Ras subclass members contain a redox-active cysteine at this position. GTPases with a redox-sensitive NKCD motif can be activated by NO_2· and other RIs; however, NO-mediated regulation is best characterized for Ras. Several cell-based and *in vitro* studies have shown that NO_2· reacts with Ras through Cys^{118} to promote nucleotide exchange and Ras activation (*57*). Our lab has employed NMR and biochemical approaches to show that S-nitrosation of Ras does not affect Ras structure or nucleotide binding (*66*). We speculated that an intermediate formed during the reaction of Ras with NO_2· modulates Ras activity and investigated several reactions involved in thiol S-nitrosation. Furthermore, we observed that $1e^-$ oxidation (radical-mediated) reactions, which have been postulated to promote thiyl radical formation, enhance nucleotide dissociation from Ras (*62*). In support of these observations, we have recently confirmed Cys^{118} radical formation upon exposure of Ras to diethylamine NONOate (NO·-generating agent) and NO_2·, using immune-spin trapping and Fourier transform ion cyclotron resonance mass spectrometry (*67*). As guanine bases are susceptible to radical-mediated oxidation, we speculated that thiyl radical generation promoted oxidation of the Ras-bound guanine nucleotide. Supporting this premise, we used mass spectrometry (MS) to demonstrate that 5-guanidino-4-nitroimidazole diphosphate (NIm-DP) is formed in the presence of NO·/O_2 and NO_2·. NIm-DP is a reported breakdown product of 5-nitro-guanine ribose diphosphate (5-nitro-GDP), which can be generated upon reaction of guanosine

diphosphate with $NO_2^{\cdot}$ (*68*). Further, mutation of the redox-sensitive cysteine (Ras^{C118S}) prevented NO-mediated nucleotide oxidation and dissociation (*69*). These results suggest that $NO^{\cdot}/O_2$ or $NO_2^{\cdot}$ can produce a Ras thiyl radical ($Ras^{C118\cdot}$) that propagates to the guanine base by electron transfer. Guanine base oxidation disrupts critical intermolecular contacts between the nucleotide and Ras nucleotide binding pocket, which enhances nucleotide dissociation. These data suggest that Ras^{C118} thiol nitrosation does not promote nucleotide exchange; rather, exchange is promoted by thiyl radical formation at Ras^{C118}. Further supporting this model, we demonstrated that nucleotide binding is not altered by either Ras^{C118} mutation or S- nitrosation (*69*). A proposed thiyl radical-based mechanism has been described in detail elsewhere (*70*) but remains inconclusive, as direct evidence to support the proposed radical intermediates has not yet been obtained.

In contrast to our observations that Cys^{118} nitrosation does not alter Ras activity, Clavreul et al suggested that covalent modification of Ras by glutathione enhances nucleotide exchange (*71*). In these experiments, Ras^{WT}, but not Ras^{C118S}, was activated by glutathiolation using peroxynitrite, and it was hypothesized that Ras^{C118} glutathiolation by $2e^-$ oxidation perturbs nucleotide binding because glutathione is negatively charged and larger than nitric oxide. Clavreul et al concluded that glutathiolation significantly altered Ras structure at the nucleotide-binding pocket and enhanced nucleotide exchange (*72, 73*). However, peroxynitrite was used in these experiments, and its breakdown products can generate RIs capable of thiyl radical formation. Peroxynitrite can undergo homolysis to generate $NO_2^{\cdot}$ and $HO^{\cdot}$. Moreover, in the presence of CO_2, peroxynitrite can produce carbonate radicals (*74*). While Kissner and Koppenol have observed that 'radical-free' peroxynitrite homolysis produces nitrite and molecular oxygen (*75*), Szabo et al discussed peroxynitrite homolysis products and concluded that it generates radical products (*76*).

Therefore, it is impossible to judge whether the effects of glutathiolation on Ras activity were induced by free radicals or direct Cys^{118} modification. While Adachi et al

suggested that Ras S-nitrosation may be an intermediate during glutathione modification of Ras, they concluded that covalent ($2e^-$) glutathione modification of Ras leads to Ras activation (*77*). However, the observation that Ras glutathiolation alters nucleotide exchange contradicts our previous studies, which demonstrated that Cys^{118} and $1e^-$ oxidants are required for regulation of Ras nucleotide binding and activity. To address this discrepancy, we have recently demonstrated that treatment of Ras with oxidized glutathione (GSSG) results in glutathiolation of Ras at Cys^{118}. However, similar to S-nitrosation, glutathione modification of Ras does not alter Ras nucleotide binding. Therefore, we propose that Ras activation requires Cys^{118} thiyl-radical formation for nucleotide dissociation and subsequent activation. One end product of Ras^{C118} thiyl-radical generation is Ras^{SSG}. Thus, the presence of Ras^{SSG} may reflect Ras activation if it was generated by a reaction with the Ras^{C118} thiyl radical; this is also the most likely mechanism in cells given the slow reaction rate for the Ras thiol and GSSG under physiological conditions.

Redox regulation of Rho GTPases by $1e^-$ and $2e^-$ mechanisms through a redox-active cysteine in the phosphoryl-binding loop

We have demonstrated that select Rho GTPases are redox sensitive; however, Rho GTPases contain a different redox motif than Ras (*78*). Over fifty percent of Rho GTPases contain a redox sensitive cysteine at the end of the nucleotide-binding p-loop motif, GXXXXGK[S/T]C. Based on the Rac1, Cdc42, and RhoA crystal structures, the solvent-exposed cysteine in the p-loop motif likely has an altered pK_a and is accessible to RIs. We have previously shown that the reactive phosphoryl binding loop (p-loop) cysteines in Rho GTPases are sensitive to oxidation, resulting in altered GTPase regulation (*79*).

Whereas treatment of RhoA with $NO_2^{\bullet}$ can promote nucleotide oxidation and dissociation similar to Rac1 and Cdc42, it can inhibit nucleotide binding in the absence of reducing agents. Distinct from Rac1 and Cdc42, RhoA contains two cysteines in its p-loop (Cys^{16} and Cys^{20}). Exposure of RhoA with $NO_2^{\bullet}$ can promote disulfide bond formation

between Cys^{16} and Cys^{20} , which occludes nucleotide binding (*80*). However, nucleotide binding can be restored with disulfide reducing agents. Our findings indicate that thiyl radical formation at $RhoA^{C20}$ upon $NO_2^{\cdot}$ treatment facilitates nucleotide oxidation and release, which increases $RhoA^{C16}$ accessibility and promotes intramolecular disulfide bond formation with Cys^{20}. RhoA disulfide-bond formation occludes nucleotide binding and promotes RhoA inactivation. Based on these observations, we postulate that RhoA is likely activated by thiyl radical-promoting RIs under conditions where the redox potential is capable of promoting disulfide reduction and restoration of RhoA nucleotide binding (*81, 82*). Redox-mediated inactivation of Ras may occur when the cellular reduction potential is reduced, such as during oxidative stress. It is intriguing to speculate that enzymes, such as thioredoxin and glutaredoxin, which are capable of reducing protein disulfides, may act on RhoA and contribute to activation.

The addition of cisplatin or arsenic trioxide has been shown to inactivate RhoA by promoting mixed disulfide formation between the two p-loop cysteines (*80*). In contrast to Ras, these results suggest that $2e^-$ oxidation can regulate RhoA activity. In support of this hypothesis, Gerhard et al showed that phenylarsine oxide (PAO) generates a mixed disulfide crosslink between RhoA Cys^{16} and Cys^{20} using MALDI-MS (matrix-assisted laser desorption/ionization-MS) and demonstrated that the modification inhibits stress fiber formation through the inactivation of RhoA in Caco-2 cells (*83*).

H_2O_2 has also been shown to regulate RhoA activity *in vitro* and in cells (*78, 81*). Unlike Ras^{C118}, $RhoA^{C20}$ directly interacts with the bound nucleotide, and $2e^-$ oxidation of this cysteine likely perturbs nucleotide binding. We observed that $2e^-$-oxidation by peroxide at the p-loop cysteines can enhance the rate of nucleotide dissociation by approximately 10-fold. In addition, $1e^-$ oxidation has also been shown to induce nucleotide dissociation. Our lab has shown that $1e^-$ oxidants ($O_2^{\cdot -}$, $NO_2^{\cdot}$, and $HO^{\cdot}$) enhance RhoA nucleotide exchange by nearly 500-fold (*78*).

While work from our lab indicates that only 1e- oxidation reactions that generate a thiyl radical at Cys^{118} in Ras affect Ras activity, discrepancies remain regarding $2e^-$ oxidation. Given the distinct Rho GTPase redox motif, $1e^-$ and $2e^-$ mechanisms can modulate their activity. RhoA is unique because 1e- oxidants can induce a disulfide bond between Cys^{16} and Cys^{20}, which can inactivate RhoA by occluding nucleotide binding. While the reduction potential under most physiological conditions will likely promote disulfide bond reduction and RhoA activation, under conditions of oxidative stress, radical quenching and/or disulfide reduction may not occur, which could render RhoA inactive (44). Further cell-based studies are needed to clarify the mechanisms of Rho GTPase regulation by redox agents.

Chapter 2: Glutathiolated Ras: Characterization and Implications for Ras Activation

Introduction

Ras proteins belong to a large superfamily of GTPases that bind to GDP and GTP with high specificity and affinity. They function as molecular switches that cycle between the inactive GDP-bound and active GTP-bound forms. Once activated, Ras GTPases interact with a variety of effectors to activate signaling pathways that regulate gene expression, cell growth and differentiation, and programmed cell death (*84-86*). The structural differences between the GDP- and GTP-bound states of Ras are primarily localized within two regions, Switch I (residues 30-37) and Switch II (residues 60-76) (*65*). The intrinsic rates of GDP exchange and GTP hydrolysis are too slow to respond to cell signaling events (*87*), and consequently, protein factors associate with Ras and accelerate these rates in a regulated manner. Guanine nucleotide exchange factors (GEFs) accelerate exchange of bound GDP for GTP, which leads to Ras activation (*88*), whereas GTPase activating proteins (GAPs) inactivate the GTPase by facilitating GTP hydrolysis (*89, 90*). Ras is considered the most prevalent oncogene in human cancer, and oncogenic mutations have been identified in approximately 30% of human tumors (*91, 92*). Oncogenic Ras mutations render Ras constitutively active by impeding down regulation by GAPs (*93*).

In addition to GEFs, reactive oxygen and nitrogen species (ROS; RNS) have been shown to enhance guanine nucleotide exchange and activate Ras (*57*). Two of the most common oxidative modifications identified for Ras *in vivo* are nitrosation and glutathiolation (*94*). Specifically, nitrogen dioxide ($NO_2^{\cdot}$) has been shown to induce Ras guanine nucleotide dissociation by causing guanine base oxidation through reaction with

cysteine 118 (Cys^{118}) (*62*). As the GTP:GDP ratio in cells is approximately 10:1, oxidation-mediated GDP dissociation can promote GTP loading of Ras, analogous to the action of GEFs (*69*). While the reaction of nitric oxide and its auto-oxidation product, $NO_2^{\cdot}$, with Ras have been characterized, it is less clear how other thiol modifications (i.e., glutathiolation) affect Ras activity. As numerous studies have described activity modulation of Ras in the presence of ROS and RNS, we refer the reader to two recent reviews that detail the redox regulation of Ras and Ras-related GTPases (*57, 95*).

Ras contains a solvent accessible cysteine (X) in the nucleotide-binding NKXD motif. While this cysteine is conserved in H-, K- and N-Ras, it does not form interactions with other residues in Ras or the guanine nucleotide ligand and is poorly conserved in the Ras superfamily. We have previously postulated that Cys^{118} is conserved in N-, K-, and H-Ras due to its role in the redox regulation of Ras (*69*). In fact, Cys^{118} has been shown to react *in vitro* and *in vivo* with a variety of thiol oxidizing agents, including oxidized glutathione, superoxide, and nitric oxide-derived oxidants (*94*). We have previously characterized a redox inactive variant of Ras (Ras^{C118S}) that retains similar structure and biochemical properties as Ras^{WT} (*21, 59*). Ras^{C118S} has been used in numerous *in vitro* and cell-based studies to discriminate between direct and indirect mechanisms of Ras activity modulation by Cys^{118}-mediated oxidation (reviewed in *57, 94*). As we have previously shown that S-nitrosation of Ras (Ras^{SNO}) at Cys^{118} does not significantly alter Ras structure, biochemical properties, or binding to the Ras-binding domain of Raf-1 (*66*), we postulated that NO modulates Ras activity by formation of a thiyl-radical intermediate, which leads to oxidation of the bound guanine base, likely through electron transfer. In support of this premise, we have previously shown that treatment of Ras with $NO_2^{\cdot}$ promotes the oxidation and release of the bound guanine nucleotide (*62*). In addition, we have recently detected the presence of a Ras-thiyl radical upon treatment of Ras^{WT} with NO using the immuno-spin trapping (IST) reagent 5,5-dimethyl-1-pyrroline N-oxide (DMPO); no radical was detected when Ras^{C118S}

was used (*67*). Thus, we propose that Ras thiyl-radical formation, as opposed to S-nitrosation, induces oxidation and release of the guanine nucleotide base, which can lead to Ras activation.

In addition to S-nitrosation, several studies have observed that Ras can undergo glutathiolation. This oxidative modification was suggested to increase nucleotide exchange and promote Ras activation (*71, 77, 96-100*). In particular, detection of Ras glutathiolation coincident with Ras activation was observed after exposure of bovine aortic endothelial cells (BAECs) to peroxynitrite (*71, 100*), addition of angiotensin II to vascular smooth muscle cells (VSMCs) (*77, 101*), and exposure of H_2O_2 to rat ventricular myocytes (*97, 99*). However, addition of these agents to cultured cells can produce redox agents capable of protein thiyl radical formation. For example, peroxynitrite can react with cellular CO_2 to produce $CO_3^{\bullet-}$ and $NO_2^{\bullet}$ radicals, and under acidic conditions (peroxynitrite pK_a is ~6.6), peroxynitrite can decompose to hydroxyl radical and $NO_2^{\bullet}$ (*102*). Furthermore, peroxynitrite and angiotensin II can dysregulate several kinase pathways, including the PI3K/Akt pathway, and increase the production of cellular NO by activation of endothelial nitric oxide synthase (eNOS) (*103, 104*). The NO produced by eNOS can auto-oxidize to produce $NO_2^{\bullet}$, which is a powerful oxidant capable of thiyl radical formation. Consistent with observations of Liaudet et al and Ushio-Fukai et al, the PI3K/Akt pathway was activated after exposure of BAECs to peroxynitrite (*71*). Intriguingly, in a pancreatic cancer cell line and a severe combined immunodeficiency/Beige mouse model, activation of PI3K has been shown to activate Ras via eNOS stimulation through a redox-mediated mechanism dependent on Cys^{118} (*63*). Furthermore, peroxynitrite and angiotensin II signaling both activate NADPH oxidase, which can produce waves of reactive oxygen species long after peroxynitrite decomposition (*105*). Lastly, H_2O_2 can produce free radicals through the Fenton reaction by reacting with transition metals present in cells. Thus, based on our previous characterization of nitrosated Ras (*66*), we postulate that Ras activation observed by Clavreul et al (*71, 100*) and Adachi et

al (*77*) results from a radical-mediated mechanism, which occurs prior to the modification by glutathione. However, due to the larger size of glutathione compared to NO•, it was hypothesized that Ras glutathiolation at Cys^{118} causes structural changes in the nucleotide binding pocket, leading to perturbation of guanine nucleotide binding and an increased rate of nucleotide exchange (*71*). As Cys^{118} is critical for the radical-mediated regulation of Ras activity, we sought to circumvent the confounding factors of peroxynitrite and angiotensin II use in cells by directly determining whether glutathiolation at Cys^{118} alters Ras structure and activity *in vitro*.

While Ras has been shown to be glutathiolated in cells (*71, 77, 97, 100*), it is unclear how glutathiolation alters Ras activity. Therefore, we employed NMR and fluorescence-based biochemical assays to assess whether glutathione modification of Ras perturbs Ras structure or activity. We find that treatment of Ras with oxidized glutathione leads to glutathiolation specifically at Cys^{118}, which does not alter Ras tertiary structure or guanine nucleotide binding. These results are consistent with our previous observations that S-nitrosation of Ras Cys^{118} does not perturb the structure or activity of Ras (*66*). Therefore, our data suggests that glutathiolation can only affect Ras activity if modification proceeds through a radical-mediated reaction. Moreover, Ras glutathiolation prevents further redox-mediated activation of Ras by free radical-based mechanisms, which may serve to protect Ras from future radical-mediated oxidation events under conditions of oxidative stress.

Materials and Methods

Ras purification and glutathiolation

Truncated human *H-ras* (H-Ras^{1-166}) was cloned into the pQlinkH vector (Addgene; Cambridge, MA), which contains an N-terminal 6x-His purification tag followed by a Tobacco Etch Virus protease cleavage site for removal of the affinity tag. The hypervariable region of Ras, including the C-terminal CAAX box, was removed as this region does not

undergo post-translational lipid modification in bacteria, is unstructured, and its removal does not affect guanine nucleotide binding or GTP hydrolysis (*106*). All proteins were expressed in BL21 (DE3) RIPL cells (Stratagene; La Jolla, CA) and purified following the Qiagen Nickel NTA purification protocol (Germantown, MD). Ras was further purified by size exclusion chromatography (Superdex-75 10/300 GL column; GE Life Sciences; Piscataway, NJ) and judged greater than 95% pure by SDS-PAGE analysis.

Ras was modified with glutathione by the addition of 1000× oxidized glutathione to purified Ras in glutathiolation buffer (50 mM Tricine pH 8.0, 50 mM NaCl, 5 mM $MgCl_2$, and 30 μM GDP) at 37˚C for 15 min. Prior the addition of glutathione, Ras was reduced with dithiothreitol (DTT) for 30 min at pH 8.5 before being buffer exchanged into glutathiolation buffer that was flushed with N_2 gas to remove dissolved oxygen and prevent auto-oxidation.

Mass Spectrometry of glutathiolated-Ras and Ras

Ras mass measurements were performed on an LTQ-Orbitrap Velos mass spectrometer (Thermo Scientific; San Jose, CA). The mass analysis of intact Ras samples was achieved in full-mass spectrometry (MS), selected-ion monitoring (SIM), and higher energy collisional dissociation-(HCD)-MS/MS modes with a resolution of 120,000 at m/z 400 Da. The intact MS spectra were deconvoluted using ProMass, and HCD-MS/MS product ion spectra were processed manually by assigning sequence ions to theoretical masses corresponding to Ras^{SSG}. The bottom-up peptide identification of trypsinized Ras samples was performed using reversed phase LC-MS/MS on a nano-LC ultra 2D plus (Eksigent Inc; Dublin, CA) coupled to an LTQ-Orbitrap Velos as described previously (*107*). Briefly, data acquisition included a full-MS scan on the Orbitrap (externally calibrated to a mass accuracy of < 1 ppm and instrumental resolving power of 60,000 at m/z 400 Da) followed by intensity-dependent CAD-MS/MS of the top 10 most abundant peptide ions. Mass spectra were processed, and peptide identification was performed using Mascot (Matrix Science

Inc.) against a Human Uniprot database. Peptides were confidently identified using a target-decoy approach with a false-discovery-rate (FDR) of 1%. A precursor ion mass tolerance of 200 ppm and product ion mass tolerance 0.5 Da with a maximum of two missed cleavages and variable modifications of cysteine glutathiolation and oxidation were used as a protein database search parameter. All peptides were filtered and reported within a mass accuracy of 5 ppm.

Nucleotide exchange and hydrolysis assays

The rate of GDP dissociation from Ras was measured using 2'-/3'-O-(N'-methylanthraniloyl)guanosine-5'-O-diphosphate (^{mant}GDP) as previously reported (*108, 109*). One micromolar Ras (Ras^{WT}, Ras^{SSG}, or Ras^{C118S}) loaded with ^{mant}GDP (BioLog; San Diego, CA) was added to 1 mL of degassed assay buffer (50 mM Tris pH 7.4, 50 mM NaCl, 5 mM $MgCl_2$, 2 mM GDP, and 100 μM diethylenetriaminepentaacetic dianhydride; DTPA), and the rate of guanine nucleotide dissociation was measured by monitoring the change in fluorescence (excitation: 365 nm; emission: 435 nm; 25˚C) over time using a Perkin Elmer LS50B fluorimeter (Waltham, MA). All experiments were performed in triplicate. Fluorescent nucleotide dissociation curves were fit to a one-phase exponential decay equation using GraphPad Prism version 3.03 (GraphPad Software; San Diego, CA). For GEF-induced Ras-GDP dissociation assays, the minimal catalytic domain of Son of Sevenless (SOS^{cat}) was used at a 1:1 ratio to Ras. This concentration of SOS^{cat} was selected as the rate enhancement of nucleotide exchange was easy to measure using fluorimetric assays and other labs have published using the GEF at this concentration. The SOS^{cat} construct (from John Kuriyan; University of California, Berkeley) was expressed and purified as previously described (*110*).

Rates of GTP hydrolysis were determined using a Spectramax M5 (Molecular Devices; Sunnyvale, CA) fluorimeter by monitoring phosphate production upon GTP hydrolysis (*111*).

FlipPi 5U (Addgene; Cambridge, MA) was used as the phosphate sensor, and the minimal catalytic domain of $p120^{GAP}$ (*112*) was added to stimulate the rate of Ras GTP hydrolysis. The expression, purification, and use of this sensor have been previously reported (*113*). Briefly, all assays used 10 μM FlipPi with 10 μM GTP-loaded Ras. GTP loading was performed as previously described (*111*). Trace phosphate was removed from all buffers using a 'phosphate mop' (*114*). The rate of GTP hydrolysis was measured by taking the ratio of the 535- and 485-nm emission wavelengths (excitation: 435 nm; 25˚C) of kinetic runs performed in triplicate and fit to a one-phase exponential association curve. For these experiments, the ratio of GAP to Ras was 1:200, and the minimal catalytic domain of p120 Ras^{GAP} was used.

Nitric oxide-induced nucleotide dissociation

To determine whether addition of nitric oxide to Ras^{WT}, Ras^{SSG}, and Ras^{C118S} alters the rates of GDP dissociation, we used the NO· donor DEANO (diethylammonium (Z)-1-(N,N-diethylamino)diazen-1-ium-1,2-diolate; Alexis Chemicals; Farmingdale, NY). Previous studies have shown that NO· in the presence of O_2 forms NO_2·, which promotes nucleotide dissociation in Ras (*62*). Therefore, all buffers used with DEANO were not degassed and were vigorously shaken prior to use. To verify the time-dependent formation of NO· by DEANO in our buffers, diaminofluorescein (DAF; Sigma) was used (data not shown). DAF displays an increased fluorescence upon exposure to NO· radicals with an excitation wavelength of 445 nm and an emission wavelength of 515 nm. All runs were performed in triplicate with 1 μM MANT-loaded Ras in assay buffer. DEANO was added at the indicated concentrations at the start of each run. Fluorescent nucleotide dissociation curves were fit using one-phase exponential decay using GraphPad Prism as described above.

NMR analysis

NMR experiments were collected on a Varian Inova 700 MHz spectrometer at 25˚C. The 2D $^{1}H-^{15}N$ heteronuclear single quantum coherence spectroscopy (HSQC) experiments

were performed with pulsed field gradient and water flip-back methods as previously described (*115*). Uniformly labeled ^{15}N-enriched Ras was purified as previously described (*116*). 2D ^{1}H-^{15}N HSQC experiments were acquired on 0.8 mM ^{15}N-enriched Ras^{WT} and Ras^{SSG} with 1,024 x 128 complex data points and a spectral width of 8,000 Hz for the ^{1}H dimension and 1,709 Hz for the ^{15}N dimension. Buffer contained 10 mM maleate (pH 6.5), 5 mM $MgCl_2$, 40 mM NaCl, 20 μM GDP, and 10% D_2O. NMR data were processed and analyzed using NMR PIPE (*117*) and NMR ViewJ (One Moon Scientific; Newark, NJ).

Results

Modification of Ras^{C118} by glutathione

As Ras^{C118} has been previously identified as the site of oxidative modification by nitric oxide (*66*), we used a combination of top-down and bottom-up MS to confirm that Cys^{118} is the preferred site of glutathiolation. Whereas partial modification of Ras by glutathione was obtained at a ratio of 50:1 GSSG to Ras upon incubation for 15 min at pH 8.5 (**Figure 3a**), increasing the GSSG to Ras ratio to 1000:1 resulted in conversion of $hRas^{1\text{-}166}$ to a predominantly single glutathiolated form. However, Ras glutathiolation was not observed when the redox insensitive Ras^{C118S} variant was treated under the same conditions (**Figure 3b**). All full-MS and selected-ion monitoring (SIM) scans corresponding to glutathiolated Ras^{C118} and redox-insensitive Ras^{C118S} are available in supporting data (Fig. S1). We have also confirmed the site-specificity of $hRas^{1\text{-}166}$ glutathiolation using top-down HCD-MS/MS of the 13^{+} charge state (Fig. S2) and bottom-up identification of surrogate triply charged tryptic peptides that constitute Cys^{118} (**Figure 3c-d**). The top-down data contain diagnostic neutral loss ions corresponding to Cys-glutathionyl and glutathione as well as backbone product ions, which suggests that the glutathione moiety is present exclusively on Cys^{118}. In concordance with $hRas^{1\text{-}166}$, bottom-up peptide mass spectra show diagnostic neutral loss of Cys-glutathionyl and sequence ions that unambiguously localize glutathione on Cys^{118}. Our

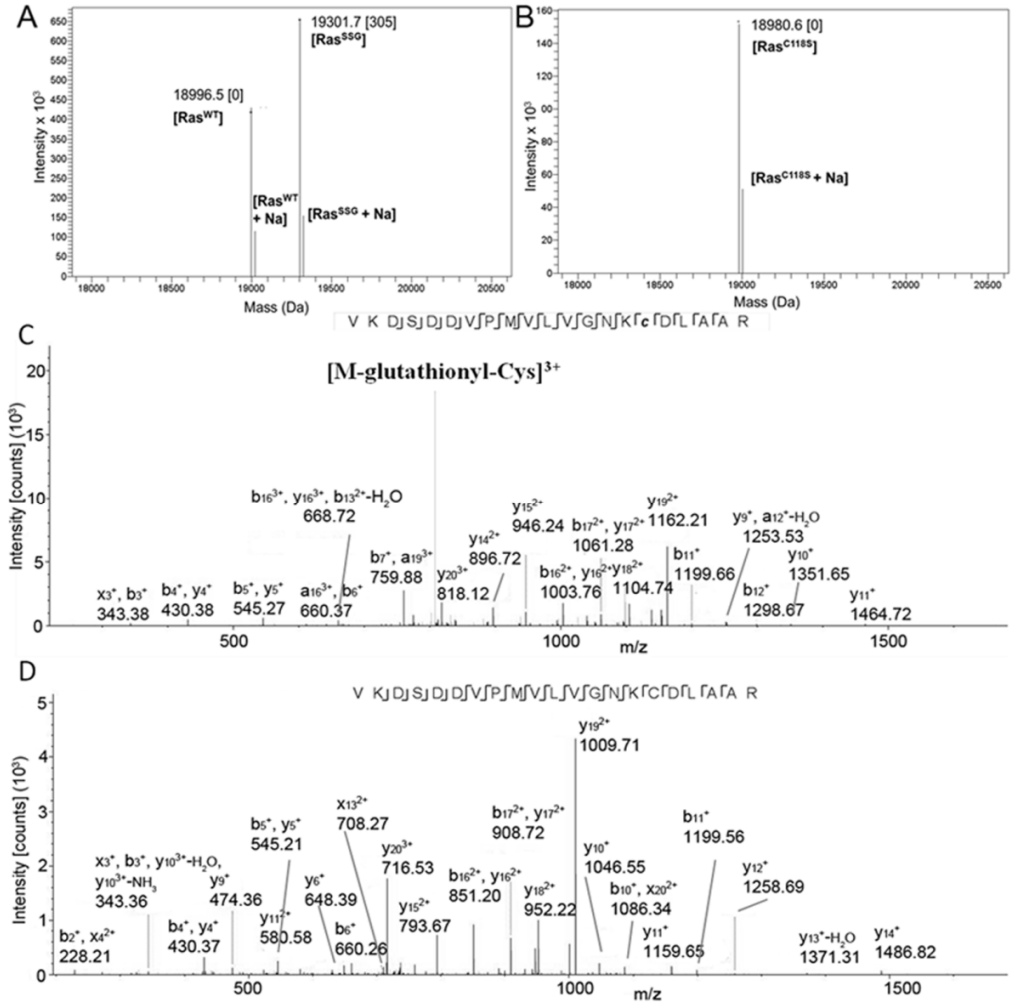

Figure 3. Mass spectrometry of glutathiolated Ras.

(a) Intact deconvoluted mass spectrum resulting from the reaction of Ras^{WT} with GSSG. The major peaks correspond to unmodified and singly glutathiolated Ras. (b) Intact deconvoluted MS resulting from the reaction of RAS^{C118S} with GSSG. The peak corresponds to unmodified RAS^{C118S}. Note: The deconvoluted mass spectra in Fig 1 a-b also consist of gas-phase sodium adducts of Ras. (c) MS/MS-CID spectrum of a triply charged RAS^{WT} peptide glutathiolated at Cys^{118}. The glutathione modification is localized at Cys^{118}, and the diagnostic neutral loss of 129 Da corresponds to glutathionyl-cysteine [60]. (d) MS/MS-CID spectrum of the unmodified triply charged peptide counterpart. Mass spectrometry data collected in collaboration with Harsha Gunawardena.

mass spectrometry data indicate that Ras^{C118}, which is solvent exposed in the structure of $hRas^{1-166}$ (pdb: 1crp), is susceptible to glutathiolation, whereas the two solvent inaccessible cysteine residues (Cys^{51} and Cys^{80}) were unmodified under the tested conditions.

Glutathiolation of Ras^{C118} does not significantly affect Ras-GDP nucleotide dissociation or GTP hydrolysis

It has previously been observed that peroxynitrite addition to BAECs and VSMCs promotes the formation of glutathiolated Ras at Cys^{118}. Moreover, glutathiolation was concluded to be an activating modification as the population of activated Ras was also glutathiolated (*71, 77, 96*). As exposure of Ras to peroxynitrite in cells could generate $Ras^{C118\bullet}$ and Ras^{SSG}, it is difficult to distinguish which modification, the thiyl radical or glutathione, leads to Ras activity changes under the experimental conditions used. To assess whether glutathiolation alters Ras guanine nucleotide binding and/or GTP hydrolysis, we performed nucleotide dissociation and GTP hydrolysis assays on unmodified and glutathiolated $hRas^{1-166}$ *in vitro*. As shown in **Figure 4a and b**, the intrinsic rates of GDP dissociation (k_{obs}) for Ras^{WT} and Ras^{SSG} (**Figure 4a-b**) were determined to be similar ($3.9 \pm 0.1\times10^{-5}$ s^{-1} vs. $4.7 \pm 0.5\times10^{-5}$ s^{-1}). As the intrinsic rate of nucleotide dissociation for Ras is slow, interactions with GEFs are required to facilitate nucleotide exchange *in vivo*. Therefore, we measured the rate of GDP dissociation in the presence of SOS, a Ras GEF, as previously described (*108*). When the minimal catalytic domain of SOS (SOS^{cat}) was added to Ras, the rate of nucleotide dissociation for Ras^{SSG} and Ras^{WT} was similar ($18.5 \pm 0.5\times10^{-4}$ s^{-1} vs. $20.2 \pm 0.7\times10^{-4}$ s^{-1}, respectively).

To determine the effect of glutathiolation on Ras-GTP hydrolysis rates, we measured the rate of GTP hydrolysis in the presence and absence of the minimal catalytic domain of the Ras-specific GAP, $p120^{GAP}$ (*112*). For this assay, the phosphate binding protein FlipPi 5U was employed as a phosphate sensor. FlipPi binds to free phosphate in solution and has a measurable change in fluorescence upon phosphate binding (*113*). By performing single-

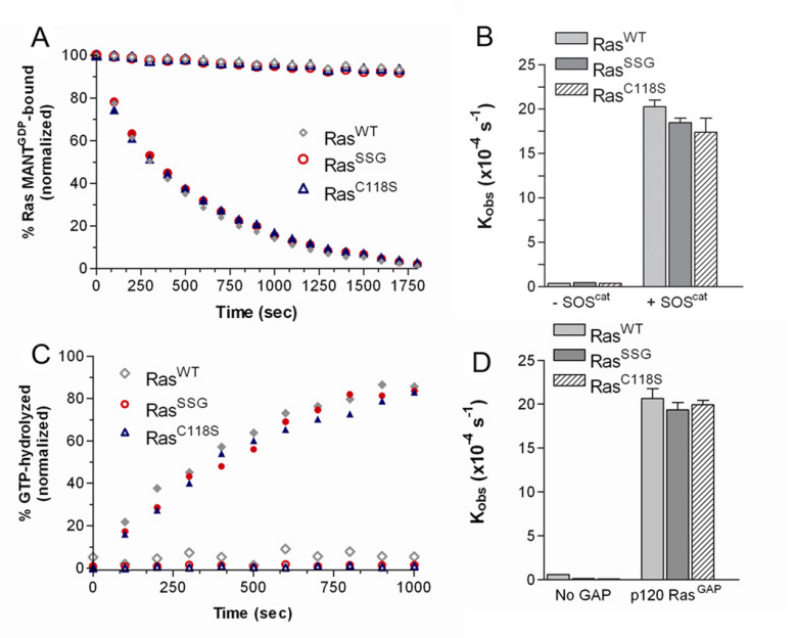

Figure 4. Biochemical characterization of glutathione-modified Ras.

(A) Rates of GDP dissociation were determined for Ras^{WT}, Ras^{C118S}, and Ras^{SSG} (1 μM). Nucleotide dissociation kinetic traces in the absence (open symbols) and presence (closed) of the GEF SOS^{cat} are shown. (B) The relative rates of GDP dissociation (k_{obs}) are presented. (C) Representative Ras GTP hydrolysis kinetic traces in the absence (open symbols) and presence (closed) of p120RasGAP^{cat}. (D) The relative rates of hydrolysis in the absence and presence of GAP are presented. All reactions were performed in triplicate and were fit to a single exponential dissociation/association curve using GraphPad Prism, and the error is reported as the standard deviation of the replicates. Normalized results are presented for graphical comparison of the experiments. The experimental conditions and data analysis for these assays are described in the Materials and Methods.

turnover hydrolysis assays, the intrinsic rate of GTP hydrolysis for Ras^{WT} was determined to be 0.6 ± 0.04×10^{-4} s^{-1} at 25˚C (**Figure 4c-d**), similar to previously reported values of 4.4×10^{-4} s^{-1}, which were performed at a higher temperature of 30˚C (*118*). The rates of GTP hydrolysis determined using the FlipPi sensor compared to previously reported values, indicating that this method is suitable for comparing GTP hydrolysis rates. The intrinsic rate of GTP hydrolysis for Ras^{SSG} was determined to be ~4-fold slower (0.14 ± 0.06×10^{-4} s^{-1}) than for Ras^{WT}. However, as the intrinsic rate of GTP hydrolysis is too slow to be biologically relevant and requires catalysis by GAPs *in vivo* to regulate Ras activity, we measured the rate of hydrolysis in the presence of catalytic amounts of $p120^{GAP}$. The rate of GAP-mediated GTP hydrolysis for Ras^{WT} and Ras^{SSG} were observed to be similar (20.6 ± 2.3×10^{-4} s^{-1} and 19.4 ± 1.7×10^{-4} s^{-1}, respectively; **Figure 4c-d**). Thus, glutathiolation of Ras^{C118} does not affect $p120^{GAP}$-mediated GTP hydrolysis.

Glutathiolation at Cys^{118} does not perturb Ras structure

As it was previously suggested that Ras glutathiolation alters the structure of Ras and leads to increased nucleotide exchange (*71*), we glutathiolated ^{15}N-enriched $hRas^{1-166}$ and performed 2D NMR HSQC analyses. A 2D ^{1}H-^{15}N NMR HSQC allows for observation of backbone and side chain N-H groups and provides a site-specific probe for every residue in a protein aside from proline. An overlay of the Ras^{WT} and Ras^{SSG} HSQC spectra is shown in **Figure 5a**. Consistent with our MS data that Cys^{118} is the site of glutathiolation, the amide resonance corresponding to Cys^{118} is perturbed upon Ras glutathiolation, whereas the chemical shifts associated with Cys^{51} and Cys^{80} are unaltered. Glutathione is a tripeptide (Gly-Cys-Glu), and modification of Ras at Cys^{118} is likely to alter the chemical environment (chemical shift) of resonances proximal to the site of modification. As shown in **Figure 5a**, most resonances are unperturbed by glutathiolation of Ras at Cys^{118}. By mapping the residues that show chemical shift perturbations (14 peaks with chemical shift differences greater than one linewidth, 0.05 ppm in the ^{1}H dimension or 0.4 ppm in the ^{15}N dimension)

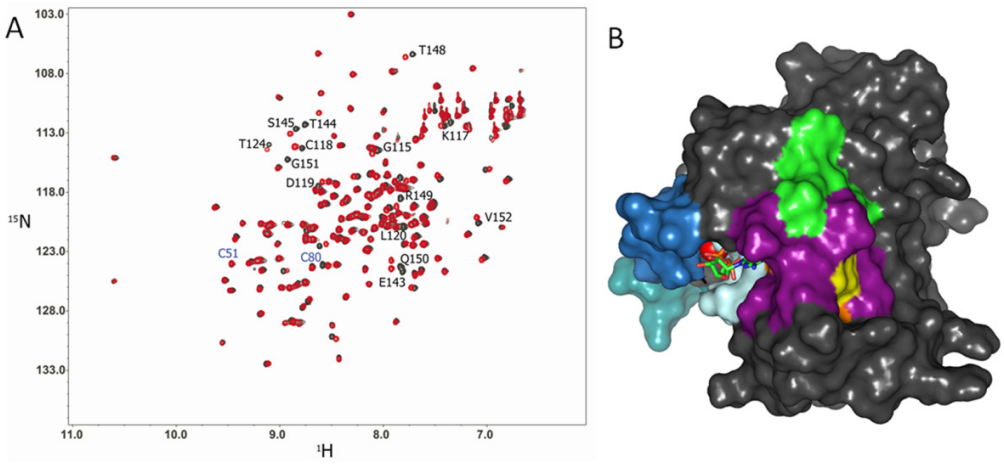

Figure 5. 2D NMR ^{1}H-^{15}N HSQC comparison of Ras^{WT} and Ras^{SSG}.

(A) A ^{1}H-^{15}N 2D HSQC overlay of Ras^{WT} (black) with Ras^{SSG} (red). The black-labeled residues indicate Ras NH resonances associated with residues that shift upon glutathione modification (peak shifts greater than 1 linewidth, 0.05 ppm in the ^{1}H dimension or 0.4 ppm in the ^{15}N dimension), and the blue-labeled residues correspond to the other two cysteines in Ras (Cys^{51} and Cys^{80}), which do not show amide peak shifts between Ras^{WT} and Ras^{SSG}. (B) Residues corresponding to the NH resonances that show chemical shift changes for Ras^{SSG} but not Ras^{SNO} are highlighted in green on a surface representation of $hRas^{1-166}$, while residues that show chemical shift changes in Ras^{SNO} are highlighted in orange. The residues that showed chemical shifts in both Ras^{SSG} and Ras^{SNO} are highlighted in purple. Cys^{118}, the site of modification, is shown in yellow, GDP is shown as sticks, magnesium is shown as a red sphere, and Switch I (blue), Switch II (teal), and the p-loop (pale blue) are shown for clarity. Surface rendering was generated with PyMol using pdb: 1crp.

onto the surface of the Ras structure (**Figure 5b**), only residues proximal to the modified cysteine show chemical shift changes. Interestingly, the chemical shift perturbations for Ras^{SSG} (green in **Figure 5B**) compared to Ras^{SNO} (orange; overlap is shown in purple, Cys^{118} in yellow) are similar, and we have previously shown that Ras^{SNO} does not alter Ras structure (*66*). Thus, the limited chemical shift changes close to the site of glutathiolation and similarity between the HSQC spectra of Ras^{WT}, Ras^{SSG}, and Ras^{SNO} suggest minimal structural perturbation by glutathiolation, consistent with our findings that the biochemical properties of Ras are unaltered. Furthermore, the residues important for Ras recognition by regulatory factors and effectors, including the p-loop (residues 10-17), Switch I, and Switch II, do not show chemical shift changes upon glutathiolation. These data are consistent with our findings that GEF- and GAP-mediated stimulation of GDP dissociation and GTP hydrolysis were unaffected by Ras glutathiolation.

Glutathiolation impedes redox-mediated nucleotide dissociation

Previous studies have shown that treatment of Ras with $NO_2^{\cdot}$ enhances the rate of nucleotide dissociation, whereas nitrosation of Ras at this site prevents radical-mediated nucleotide dissociation (*69*). To determine whether Ras glutathiolation, like nitrosation, impedes free radical-mediated dissociation in Ras, the rate of nucleotide dissociation was determined using a ^{MANT}GDP-dissociation assay in the presence of the NO$^{\cdot}$-releasing agent DEANO (*1*). As shown in **Figure 6a**, we observe an enhanced rate of Ras^{WT}-GDP dissociation in the presence of DEANO (greater than 200-fold faster). In contrast, the rate of GDP dissociation for the redox inactive Ras^{C118S} variant was insensitive to the presence of DEANO. Furthermore, Ras^{SSG} was resistant towards DEANO-mediated nucleotide dissociation. Although 1 mM DEANO was used in these experiments, only a small fraction generates $NO_2^{\cdot}$. DEANO releases NO$^{\cdot}$ with a half-life of 15 minutes at pH 7.0, and NO$^{\cdot}$, once generated, reacts with O_2 to generate $NO_2^{\cdot}$ (*119, 120*). Moreover, the estimated dissolved oxygen content in aqueous solution is only 250 μM, which limits the amount of $NO_2^{\cdot}$ that can

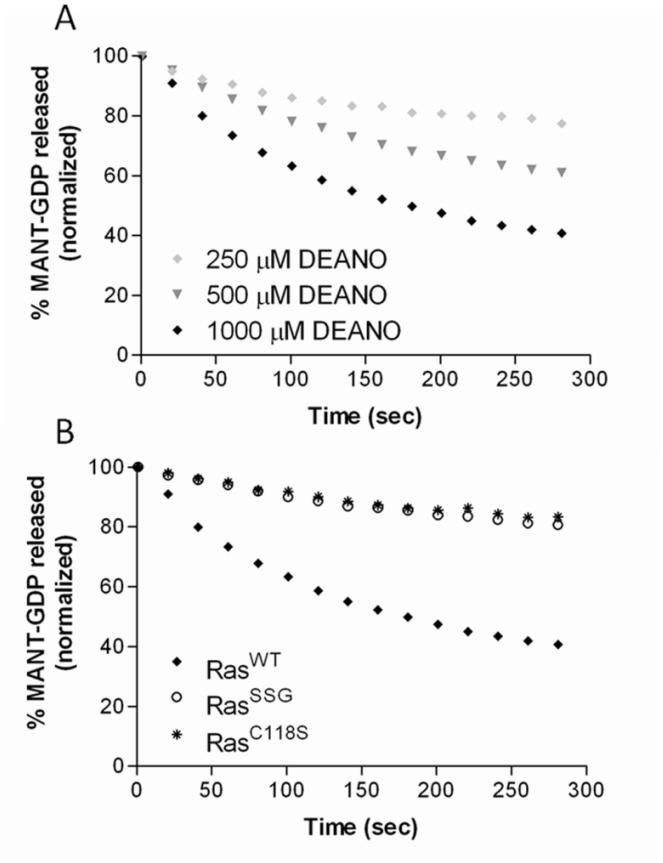

Figure 6. ^{MANT}GDP nucleotide dissociation assays in the presence of the NO-generating agent DEANO.

(A) Ras^{WT} was pre-loaded with ^{MANT}GDP and exposed to increasing concentrations of DEANO in the absence of unlabeled GDP. All conditions contained 1 μM Ras^{WT} and ♦ 250 μM DEANO, ▼ 500 μM DEANO, or ♦ 1 mM DEANO added at the start of the experiment. (B) ♦ Ras^{WT}, * Ras^{C118S}, and ○ Ras^{SSG} (1 μM) were preloaded with ^{MANT}GDP and exposed to 1 mM DEANO. All reactions were performed in triplicate and were fit to a single exponential dissociation curve using GraphPad Prism. Normalized results are presented for graphical comparison of the experiments.

be formed. Thus, our results show that glutathiolation impedes free radical-dependent Ras GDP dissociation, whereas glutathiolation does not significantly affect Ras structure, activity, or interactions with modulatory proteins.

Discussion

A number of studies have reported Ras activity modulation by ROS and RNS (*94*). Most of these studies point to Ras^{C118} as the redox-sensitive site because this cysteine has been shown to be oxidized by a number of cysteine-modifying agents and is required for redox-mediated regulation of Ras activity (*57*). Two of the most common oxidative modifications identified for Ras *in vivo* are nitrosation and glutathiolation. We have previously reported that radical-mediated nitrosation of Ras leads to increased guanine nucleotide dissociation (*68*), whereas non-radical-mediated nitrosation of Ras^{C118} does not affect Ras guanine nucleotide binding (*66*). Given these observations, we were intrigued by reports that glutathiolation of Ras alters Ras activity (*71, 77, 96, 100*).

To better understand how Ras activity is modulated by glutathione, we considered radical- and non-radical-mediated reactions that can result in Ras glutathiolation. Three potential pathways of glutathiolation are presented in **Figure 8** (radical-mediated, 8a; and non-radical-mediated, 8b and 8c). Earlier reports have suggested that glutathiolation leads to Ras activation. For example, the fraction of activated GTP-bound Ras was higher in the pool shown to be glutathiolated upon peroxynitrite exposure to BAECs (*71*) and after administration of angiotensin II to VSMCs (*77*). However, angiotensin II and peroxynitrite produce free radicals. Angiotensin II produces ROS through NAD(P)H oxidase activation (*104, 121*), and peroxynitrite can undergo homolysis to generate ROS and RNS. In fact, under most physiological conditions, CO_2 reacts with peroxynitrite to generate $CO_3^{\bullet-}$ and $NO_2^{\bullet}$ byproducts in fairly high yields (>30%) (*75, 76*); in addition, under acidic conditions, peroxynitrite can undergo proton catalyzed homolysis to form $HO^{\bullet}$ and $NO_2^{\bullet}$ (*74*). An

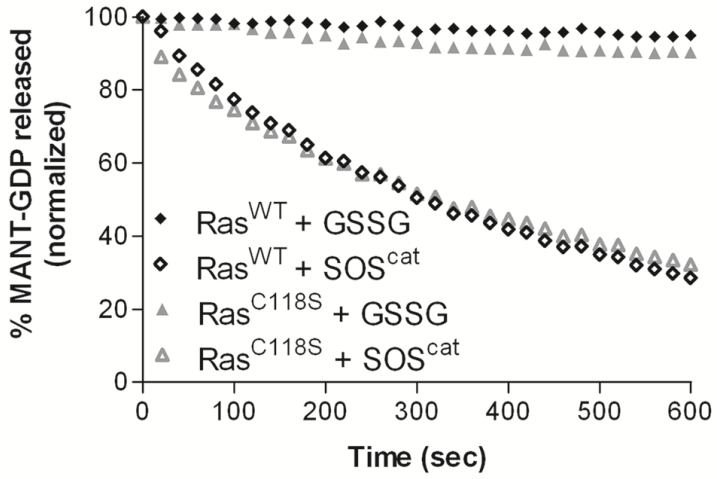

Figure 7. Effect of oxidized glutathione on nucleotide binding in Ras.

^{mant}GDP dissociation measured for Ras^{WT} (♦) and Ras^{C118S} (▲) in the presence of 100 μM GSSG (closed symbols) and in the presence of SOS^{cat} (open symbols). ^{mant}GDP nucleotide dissociation was performed as described; however, no unlabeled GDP was present and 100 μM oxidized glutathione was added to the reaction cuvette. All reactions were performed in triplicate and were fit to a single exponential dissociation curve using GraphPad Prism. Error bars have been removed for clarity. Ras and Ras^{C118S} with 1 μM GEF are shown for comparison. Normalized results are presented for graphical comparison of the experiments.

important consideration that must guide *in vitro* experimentation with peroxynitrite is that in the absence of CO_2, peroxynitrite reacts directly with many biochemical targets, particularly thiols. This oxidative reaction produces predominately non-radical oxidativeproducts and is faster than its homolysis to $HO^{\cdot}$ and $NO_2^{\cdot}$. Therefore, peroxynitrite reactions are heavily context dependent. Importantly, given the high glutathione concentration in cells, once peroxynitrite is decomposed and the free radical chain reactions are completed, glutathiolated Ras will predictably be a major end product that is indistinguishable by all means from the end product produced directly by the reaction of oxidized glutathione with Ras^{WT}. Therefore, we postulate that the exogenous addition of peroxynitrite and angiotensin II promotes Ras thiyl radical-mediated oxidation of the bound guanine nucleotide, leading to Ras activation. Further, the resulting thiyl radical can react with glutathione to produce $Ras^{SSG\cdot}$, which aerobically decays to Ras^{SSG} and $O_2^{\cdot-}$. This route of activation is shown in **Figure 8A**, and based on our analysis, is the likely pathway of glutathiolation that would result in Ras activation *in vivo*. Interestingly, Ras glutathiolation appears to protect Ras from further free radical-mediated events. We evaluated guanine nucleotide binding of Ras^{WT}, Ras^{C118S}, and Ras^{SSG} in the presence of the NO-releasing agent DEANO. In these experiments (**Figure 6**), glutathiolated Ras was protected from free radical-mediated nucleotide dissociation. Therefore, glutathione, which likely modifies Ras after an initial activating event, could protect Ras from over-oxidation in cells under conditions of oxidative stress.

The other potential pathways of Ras glutathiolation shown in **Figure 8** are unlikely to lead to Ras activation (**Figure 8b** and **8c**). To demonstrate this, we generated glutathione-modified Ras through a non-radical-mediated pathway by treating Ras with oxidized glutathione (**Figure 8b**), which glutathiolates Ras at Cys^{118}, and find that neither the intrinsic or regulator (GEF/GAP)-mediated rates of guanine nucleotide dissociation and hydrolysis are altered (**Figure 4**). However, as the cellular concentration of oxidized

glutathione is generally quite low (GSH:GSSG ratio in cells is >100:1) (*122*) and the reaction rate slow, this is an unlikely pathway of Ras glutathiolation in cells. To experimentally validate the role of glutathione on nucleotide exchange, we exposed Ras^{WT} and Ras^{C118S} to oxidized glutathione (similar to the pathway presented in **Figure 8b**) and found that Ras guanine nucleotide binding was not affected by the presence of oxidized glutathione (**Figure 7**). While this data appears contradictory to the results described by Clavreul et al (*71*), identical levels of Ras nucleotide dissociation were observed, which was approximately 5% of the bound nucleotide after 300 s. In our experiments, we also tested Ras^{C118S} and observed identical levels of nucleotide dissociation, indicating that glutathione does not promote guanine nucleotide release from Ras. We also present GEF-induced dissociation of Ras^{WT} and Ras^{C118S} within **Figure 4** to highlight the difference in GSSG-mediated dissociation and GEF-mediated dissociation. Furthermore, as the experimental conditions used in Clavreul et al (*71*) were not conducive to peroxynitrite-mediated radical formation [7], glutathiolation is unlikely to result in Ras activation. Thus, results from this study do not support Ras activity modulation due to the presence of the glutathione moiety on Ras.

Seemingly in direct contradiction with our results, Adachi et al observed that overexpression of glutaredoxin-1 (GRX-1) in VSMCs inhibited Ras glutathiolation and activation upon stimulation with peroxynitrite (*77*). However, overexpressed redox proteins can have profound effects on the cellular oxidation state, and it has been previously shown that downregulation of GRX-1 can sensitize lens epithelial cells to oxidative stress-induced apoptosis (*123*). Moreover, overexpression of GRX-1 protects against doxorubicin-induced cell death (*124, 125*), which mediates cell death through increased oxidative stress (*126*). Therefore, overexpression of GRX-1, as in Adachi et al, likely decreased the level of oxidative stress, which would result in reduced Ras activation by radical-mediated oxidation.

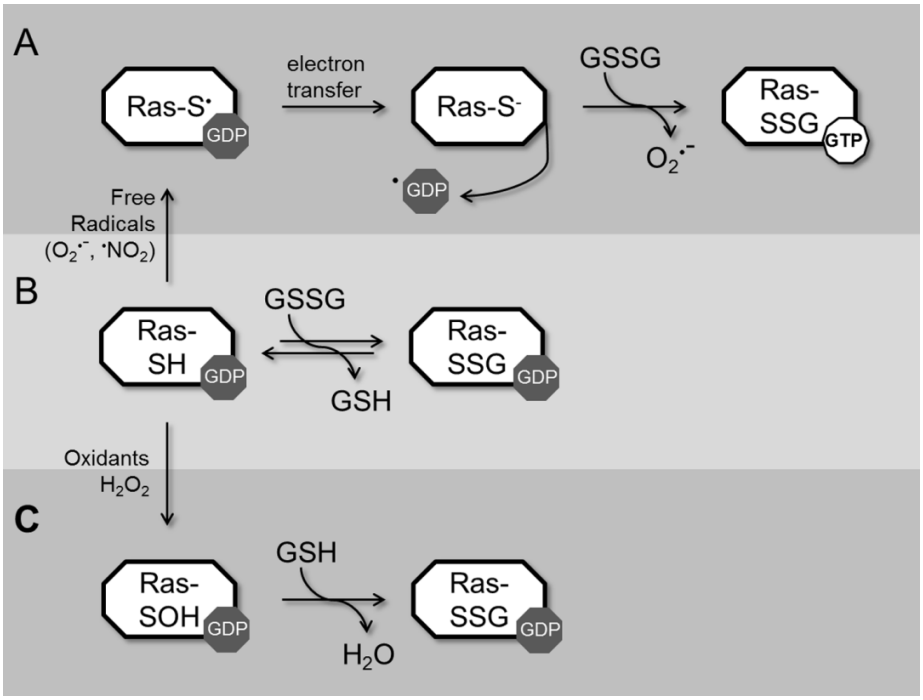

Figure 8. Modification of Ras by glutathione can proceed by three different mechanisms. In pathway A, redox agents capable to generating a Ras thiyl radical can induce radical formation on Ras^{C118}; electron transfer results in guanine-radical formation, guanine-base oxidation, and release of the oxidized base from Ras. Given the ratio of GTP/GDP in cells (~10:1), release of GDP promotes GTP binding. Free radical-induced oxidation leaves Ras in the thiyl anion form, which is more reactive to oxidation and can result in glutathione modification. In pathway B, Ras can react with oxidized glutathione through disulfide exchange to form glutathiolated Ras. Given the slow rate of this reaction and concentration of GSSG in cells, this pathway is unlikely to have a large contribution to Ras glutathiolation *in vivo*. In pathway C, Ras is oxidized by a non-radical oxidant, such as H_2O_2, which results in sulfenic acid formation at Ras^{C118}. Sulfenic acids are an intermediate step in disulfide bond formation; therefore, this form of Ras can interact with reduced glutathione to form glutathiolated Ras. However, Ras^{SSG} formed by non-radical means does not affect guanine nucleotide binding, nucleotide hydrolysis, or Ras activation. Thus, Ras activation and glutathiolation likely occurs in cells by reaction of Ras with thiyl radical-generating agents (pathway A), which promotes activation through nucleotide dissociation and GTP binding.

Another possible reaction pathway to consider is shown in **Figure 8c**. As disulfide bond formation generally proceeds through a sulfenic acid intermediate, it is possible that oxidation of Cys^{118} to a sulfenic acid will lead to Ras^{SSG} formation in the presence of reduced glutathione, which is present at a high levels in cells (GSH:GSSG ratio in cells is >100:1). Asthis pathway does not generate radical intermediates, we postulate that it is unlikely to alter Ras activity. While the products of angiotensin II or peroxynitrite exposure to cells can lead to Ras glutathiolation by the pathway presented in **Figure 8c**; the relative rate of oxidation is likely too slow to be physiologically relevant. It is more likely that glutathiolation occurs through radical-mediated interactions in cells. However, as Ras glutathiolation can proceed through pathways that do not alter Ras activity, it is difficult to use Ras glutathiolation as a marker of Ras activity regulation unless Ras radical formation can be detected coincident with Ras glutathiolation.

Conclusions

We have previously shown that $NO_2^{\cdot}$ can increase the rate of nucleotide dissociation in Ras and that modification of Ras by $NO^{\cdot}$ renders Ras less sensitive to radical-mediated oxidation (*66*). Consistent with these observations, Ras^{SSG} does not affect the structure or activity of Ras. When considering the faster reaction rates of radical vs. non-radical-mediated cysteine oxidation, we postulate that activation mediated through oxidation of Ras *in vivo* occurs through the formation of a Ras thiyl-radical intermediate (**Figure 8**). The Ras thiyl radical can promote Ras activation under appropriate redox conditions by facilitating nucleotide exchange and can react with $NO^{\cdot}$ or $GS^{\cdot}$ radicals to form Ras^{SNO} or Ras^{SSG} (**Figure 8**). While these end products do not alter Ras guanine nucleotide binding or hydrolysis, they impede Cys^{118} from engaging in further free radical-mediated reactions. Therefore, we postulate that coincident detection of Ras glutathiolation and activation results from Cys^{118} thiyl radical-mediated oxidation of the guanine base and GDP release.

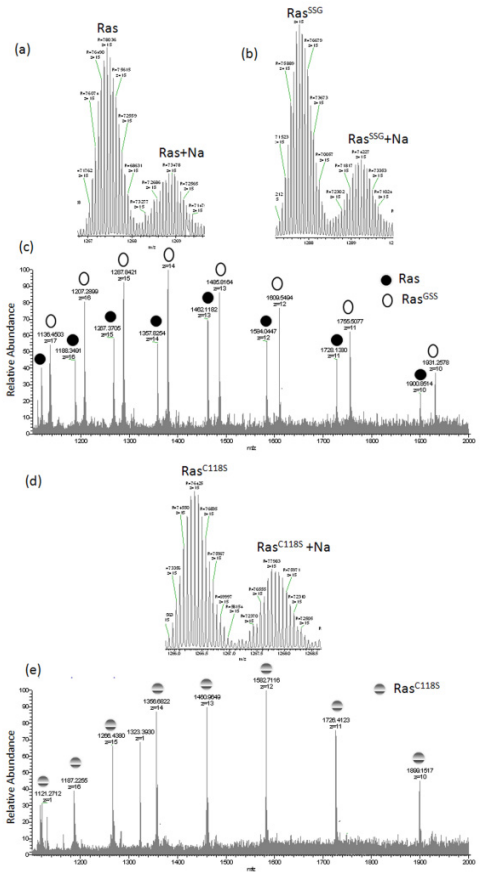

Supplemental Figure 1. Intact mass spectra resulting from the reaction of Ras^{WT} and Ras^{C118S} with GSSG.

(a) ESI-SIM scan of 15+ Ras. (b) ESI-SIM scan of 15+ Ras^{SSG}. (c) ESI-Full MS scan of unmodified and singly glutathiolated Ras^{WT}. (d) ESI-SIM scan of 15+ Ras^{SSG}. (e) ESI-Full MS scan of Ras^{SSG}. Mass spectrometry data collected in collaboration with Harsha Gunawardena.

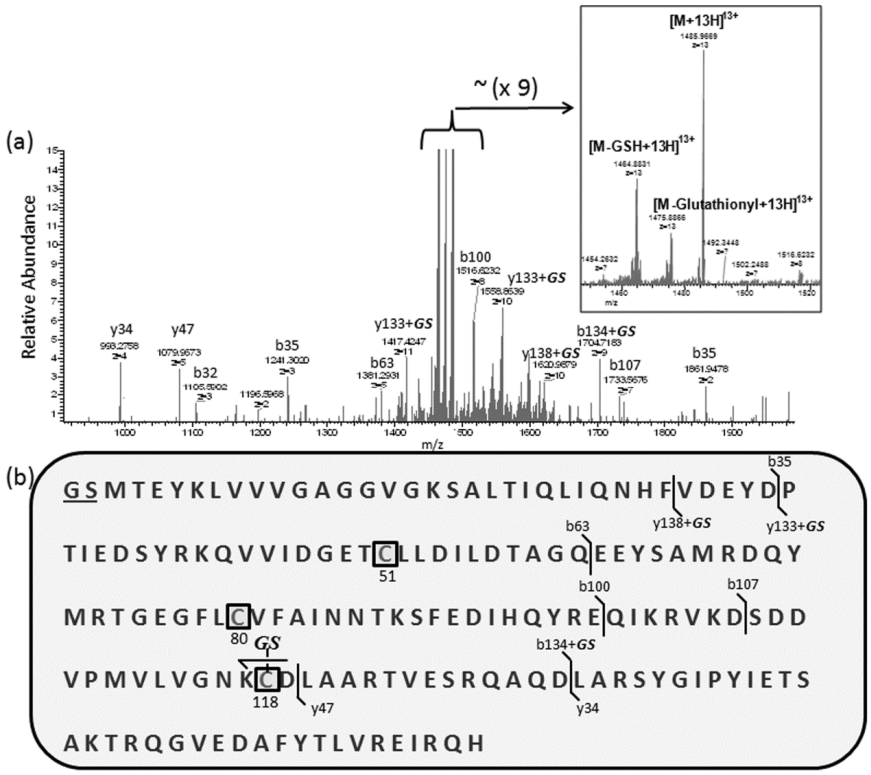

Supplemental Figure 2. Detection of glutathiolated Ras at Cys^{118}.

(a) HCD-MS/MC spectrum of z=13+ glutathiolated RasWT with inset showing neutral loss of ions corresponding to cys-glutathionyl and glutathione (GSH). (b) Sequence ions mapped to the theoretical sequence of the Cys^{118} glutathiolated Ras constructs. The sequence ions b63, b100, b107, and (b134+GS) were used to localize the single glutathione exclusively on Cys^{118}. (Note that Ras constructs contained two additional residues on the N-terminus that were ignored in the positional annotation of cysteine residues of Ras. Mass spectrometry collected in collaboration with Harsha Gunawardena.

Chapter 3: Characterization and Nitrosation of Oncogenic K-Ras^{G12C}

Introduction

Ras GTPases are part of the Ras superfamily of GTPases, which play a major role in many cellular signaling pathways, including gene expression, cell growth, transport, and apoptosis (*84*). These proteins function as molecular switches by cycling between the active GTP- and inactive GDP-bound states to regulate activity. Ras alternates between the GTP-bound and GDP-bound forms through regulation by GTPase activating proteins (GAPs) and guanine nucleotide exchange factors (GEFs). GAPs bind and stimulate GTP hydrolysis to GDP, which inactivates the GTPase, whereas GEFs promote activation by facilitating the exchange of GDP for GTP (*127*).

Mutations to Ras family proteins account for approximately 30% of all oncogenic mutations (*128*). There are three isoforms of Ras in the cell, H-Ras, N-Ras, and K-Ras. However, K-Ras is the most frequently mutated isoform in cancer (*128*). Oncogenesis due to Ras most commonly arises from single mutations at Gly^{12}, Gly^{13}, and Gln^{61}. Gly^{12} and Gly^{13} are within the phosphoryl binding loop (p-loop), a structural motif in Ras to interacts with the phosphate moieties of the bound nucleotide. Gln^{61} functions as the catalytic residue of GTP hydrolysis and serves as the catalytic base in cleavage of the γ phosphate of GTP (*90*). Mutations to these specific residues often result in loss of GAP sensitivity and constitutive activation (*93, 129*). For K-Ras, the majority of the mutations occur at Gly^{12} and account for the majority of mutations in lung and pancreatic cancers; the most common Gly^{12} mutations in K-Ras are K-Ras^{G12C}, K-Ras^{G12D} and K-Ras^{G12V} (*128, 130*).

Ras has been shown to be susceptible to oxidation by small molecule oxidants, which induce nucleotide dissociation and activate Ras (*57*). Ras GTPases are sensitive to free

radical oxidation; *in vivo*, this can occur by interaction with various reactive nitrogen and oxygen species (RNS, ROS), which are often produced by enzymes such as nitric oxide synthases (NOS) and NADPH oxidases. In the cell, endothelial NOS (eNOS) specifically catalyzes NO· synthesis, which promotes Ras activation through the reaction of Cys^{118} (*63*). The free radical NO_2· has been shown to react with the thiol of Cys^{118} and produce a thiyl radical (RS·), which likely results in degradation of the base and nucleotide dissociation (*62, 67*). The redox sensitivity and importance of Cys^{118} was further confirmed from the characterization of the variant Ras^{C118S}, which was found to be insensitive to oxidants but otherwise behaved identically as Ras^{WT} (*21*).

The Ras^{G12C} mutation, which is common in lung cancer, places a thiol in the p-loop of Ras. Thus, given the reactivity of Cys^{118} to oxidants and the altered redox environment in the lung, it was proposed that Ras^{G12C} may be redox sensitive. Toward this end, K-Ras was modified with the fluorophore ABD-F (4-fluoro-7-aminosulfonylbenzofurazan), which preferentially interacts with the thiolate state, and was used in a pH screen to determine the pK_a of the thiol of Ras^{G12C}. Ras^{G12C} was s-nitrosated using nitric oxide and CysNO, a non-radical nitrosating agent, to determine the effects of oxidation at this cysteine. Further, while all mutations at Gly^{12} are predicted to decrease GAP sensitivity, Ras^{G12C} has not been studied. Therefore, we investigated the GAP sensitivity of Ras^{G12C} to the catalytic domains of RasGAP and NF1, two Ras-specific GAPs. The stability and secondary structure of native K-Ras and K-Ras^{G12C} was analyzed using circular dichroism (CD) spectroscopy. In addition, we performed NMR spectroscopy to determine whether Ras^{G12C} showed an altered structure from other oncogenic Gly^{12} mutants, such as Ras^{G12D}. We found that K-Ras^{G12C} has an altered pK_a and was susceptible to free radical and two-electron oxidation. Gly^{12} mutants were also reaffirmed to have reduced sensitivity to GAPs, and the structure of Ras^{G12C} was not significantly altered when compared to other Gly^{12} mutants.

Methods

Purification of Ras proteins

Protein purification was performed exactly as previously described (*131*). K-Ras was a gift of Genentech and is in the pET52b vector, which contains a 6x-His purification tag and a TEV (tobacco etch virus) protease site to remove the His tag. This vector was expressed in BL21 (DE3) Rosetta 2 pLysS cells, purified following the Qiagen nickel NTA purification protocol, and verified by SDS-PAGE.

ABD-F modification assays

ABD-F modification buffer (15 mM MES [(2-(N-morpholino)ethanesulfonic acid], 5 mM MgCl2, 30 mM NaCl, 200 μM DTPA, pH 8.0) was prepared with 10 mM dithiothreitol (DTT). An Amicon centricon was used to buffer exchange K-Ras and the protein was reduced for 30 minutes on ice. At the same time, ABD-F modification buffer without DTT was sparged with N_2 gas to remove dissolved oxygen. The protein was exchanged into this buffer to remove DTT from the sample prior to reaction with ABD-F.

In a black 96-well plate, 20 μM K-Ras was added in 100 μL of reaction buffer (100 mM MES, 100 mM HEPES, 5 mM MgCl2, 200 μM DTPA) with a pH that was predetermined. To a separate plate, ABD-F was added to 2 mM in 100 μL of reaction buffer at the same pH as the corresponding well in the original plate. Using a multi-channel pipette, ABD-F was added to the K-Ras plate to start the reaction. The fluorescence of the reaction was monitored using a Spectramax M5 plate reader over a pH range of 5.8 to 8.5. The excitation wavelength for ABD-F is 389 nm, and the emission wavelength is 513 nm.

Nucleotide exchange and hydrolysis assays

K-Ras was loaded with ^{mant}GDP (2'-/3'-O-(N'-methylanthraniloyl)-GDP) for nucleotide exchange as previously described (*108, 109, 131*). K-Ras was added to 1 μM in 1 mL of exchange buffer, and the rate of nucleotide dissociation was determined by monitoring the

change in fluorescence of the ^{mant}GDP-loaded protein (excitation wavelength of 365 nm, emission wavelength of 435 nm) using a fluorimeter.

The nitrosating agent CysNO was generated for usage in the dissociation assays by reacting 100 μL of 50 mM L-cysteine (in 0.2 M HCl) with 100 μL of 50 mM $NaNO_2$. The reaction was allowed to proceed in the dark for 10 min, after which 20 μL of 40 mM ammonium sulfamate was added to remove any unreacted nitrate. After allowing 2 min for the reaction to quench, the CysNO solution was diluted to 1100 μL with 100 mM Hepes, 5 mM $MgCl_2$, and 1 mM DTPA (pH 7.5) to neutralize the acidic pH and remove free metal ions aside from Mg^{2+} (*132*). The concentration of CysNO was determined from an absorbance measurement taken at 336 nm (ε = 900 $M^{-1}cm^{-1}$).

The reactions with RNS were performed with either CysNO or DEANO NONOate (diethylammonium(Z)-1-(N,N-diethylamino)dia-zen-1-ium-1,2-diolate). DEANO was added in an excess of 40:1 to the protein to induce nucleotide dissociation by free radical oxidation. Nucleotide dissociation assays with CysNO were performed with 100:1 CysNO to induce modification by two-electron/non-radical oxidation. The addition of the oxidants was performed in the presence of 2 mM unlabeled GDP.

GTP hydrolysis assays with K-Ras were performed as previously described (*111, 133*) using FlipPi (Addgene; Cambridge, MA, USA) as the phosphate sensor (*113*). K-Ras (10 μM) was loaded with GTP and used with 10 μM FlipPi. Trace phosphates were removed from all reaction components to minimize background fluorescence. The rate of hydrolysis was determined from the fluorescence ratio of the emission wavelengths at 535 and 485 nm with an excitation wavelength of 435 nm as previously described (*113*).

Circular dichroism (CD) spectroscopy

Circular dichroism data were collected on a JASCO J-815 CD spectrometer with a JASCO Peltier device and water bath to control the temperature. Experiments were performed in a 1-mm cuvette at a protein concentration of 15 μM in 10 mM Tris, 1 mM

$MgSO_4$ (pH 7.45) and 10 μM GDP. Far UV scans were from 200 nm to 250 nm. Thermal denaturation of RhoA and the selected variants were monitored at a 221 nm to estimate the protein melting temperature. The temperature ramp rate was 1˚C/min and data points were collected every 1˚C. All data are reported in units of mean residue ellipticity, which was calculated as follows:$[\theta]_{MRE}=(\theta_{raw}\times MRW)/(10\times c\times l)$, where θ_{raw} is the ellipticity in degrees, MRW is (Molecular Weight (Da))/((no.of residues)-1), c is the protein concentration in g/ml, and l is the pathlength of the cuvette in cm, according to (*134*). For nitrosated Ras, Ras was reacted with 50× CysNO for 10 min, which was prepared as previously stated, prior to performing the CD analysis.

NMR analysis

NMR experiments were collected on a Varian Inova 700 MHz spectrometer at 25˚C. The 2D $^{1}H-^{15}N$ heteronuclear single quantum coherence spectroscopy (HSQC) experiments were performed with pulsed field gradient and water flip-back methods as previously described (*115*). Uniformly labeled ^{15}N-enriched Ras was purified as previously described (*116*). 2D ^{1}H-^{15}N HSQC experiments were acquired on 0.8 mM ^{15}N-enriched Ras^{WT} and Ras mutants with 1,024 x 128 complex data points and a spectral width of 8,000 Hz for the ^{1}H dimension and 1,709 Hz for the ^{15}N dimension. Buffer contained 10 mM maleate (pH 6.5), 5 mM $MgCl_2$, 40 mM NaCl, 20 μM GDP, and 10% D_2O. NMR data were processed and analyzed using NMR PIPE (*117*) and NMR ViewJ (One Moon Scientific; Newark, NJ).

Results

The thermal stability of K-Ras^{G12C} is not altered

As shown in **Figure 9A**, the CD spectra for K-Ras^{G12C} shows that there were no significant changes in the secondary structure of oncogenic K-Ras. Interestingly, the modification of the protein with CysNO does not influence the overall secondary structure of

the protein. To avoid modification at Cys^{118}, all mutations were performed in the K-Ras^{C118S} background. Thus, all proteins are in the context of additional mutations beyond Ras^{C118S}. The thermal denaturation study indicates that there is no significant loss in overall protein stability resulting from the K-Ras^{G12C} mutant or s-nitrosation (**Figure 9, Table 1**). Furthermore, modification by CysNO resulted in a slightly increased thermodynamic stability compared to K-Ras^{WT} and K-Ras^{G12C}; however, the increased stability was not significant.

K-Ras^{G12C} has an altered pK_a

Figure 10 shows that K-Ras^{G12C} is susceptible to modification by ABD-F in a pH-dependent manner. **Figure 10B** shows that there is a shift in the pK_a of K-Ras^{G12C} with respect to K-Ras^{WT}. The pK_a for K-Ras^{G12C} and H-Ras^{G12C} was found to be ~7.5; however, the pH screen used for the ABD-F assay did not extend far enough to allow for the pH plot of K-Ras^{WT} to reach a plateau. As Ras has been shown to be unstable above pH 8.5, it was not possible to determine the pK_a of Cys^{118}. However, this cysteine is not predicted to have an altered pK_a as it is solvent accessible and has no intra-protein contacts.

K-Ras^{G12S} was used as a negative control for this experiment. Aside from Cys^{118}, K-Ras has two other cysteine residues; however, these sites are not solvent accessible and are unlikely to be modified during reaction with ABD-F. Thus, mutation at Gly^{12} in combination with C118S results in only G12C modification by ABD-F, an observation that was further determined using mass spectrometry (data not shown). This is clearly shown from the superimposed ABD-F plot of K-Ras^{G12S} in **Figure 10A**. This analysis confirmed that ABD-F modification was specific to residue 12 in K-Ras^{G12C} as modification was not observed in K-Ras^{G12S}.

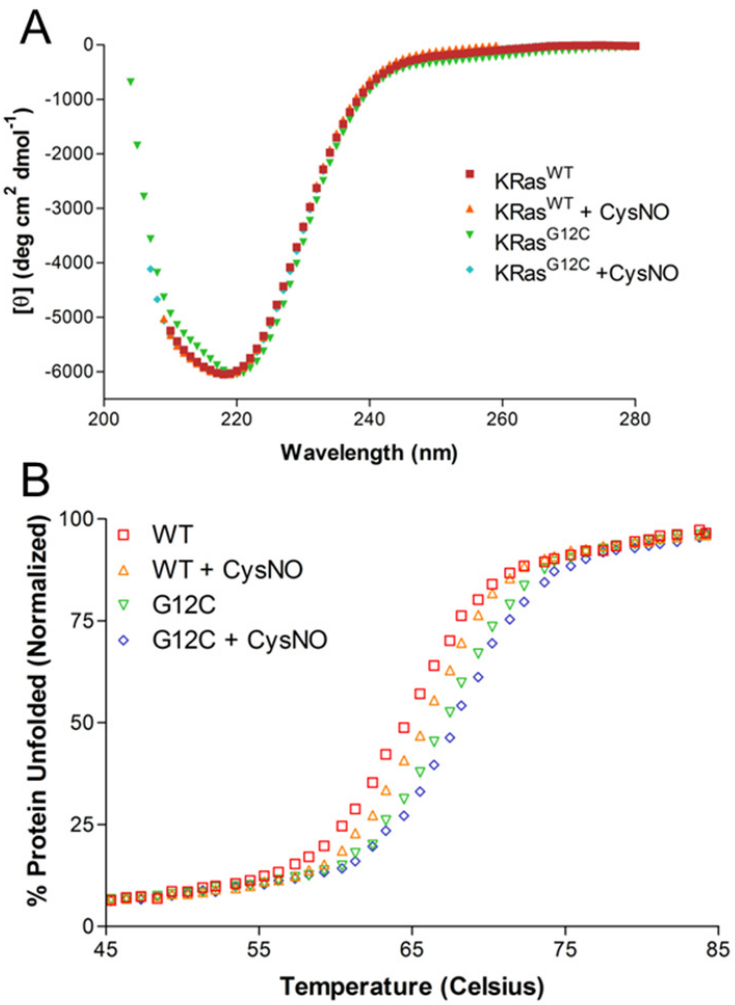

Figure 9. CD spectroscopy of K-Ras^{WT} and K-Ras^{G12C}.

(A) Far-UV CD scan of K-Ras. K-Ras was used at 25 μM. The raw data was used to calculate the mean residue ellipticity (Θ) for each protein sample.(B) The thermal stability of K-Ras. Each curve was normalized to total % of protein unfolding. The data were fitted to a Boltzmann sigmoidal curve to determine the melting temperature, which corresponds to the protein's respective T_m (melting temperature).

Table 1. T_m of K-Ras determined by CD spectroscopy

Protein	$\mathbf{T_m}$
$K\text{-}Ras^{WT}$	64.51°C
$K\text{-}Ras^{WT}$ + CysNO	65.73°C
$K\text{-}Ras^{G12C}$	67.12°C
$K\text{-}Ras^{G12C}$ + CysNO	67.83°C

Nitrosation of K-Ras^{G12C}

It is important to note that although Ras is specifically sensitive to radical oxidation (*21, 62*), the rates of dissociation shown here cannot be directly compared for computational purposes for several reasons. As shown in **Figure 11**, the amount of CysNO and DEANO added to react with K-Ras were not identical, so equimolar reactions did not occur. In addition, DEANO is initially slower to modify K-Ras than CysNO because it must first decompose and recombine with O_2 in solution to form $NO_2^{\cdot}$ that can oxidize G12C. As shown in **Figure 11**, modification at G12C by RNS (CysNO and DEANO) causes complete loss of ^{mant}GDP fluorescence over the course of the reaction. The ratios of oxidant to protein were selected to ensure complete modification of K-Ras on an appropriate timescale. Higher and lower ratios of oxidant to protein were also tested; however, the ratios plotted here were sufficient in showing a moderate rate of modification.

After completion of the NO reaction, DTT was added in equimolar concentrations to the CysNO/DEANO reaction cuvettes to reduce the protein to determine whether the reaction was reversible (resulting in nucleotide re-binding). This additional step resulted in a 60-70% recovery of fluorescence in the CysNO and DEANO reactions. However, because these assays were performed with an excess of GDP present in the solution (about 1000:1 excess GDP compared to ^{mant}GDP), a fluorescence recovery of this magnitude should not be expected as this implies that K-Ras is selectively rebinding with the released ^{mant}GDP.

Mutations at Gly^{12} result in a loss of GAP-mediated hydrolysis

Intrinsic and GAP-mediated GTP hydrolysis rates are shown **Figure 12**. Results from these analyses confirm that mutations at position 12 impair the rate of GAP-mediated GTP hydrolysis. At ratio of GAP:Ras that resulted in catalytic GTP hydrolysis in Ras^{WT}, we observed minimal increase in the rate of hydrolysis with Gly^{12} mutants, which is consistent with the current model on GAP-mediated hydrolysis (*112*). Although Ras^{G12C} had not been tested before, this mutation, as likely with all mutations at Gly^{12}, effectively make K-Ras

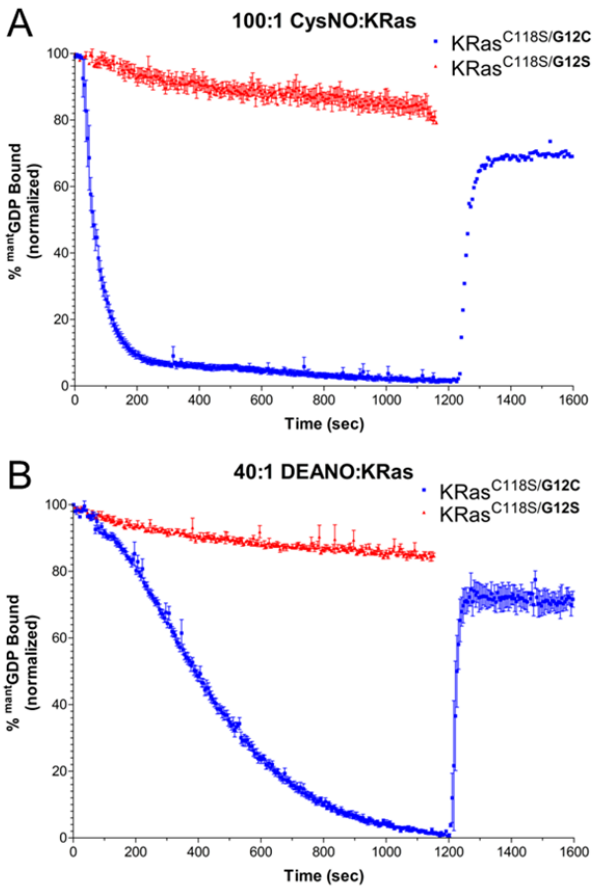

Figure 10. Nitrosylated K-Ras and nucleotide binding.

(A) CysNO modification of K-Ras. K-Ras was preloaded with ^{mant}GDP and added to the cuvette at 1 µM. CysNO was added at a final concentration of 100× to the reaction cuvette at the start of the experiment. (B) Oxidation of K-Ras^{G12C} with DEANO. DEANO was added at a final concentration of 40 µM. DTT was added to the reaction cuvette after 1200 s to reduce nitrosylated Ras. All reaction were performed in the presence of 2 mM GDP at pH 7.4. ^{mant}GDP fluorescence was measured as previously described.

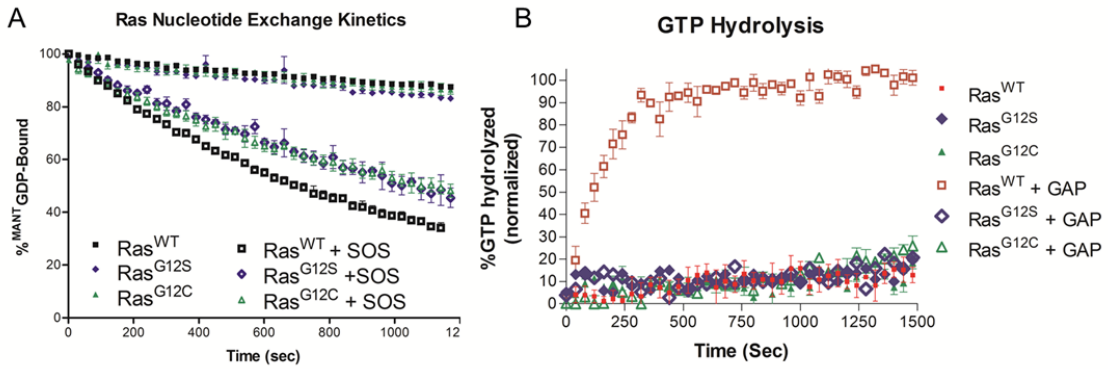

Figure 11. Nucleotide exchange and hydrolysis kinetics of Ras^{G12C} and Ras^{G12S}.

(A) Rates of GDP dissociation were determined for Ras^{WT}, Ras^{G12S}, and Ras^{G12C} (1 μM). Nucleotide dissociation kinetic traces in the absence (closed symbols) and presence (open) of the GEF SOS^{cat} are shown. GEF-mediated dissociation rates for the Gly^{12} mutants were approximately 2-fold slower compared to Ras^{WT}. (B) Representative Ras GTP hydrolysis kinetic traces in the presence (open symbols) and absence (closed) of $p120RasGAP^{cat}$. All reactions were performed in triplicate and were fit to a single exponential dissociation/association curve using GraphPad Prism, and the error is reported as the standard deviation of the replicates. Normalized results are presented for graphical comparison of the experiments. The experimental conditions and data analysis for these assays are described in the Materials and Methods.

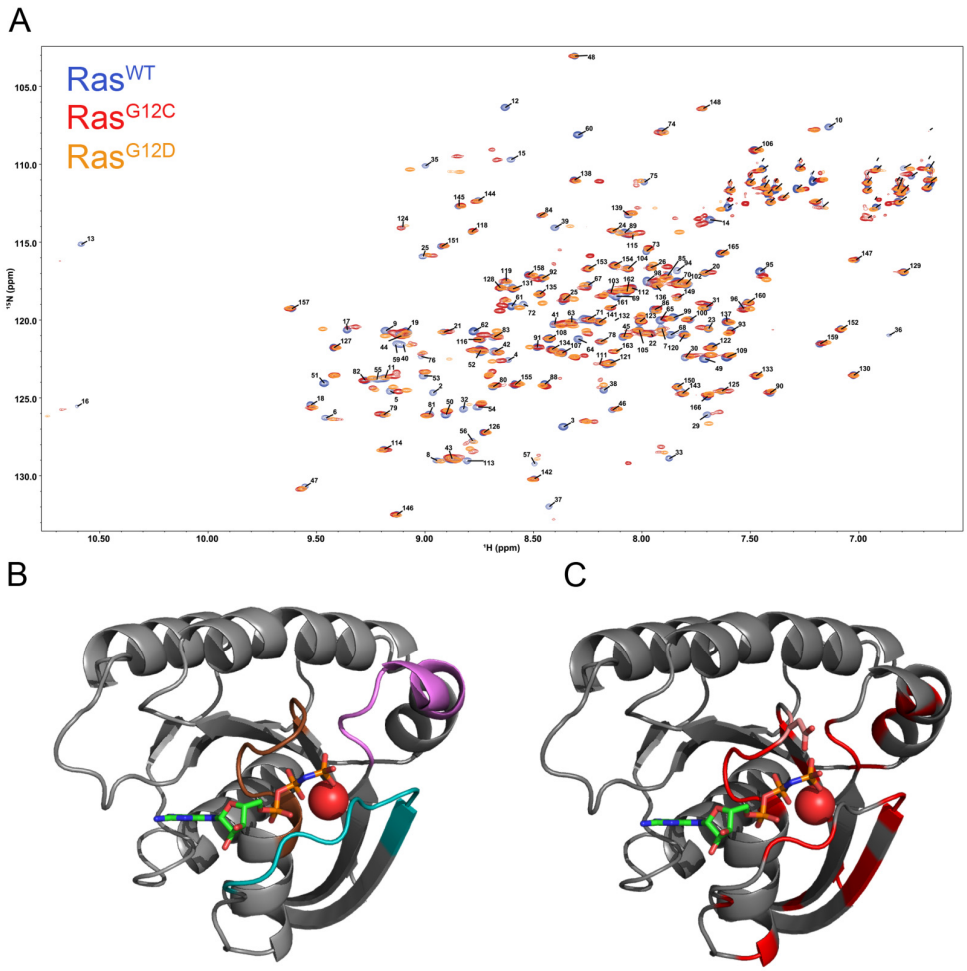

Figure 12. NMR analysis of Ras position 12 mutants.

(A) HSQC spectra of Ras^{WT} (black) overlaid with Ras^{G12C} (red) and Ras^{G12D} (yellow). All proteins were ^{15}N-enriched and data collection was at 0.8 mM protein. Figure was prepared with NMRViewJ. Numbering represents the Ras^{WT} assignments. (B) Ras^{G12D} (pdb 1AGP) crystal structure shown for reference. The nucleotide is shown in colored sticks, Mg^{2+} is a red sphere, switch I is shown in cyan, switch II is in purple, and the p-loop is in brown. (C) The Ras^{G12D} crystal structure with residues showing a chemical shift in Ras^{G12C} HSQC spectra plotted on the structure in red (peak shifts greater than 1 linewidth, 0.05 ppm in the ^{1}H dimension or 0.4 ppm in the ^{15}N dimension). The RasG12D residue is shown in pink sticks.

GAP-dead.

HSQC analysis of Ras^{G12C} shows minimal chemical shifts

As the Ras^{G12C} structure has not been reported, we wished to determine whether the structure of this mutant was significantly different from other Ras mutants. However, as many Gly^{12} mutants have been solved, including Ras^{G12D} (*135*), Ras^{G12V} (*136*), and Ras^{G12P} (*135*), we opted against determining yet another Ras structure. Instead, we analyzed the 2D HSQC data of Ras and two variants, Ras^{G12C} and Ras^{G12D}, to determine whether the Ras^{G12C} variant was likely to have a significantly different structure. As the Ras^{G12D} structure had been previously determined, this mutant was used to compare the chemical shifts of a mutant with a structure known to be similar to Ras^{WT}. Thus, the data show that mutation of Ras^{G12C} has a similar spectra to Ras^{G12D}, which was expected, and helps confirm that the Ras^{G12C} mutant does not have a significantly altered structure.

Discussion

Activating mutations in Ras lead to the development of cancer in humans. Mutations at positions 12, 13, and 61 alter GAP-mediated nucleotide hydrolysis, which leads to Ras activation in cells. Gly^{12} mutants are present in developmental disorders, such as Costello syndrome and Cardio-facio-cutaneous (CFC) syndrome (*137*), and have been associated with an increased occurrence of tumorigenesis. Mutations at this site lead to non-small cell lung cancer occurring in 30-50% of human lung cancer patients (*138, 139*) and any mutation at this position (except proline) leads to Ras activation (*140, 141*).

According to the model put forth by Scheffzek et al on GAP-mediated hydrolysis, mutations at position 12, 13, and 61 all interfere with GAP-mediated hydrolysis by steric clashes. The mutations prevent the arginine finger of the GAP from aligning the γ phosphate for hydrolysis. Specifically, at position 12, the model suggests that any mutation would lead to steric clashes and prevent nucleotide hydrolysis (*112*). This model is supported by data

that shows that Ras^{G12A} , in addition to other Gly^{12} mutants, is resistant to GAP-mediated hydrolysis (*142*). Therefore, one would expect all Gly^{12} mutations to show similar phenotypes *in vivo*. However, various mutations found at Gly^{12} lead to different levels of Ras activation, for example, the Ras^{G12C} substitution is less transforming than the Ras^{G12D} mutation, but both variants are associated with poor patient survival (*143*). In murine lung cancer studies, lesions harboring Val^{12} or Asp^{12} mutations were more likely to progress to adenocarcinomas than the Cys^{12} mutants (*143, 144*). However, increased expression of the Ras^{G12C} in mice displayed a higher occurrence of hyperplasia and adenomas (*138*).

Redox agents have been shown to modulate Ras superfamily GTPases at the NKCD motif (*62, 69, 84, 86, 145-148*). In particular, ROS and RNS activate Ras superfamily GTPases by increasing the rate of nucleotide exchange (*65, 68, 80, 149, 150*). ROS and RNS activate select redox-sensitive GTPases by reacting with the thiol of a solvent-accessible cysteine residue. Distinct from the NKCD motif in Ras (*78*), Rho GTPases contain a redox-sensitive cysteine at the end of the p-loop (GXXXXGK(S/T)C) (*151-153*). Ras^{G12C} is located in the p-loop similarly to Rho GTPases and given their redox reactivity, we hypothesized that the Ras^{G12C} mutant results in the generation of a new redox-sensitive cysteine that may alter the interaction with modulatory proteins (i.e., GAP proteins) and oxidants compared to other Gly^{12} mutants.

Ras Gly^{12} mutants have been shown to have varying phenotypes in tumors, with tumor aggressiveness being Ras^{G12V}>Ras^{G12D}>Ras^{G12C} (*154, 155*). The Ras^{G12C} mutant introduces a thiol into the p-loop of Ras, which could potentially generate an oncogenic variant with a redox-sensitive thiol. We used the thiolate-specific compound ABD-F to measure the reactivity of the thiol in $Ras^{G12C/C118S}$. In these experiments, we used the Ras^{C118S} variant to detect only the Ras^{G12C} thiol. As the Ras^{C118S} variant has no reactivity to ABD-F, it was determined that the fluorescence observed in the ABD-F pK_a assay was the result of Ras^{G12C} modification. From this study, we determined that Ras^{G12C} has an altered pK_a of ~7.5

(**Figure 10**). As a free cysteine in solution has a pK_a of ~8.5, this pK_a indicates that Ras^{G12C} has an altered pK_a and is solvent accessible, which are two requirements for a thiol to be redox sensitive.

To test the reactivity of Ras^{G12C} to oxidants, we treated ^{mant}GDP-loaded Ras^{G12C} with CysNO and NO$^{\cdot}$ from DEANO (**Figure 11**). Exposure to both nitrosation agents resulted in a rapid and complete loss of ^{mant}GDP fluorescence. As it has been surmised that Ras^{G12V} is more oncogenic than Ras^{G12D} because of steric repulsions between the aspartate residue and negatively charged phosphates (*156*), we postulated that the loss of ^{mant}GDP fluorescence was due to the presence of negatively charged oxygen on nitric oxide decreasing the binding affinity for the nucleotide.

However, the loss of fluorescence from modification of K-Ras upon addition of CysNO/DEANO may be the result of a conformational change in the protein and does not effect nucleotide binding. This hypothesis is supported by the reduction the Cys-NO bond using DTT after treatment with both oxidants. After treatment with NO in the presence of 1000× unlabeled GDP, the addition of DTT and the reduction of the nitroso-thiol should result in a minimal gain of ^{mant}GDP fluorescence. However, we observed nearly 70% of the fluorescence due to ^{mant}GDP return, which indicates that the ^{mant}GDP never dissociates from the GTPase. The ^{mant}GDP fluorescence may have been quenched by the modification with NO. This conformational change may have altered the effective environment that the fluorophore experiences without changing the secondary structure (**Figure 9**), thereby changing the observed fluorescence. Further experimentation will be needed to determine the reason behind the loss of fluorescence and what changes result from NO modification. A proposed test to investigate this behavior will be to modify K-Ras with each respective RNS and examine the protein for any changes in structure or the dissociation of bound nucleotide with mass spectrometry or x-ray crystallography.

In summary, we have shown that K-Ras^{G12C} is a thermodynamically stable mutant and mutation does not effect protein structure. The Ras^{G12C} mutation resulted in a lowered pK_a for the thiol, which is likely to be reactive to RNS and ROS under physiological conditions. The Ras^{G12C} mutation has been shown to be modified by nitric oxide in vitro; however, the physiological consequences of this modification are not currently understood. Further experiments to examine the structural changes to K-Ras because of nitric oxide modification will be performed to determine the exact source of the fluorescence change and to what extent nitrosation effects nucleotide binding.

Chapter 4: Oxidation of RhoA at Cys^{20} regulates nucleotide binding

Introduction

RhoA is part of the Rho family of GTPases, which comprise a distinct subclass of Ras GTPases. Rho family GTPases regulate pathways involved in cell growth, differentiation, cell death (*145, 157, 158*), regulation of cell morphology and motility through cytoskeletal rearrangements (*159-163*). Rho GTPases behave as molecular switches and cycle between the GTP-bound 'on' and GDP-bound 'off' states. Like most Ras superfamily GTPases, Rho GTPases have regulatory proteins that catalyze nucleotide exchange (guanine nucleotide exchange factors; GEFs), which activate the GTPase, and GTP hydrolysis (GTPase accelerating proteins; GAPs), which deactivate the GTPase by hydrolyzing GTP to GDP. In addition, Rho GTPases are bound to guanine dissociation inhibitors (GDIs) when in the GDP-bound state, which sequesters the GTPase from the membrane and maintains the inactive state.

In addition to protein regulatory factors, select Ras family GTPases have been shown to be regulated by reactive oxygen and reactive nitrogen species (ROS and RNS, respectively) (*164*). The role of reactive species (RNS, ROS) in regulating Ras superfamily GTPases is best characterized for the Ras subclass, where select free radical oxidants have been shown to induce nucleotide dissociation through a redox-sensitive motif at Cys^{118} (*67, 69*). In contrast to Ras GTPases, Rho GTPases contain a distinct redox-sensitive motif in the phosphoryl-binding loop (p-loop; GXXXXGK(S/T)C^{20}). Nearly 50% of Rho GTPases contain a cysteine immediately adjacent to the p-loop. In addition, many Rho GTPases, including RhoA, RhoB, and RhoC, possess a second cysteine within the p-loop motif (GXXC^{16}XGKTC^{20}), which makes these GTPases susceptible to internal disulfide bond formation and inactivation. Free

radical-mediated oxidants, such as nitrogen dioxide ($NO_2^{\cdot}$) and superoxide ($O_2^{\cdot-}$), have been shown to induce nucleotide dissociation in Rho GTPases by directly reacting with the redox-sensitive cysteine (*79*). In addition, it has been shown that exposure to non-radical oxidants, such as H_2O_2, can effect nucleotide binding as well as increase the rate of nucleotide exchange (*79*), presumably due to perturbation of the nucleotide binding pocket. As the cellular GTP concentration is approximately 10-fold greater than GDP, events that increase the rate of nucleotide exchange will populate the GTPases in the active, GTP-bound state. Thus, oxidation of these cysteines in Rho family GTPases has been shown to effect nucleotide binding and activation.

In addition, the p-loop has been shown to be critical for Mg^{2+} and nucleotide binding (*165*). From the crystal structure, many residues within the p-loop make direct interactions with the bound nucleotide. Furthermore, Mg^{2+} has been shown to stabilize nucleotide binding and play a role in GEF-mediated nucleotide exchange (*166*). While the K_d of RhoA for GDP and GTPγS do not vary greatly with and without Mg^{2+}, the k_{off} rate of nucleotide dissociation is greatly enhanced in the absence of Mg^{2+}. Therefore, Mg2+ is considered a gatekeeper of nucleotide binding. Thus, oxidation of Cys20 and Cys16 could mediate effects on RhoA activity by regulating Mg^{2+} binding.

RhoA has been shown to be activated and deactivated by ROS/RNS in cell-based experiments (*81, 83, 167*), which has complicated observations of RhoA function due to oxidants. While activation is likely due to oxidation of Cys^{20} and increasing the rate of nucleotide dissociation (*79*), deactivation likely occurs because RhoA possesses two cysteines within the p-loop (Cys^{16} and Cys^{20}) that can form a disulfide (*80, 83*). However, many of these studies have not discriminated between direct and indirect oxidation nor have these studies determined the oxidative modification. Further, the use of exogenous oxidants and non-physiological concentrations of oxidants have made interpretation of these data difficult.

We have previously shown that exposure of RhoA to $NO_2^{\cdot}$ in vitro promotes disulfide formation and occludes nucleotide binding (*80*). Consistent with this observation, RhoA shows decreased GTP binding when exposed to the nitric oxide-generating species PAPA-NONOate in vascular smooth muscle cells (*167*). In this study, it was shown that RhoA was s-nitrosated using a nitrosocysteine-specific antibody. It is also possible that a disulfide was formed between Cys^{16} and Cys^{20}, with the nitrosated product an intermediate to disulfide bond formation; however, other oxidation states aside from nitrosation were not tested. Furthermore, RhoA has been shown to be modified by phenylarsine oxide (PAO). Whereas PAO is a thiol-modifying compound that was originally developed as a protein tyrosine phosphatase inhibitor, RhoA can be modified and inactivated after PAO exposure in Caco-2 cells. Analysis by mass spectrometry showed mixed disulfide formation between Cys^{16} and Cys^{20} (*83*), resulting in deactivation of RhoA by occluding nucleotide binding; however, Rac1, which only has one p-loop thiol, was not inactivated upon exposure to PAO.

In contrast to the studies showing RhoA inactivation by oxidants, Cys^{16} and Cys^{20} of RhoA have been shown to be critical for peroxide-mediated activation of RhoA in REF52 cells (*81*). In this study, RhoA and a redox-insensitive variant, C16A/C20A, were ectopically expressed and exposed to exogenous and endogenous peroxide. $RhoA^{WT}$ was activated by peroxide under serum free conditions, whereas $RhoA^{C16A/C20A}$ was not activated under identical conditions. RhoA activation by peroxide concentrations as low as 0.1 μM was observed using the Rhotekin-RBD pull-down assay and microscopy to observe stress fiber formation, which is indicative of RhoA activation; however, $RhoA^{C16A/C20A}$ was not activated due to exogenous or endogenously produced peroxide (through antimycin A).

While there are a numerous studies that have observed regulation of RhoA activity through oxidation, many of these studies have shown that RhoA activity is indirectly regulated by ROS and RNS. According to Chang et al (*168*), $NO^{\cdot}$-induced activation of SHP-2 led to the inactivation of RhoA in rat aortic smooth muscle cells. However, the RhoA

pathway was activated by 3-morpholino-sydnonimine (SIN-1), a NO· donor, and peroxide through oxidant-mediated activation of Protein Kinase C (PKC) in bovine aortic endothelial cells. In this study, PKC was activated by oxidation, which in turn, activated RhoA through p115-Rho-GEF (*169*). However, in both of these studies, RNS were used to regulate RhoA-mediated pathways in the cell, but direct oxidation of RhoA was not probed. Therefore, while it would be useful to directly determine the types of modifications and oxidation events in the cell, the level of oxidation is likely small, which would make direct detection difficult. Thus, a carefully designed redox-insensitive variant that functions similarly to $RhoA^{WT}$ would aid in determining whether the effects of oxidants on RhoA are direct, or the result of indirect activation.

Thus, in this study, we characterized redox-insensitive variants of RhoA, demonstrate that Cys^{20} has an altered pK_a, and Cys^{20} sensitizes RhoA to free radical and nonradical oxidants. Our data also indicate that oxidation of Cys^{20} by glutathione increases the rates of nucleotide exchange whereas nitrosation does not increase nucleotide exchange rates. Further, we generated a $RhoA^{C20D}$ variant, which is a structural mimic of sulfinic acid. RhoAC20D, like glutathiolated RhoA, showed greatly enhanced rates of nucleotide exchange but did not affect GAP-mediated hydrolysis. Consistent with these observations, RhoAC20D was constitutively active in Swis3T3 cells, most likely due to the high rate of nucleotide exchange, and may prove as a useful oxidation mimetic. These results show that RhoA can be directly activated by oxidants and that activation is mediated through Cys^{20}. In the future, studies looking at RhoA-mediated signaling regulation by oxidants should consider the direct activation of RhoA, which can be tested using the $RhoA^{C20S}$ variant, in addition to the indirect activation of the RhoA signaling pathway.

Methods

RhoA protein purification

Truncated human *RhoA* ($RhoA^{1-181}$) was cloned into the pQlinkH vector (Addgene; Cambridge, MA), which contains an N-terminal 6x-His purification tag followed by a Tobacco Etch Virus protease cleavage site for removal of the affinity tag. The hypervariable region of RhoA, including the C-terminal CAAX box, was removed as this region does not undergo post-translational lipid modification in bacteria, is unstructured, and its removal does not affect guanine nucleotide binding or GTP hydrolysis in Ras GTPases (*106*). All proteins were expressed in BL21 Rosetta2 cells (Millipore; Darmstadt, Germany) and purified following the Qiagen Nickel NTA purification protocol (Germantown, MD). RhoA was further purified using size exclusion chromatography (Superdex-75 10/300 GL column; GE Life Sciences; Piscataway, NJ) and judged greater than 95% pure by SDS-PAGE analysis.

Nucleotide exchange and hydrolysis assays

The rate of GDP dissociation from Rho proteins was measured using 2'-/3'-O-(N'-methylanthraniloyl)guanosine-5'-O-diphosphate (^{mant}GDP) as previously described (*108, 109*). Briefly, 1 μM RhoA and RhoA variants were preloaded with ^{mant}GDP (BioLog; San Diego, CA) and added to 1 mL of degassed assay buffer (50 mM Hepes pH 7.4, 50 mM NaCl, 5 mM $MgCl_2$, 2 mM GDP, and 200 μM diethylenetriaminepentaacetic dianhydride; DTPA), and the rate of guanine nucleotide dissociation was measured by monitoring the change in fluorescence (excitation: 365 nm; emission: 435 nm; 25˚C) over time using a Perkin Elmer LS50B fluorimeter (Waltham, MA). All experiments were performed in triplicate. Fluorescent nucleotide dissociation curves were fit to a one-phase exponential decay equation using GraphPad Prism version 3.03 (GraphPad Software; San Diego, CA). For GEF-induced RhoA-GDP dissociation assays, the minimal catalytic domain of Dbs ($Dbs^{DH/PH}$) was used at a 1:10 ratio to RhoA. This concentration of $Dbs^{DH/PH}$ was selected as

the rate enhancement of nucleotide exchange was easy to measure using the fluorimetric assays. The Dbs construct was expressed and purified as previously described (*170*). For experiments where CysNO was employed, the oxidant was generated exactly as previously described and then diluted into 100 mM Hepes (pH 7.4) and 1 mM DTPA.

Rates of GTP hydrolysis were determined using a Spectramax M5 (Molecular Devices; Sunnyvale, CA) fluorimeter by monitoring phosphate production upon GTP hydrolysis (*111*). FlipPi 5U (Addgene; Cambridge, MA) was used as the phosphate sensor, and the expression, purification, and use of this sensor have been previously reported (*113*). Briefly, all assays used 10 μM FlipPi with 10 μM GTP-loaded RhoA. GTP loading was performed as previously described with minor modifications (*111*). Briefly, RhoA was loaded with GTP in loading buffer (20 mM Hepes, 50 mM NaCl, 1 mM EDTA, 20 mM $(NH_4)_2SO_4$ and 1 mM inosine, pH 8.0) for 3 min at 37˚C. Excess nucleotide was removed using a PD-10 desalting column with hydrolysis buffer (20 mM Hepes, 50 mM NaCl, 100 μM EDTA, and 1 mM inosine, pH 7.4) and placed in a 96-well plate. Hydrolysis was initiated by adding 1 mM $MgCl_2$ to the well. Trace phosphate was removed from all buffers using a 'phosphate mop' (*114*). The rate of GTP hydrolysis was measured by taking the ratio of the 535- and 485-nm emission wavelengths (excitation: 435 nm; 25˚C) of kinetic runs performed in triplicate and fit to a one-phase exponential association curve. For these experiments, the ratio of GAP to RhoA was 1:1000, and the minimal catalytic domain of p50 RhoGAP was used for hydrolysis.

4-fluoro-7-aminosulfonylbenzofurazan (ABD-F) modification of RhoA

To modify RhoA and select variants with ABD-F, Rho proteins were reduced with DTT before reaction. RhoA and RhoA variants were reduced using 5 mM DTT for 30 min on ice on the day of the experiment in reducing buffer (20 mM HEPES pH 8.0, 50 mM NaCl, 5 mM $MgCl_2$, and 200 μM DTPA) before being buffer exchanged into ABD-F reaction buffer (100 mM MES pH 6.5 and 5 mM $MgCl_2$) that was sparged with N_2 gas to remove oxygen content in the buffer and limit air oxidation during the reaction.

The reaction was performed in a Spectramax M5 plate reader using 96-well black plates. All reactions were performed in triplicate in ABD-F reaction buffer at a final volume of 200 µl with 10 µM protein and 1 mM ABD-F. ABD-F was stored at -20˚C in DMSO, and the concentration of ABD-F was determined using the extinction coefficient of 4200 $M^{-1}cm^{-1}$ at 313 nm. The fluorescence of ABDF was measured at an excitation wavelength of 389 nm and emission wavelength of 513 nm.

Circular Dichroism spectroscopy

Circular Dichroism data were collected on a JASCO J-815 CD spectrometer with a JASCO Peltier device and water bath to control the temperature. Experiments were performed in a 1-mm cuvette at a protein concentration of 15 µM in 10 mM potassium phosphate (pH 6.5) containing 500 µM $MgCl_2$ and 10 µM GDP. Far UV scans were from 200 nm to 250 nm. Thermal denaturation of RhoA and the selected variants were monitored at a 221 nm to estimate the protein melting temperature. The temperature ramp rate was 1˚C/min and data points were collected every 1˚C. CD scans are reported in units of mean residue ellipticity, which was calculated as follows:$[\theta]_{MRE} = \frac{\theta_{raw} \times MRW}{10 \times c \times l}$, where θ_{raw} is the ellipticity in degrees, MRW is $\frac{Molecular\ Weight\ (Da)}{(no.of\ residues)-1}$, c is the protein concentration in g/ml, and l is the pathlength of the cuvette in cm, according to (*171*).

Glutathiolation and oxidation of Rho samples

Before the addition of oxidants, RhoA was reduced with DTT for 30 min at pH 8.0 before being buffer-exchanged into the selected buffer that was flushed with N_2 gas to remove dissolved oxygen and prevent autoxidation. $RhoA^{WT}$ and $RhoA^{C16S}$ were modified with glutathione by the addition of 1000× oxidized glutathione to purified protein in glutathiolation buffer (50 mM NaH_2PO_4, pH 6.5, 100 mM NaCl, 10 mM $MgCl_2$, and 50 µM

GDP) for 30 min at room temperature. After, the samples were dialyzed into glutathiolation buffer without glutathione at 4˚C overnight.

To oxidize Rho with peroxide, the samples were reduced as described above. After, the samples were exposed to 250× hydrogen peroxide for 1.5 h at room temperature in oxidation buffer (50 mM Hepes pH 7.4, 50 mM NaCl, 5 mM EDTA, and 200 μM DTPA). After the samples were run over a PD-10 column equilibrated with assay buffer. The oxidized proteins were used in nucleotide association assays.

Mass spectrometry of Rho Samples

To prepare Rho samples for MS, the proteins were first modified with the selected oxidant before denaturation in 100 mM NH_4CO_3 (pH 7.8), 6 M urea, and 10 mM iodoacetamide (IAA). The iodoacetamide-containing buffer was prepared fresh daily and used in amber-colored eppendorf tubes. The reaction was performed in the dark as IAA is deactivated by light. After reaction for 1 h at room temperature, the Rho proteins were buffer exchanged into 50 mM NH_4CO_3 (pH 7.8) and digested with trypsin overnight at 37˚C. The peptides were cleaned up using a C-18 spin column (Pierce) following the manufacturer's recommended protocol. The cleaned peptide samples were lyophilized in a speedvac to powder and suspended in H_2O with 0.1% formic acid. The bottom-up peptide identification of trypsinized Rho samples was performed using reversed-phase LC–MS/MS on a nano-LC Ultra 2D Plus (Eksigent; Dublin, CA, USA) coupled to an LTQ-Orbitrap Velos as described previously [35]. Briefly, data acquisition included a full-MS scan on the Orbitrap (externally calibrated to a mass accuracy of <1 ppm and instrumental resolving power of 60,000 atm/z 400 Da) followed by intensity-dependent CAD–MS/MS of the top 10 most abundant peptide ions. Mass spectra were processed, and peptide identification was performed using Mascot (Matrix Science) against a Human UniProt database. Peptides were confidently identified using a target–decoy approach with a false discovery rate of 1%. A precursor ion mass tolerance of 200 ppm and product ion mass tolerance 0.5 Da with a maximum of two missed

cleavages and variable modifications of cysteine glutathiolation and oxidation were used as a protein database search parameter. All peptides were filtered and reported within a mass accuracy of 5 ppm.

NMR spectroscopy

NMR experiments were collected on a Varian Inova 700 MHz spectrometer at 25˚C. The 2D $^{1}H-^{15}N$ heteronuclear single quantum coherence spectroscopy (HSQC) experiments were performed with pulsed field gradient and water flip-back methods as previously described (91). Uniformly labeled ^{15}N-enriched Rho was purified as previously described. 2D ^{1}H-^{15}N HSQC experiments were acquired on 0.5 mM ^{15}N-enriched $RhoA^{WT}$, $RhoA^{C20S}$, $RhoA^{C16S/C20S}$, and $RhoA^{C20D}$ with 1,024 x 128 complex data points and a spectral width of 8,000 Hz for the ^{1}H dimension and 1,709 Hz for the ^{15}N dimension. Buffer contained 10 mM MOPS, 100 mM NaCl, 10 mM $MgCl_2$, 10 μM GDP, 0.1% azide, and 10% D_2O. NMR data were processed and analyzed using NMR PIPE and NMR ViewJ (One Moon Scientific; Newark, NJ).

Results

While RhoA activity can be modulated by cysteine oxidation in vitro (*79, 80*), few studies have demonstrated direct oxidation of RhoA in cellular-based experiments. The lack of studies that have directly detected oxidized RhoA in cells is likely a result of the difficulty detecting low levels of oxidation in physiological settings. However, mass spectrometry was used to verify direct oxidation of RhoA by PAO in Caco-2 cells (*83*), which was shown to inhibit RhoA by occluding nucleotide binding. RhoA has been shown to be directly activated by both exogenous and endogenous peroxide in REF52 cells, and RhoA activation was shown to be regulated through Cys^{16} and Cys^{20} (*81*). Other studies have tied RhoA regulation to oxidants through indirect oxidation (*168, 169*), although similar oxidants were used that have been previously been shown to activate RhoA in vitro (*79, 80*). The only variants

previously used as redox-insensitive controls, which mutated Cys^{16} and Cys^{20} to alanine, were not biochemically characterized (*80, 81*). Thus, we have shown that Cys^{20} of RhoA has an altered pK_a and characterized the effect of oxidation at Cys^{20} by glutathione, peroxide, and NO. We characterized the previously used $RhoA^{C16A/C20A}$ variant and determined that this variant has altered nucleotide-binding properties. Therefore, we characterized several redox-insensitive variants, which should serve as powerful tools to determine the effects of RhoA oxidation in cells.

Thiol accessibility and 4-fluoro-7-aminosulfonylbenzofurazan (ABD-F) modification of RhoA

Due to the observed reactivity of RhoA Cys^{20} to oxidants, we hypothesized that RhoA Cys^{20} has an altered pK_a. We tested the reactivity of the cysteines in RhoA by monitoring the reaction of RhoA at various concentrations of ABD-F. ABD-F reacts with the thiolate state of cysteine residues with an approximate 10-fold faster rate than the thiol state and shows enhanced fluorescence upon modification.

The computational program nAccess was used to probe the surface of RhoA thiol side chains that are accessible to the solvent relative to an Ala-x-Ala peptide, where x is the residue being considered (**Table 2**). Analysis with nAccess indicates that only Cys^{20} is solvent accessible in the GTP-bound states when accounting for the bound nucleotide. However, as the guanine nucleotide is exchangeable, we performed nAccess without considering the bound nucleotide. By omitting the bound nucleotide, the relative accessibility of Cys^{20} is increased. In the GEF-bound state, which is not bound to nucleotide, the solvent accessibility of Cys^{20} is similar to RhoA without the considering the bound nucleotide. In GAP, GDI, and effector bound states, the relative accessibility of all thiols is minimal. The only other thiol that is readily accessible in any structure is Cys^{107}. However, nAccess considers the relative accessibility of the entire side chain. In Cys^{107}, visual analysis of the structures indicate that the majority of Cys^{105} that is solvent accessible is the β carbon. Thus,

Table 2. Thiol accessibility in RhoA crystal structures

	Cys^{16}	Cys^{20}	Cys^{83}	Cys^{107}	Cys^{159}
$RhoA^{GTP}$ 1A2B	1.9	4.3	0.0	7.9	1.3
RhoA 1A2B	1.9	35.4	0.0	7.9	1.3
$RhoA^{GDP}$ 1FTN	1.8	0.0	0.0	5.4	0.0
RhoA 1FTN	1.8	19.7	0.0	5.4	0.0
RhoA-RhoGEF 3T06	3.0	33.5	0.1	3.7	0.0
RhoA-RhoGAP 1OW3	3.5	2.2	0.0	4.0	0.5
RhoA-GDI 1CC0	1.8	0.0	0.0	4.8	0.0
RhoA-PKN/PRK 1CXZ	2.3	2.4	0.0	4.9	0.3

All values are presented as % accessibility compared to an Ala-x-Ala peptide. Value considers the total side chain solvent accessibility. In the second and fourth rows, nAccess was performed on crystal structures where the bound nucleotide was omitted.

this data suggests that Cys^{20} is the most accessible thiol in RhoA. As the GDP-bound form is generally bound to GDI in cells, it is likely that RhoA will only be accessible to oxidation in the GTP-bound form in the cellular context.

As RhoA contains a solvent-accessible cysteine at position 105 that does not play a role in nucleotide binding or effector interaction, we tested ABD-F reactivity at a pH (pH 6.5) that was unlikely to modify accessible thiols that do not possess altered reactivity (**Figure 14**). Thus, if Cys^{20} has an altered pK_a, this pH should highlight the reactivity of this residue while minimizing modification at other sites. The ABD-F fluorescence intensity was found to be the highest for $RhoA^{WT}$ upon modification with ABD-F, and $RhoA^{C16S}$ resulted in 40% of the fluorescence observed for $RhoA^{WT}$. In contrast, $RhoA^{C20S}$ and $RhoA^{C16S/C20S}$ showed only ~15% of the fluorescence of $RhoA^{WT}$. Mass spectrometry confirmed that Cys^{20} was modified in $RhoA^{WT}$. Lastly, Cys^{159}, which is buried by the bound nucleotide (**Table 2**), was also partially modified by ABD-F in all RhoA proteins tested. This data, in combination with the nAccess study, suggests that oxidation of RhoA will primarily occur at Cys^{20}.

Oxidation of RhoA differentially effects nucleotide binding

To test the effect of RhoA oxidation, we exposed RhoA to CysNO, peroxide, and glutathione in vitro. Interestingly, we observed different nucleotide binding in response to the tested oxidants. As exposure to $NO_2^{\cdot}$ radicals can promote disulfide formation between Cys^{16} and Cys^{20}, we used CysNO, which nitrosates cysteines by non-radical oxidation, to determine the effect of $2e^-$ nitrosation on RhoA. As shown in **Figure 15A**, oxidation of RhoA and $RhoA^{C20S}$ by CysNO had no effect on nucleotide exchange rates. Thus, the rate of nucleotide exchange after CysNO addition was nearly identical to the rate observed prior to the addition of the oxidant.

We also treated RhoA with peroxide and observed nucleotide association. However, treating ^{mant}GDP-loaded RhoA with peroxide in the reaction cuvette did not appear to effect nucleotide dissociation rates by the ^{mant}GDP assay, which prevented the measurement of

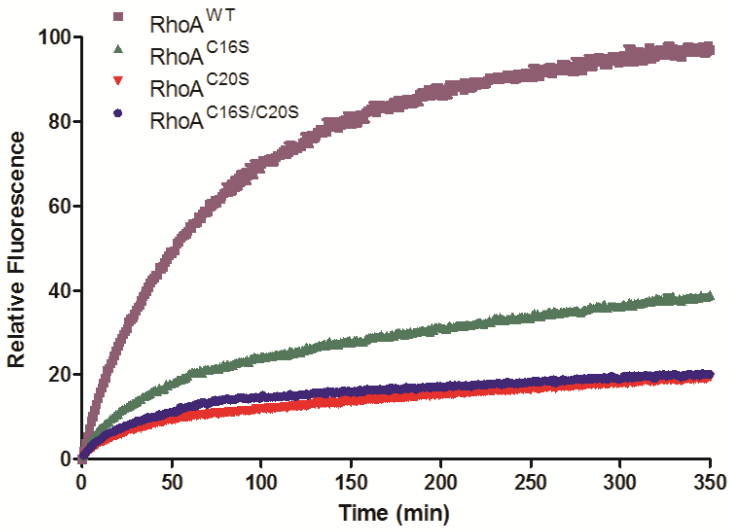

Figure 13. Reaction of RhoA and RhoA variants with ABD-F.

Reaction of RhoA with ABD-F shows increased reactivity at Cys^{20}, likely because of a decreased pK_a of the thiol moiety. All reactions were performed with 10 μM $RhoA^{WT}$, $RhoA^{C16S}$, $RhoA^{C20S}$, or $RhoA^{C16S/C20S}$ and 1 mM ABDF at pH 6.5 for 350 minutes. Reactions were performed in triplicate using a 96-well plate reader and were plotted using GraphPad Prism. Data are presented as a relative % modification by counting the maximal RhoA modification to be 100%.

nucleotide dissociation due to direct peroxide exposure (data not shown). We treated RhoA, RhoA^{C20S}, and RhoA$^{C16S/C20S}$ with 250× peroxide for 1.5 h prior to measuring nucleotide association using ^{mant}GDP (**Figure 15B**). While RhoA^{C20S} and RhoA$^{C16S/C20S}$ were unaffected due to peroxide treatment, RhoA^{WT} showed decreased nucleotide association, which suggests that oxidation proceeds initially through Cys^{20} of RhoA.

Further, we also treated RhoA^{WT} with oxidized glutathione and used MS to analyze the consequences of RhoA oxidation. We find that glutathiolation is specific to Cys^{20} of RhoA (data not shown). Glutathiolation at Cys^{20} resulted in significantly enhanced nucleotide dissociation rates with an approximate 140-fold increase in intrinsic exchange in RhoA^{WT} and 250-fold in RhoA^{C16S}. As we were unable to preload glutathiolated RhoA with ^{mant}GDP, we measured nucleotide cycling with 0.1 μM ^{mant}GDP and 1 μM protein and measured the subsequent dissociation curves (**Figure 15C**). Association was performed for 30 s to 1 min (data not shown) and dissociation was initiated by adding 2 mM GDP into the reaction cuvette. The results show that glutathiolated RhoA is able to bind nucleotide and that glutathiolated RhoA shows greatly enhance nucleotide exchange rates.

As sulfenic acid-modified proteins are generally unstable and in equilibrium with sulfinic and sulfonic acid oxidation states, we used the RhoA^{C20D} variant to serve as an oxidation mimetic (**Figure 16**). As Cys^{20} is the initial site of oxidation, the RhoA^{C20D} variant allows for studies of oxidized RhoA that cannot form a disulfide with Cys^{16}. As shown in **Figure 16**, we characterized intrinsic and GEF/GAP-mediated rates of nucleotide exchange and hydrolysis. We find that the RhoA^{C20D} variant possess greatly enhanced rates of nucleotide dissociation, which was ~480-fold faster than intrinsic nucleotide dissociation. The rate of intrinsic GTP hydrolysis was slower than RhoA^{WT}, which was likely due to the fast exchange rate as we employed a single-turnover hydrolysis assay. In the presence of GAP, the rate of hydrolysis was restored to a rate that was similar to RhoA^{WT}.

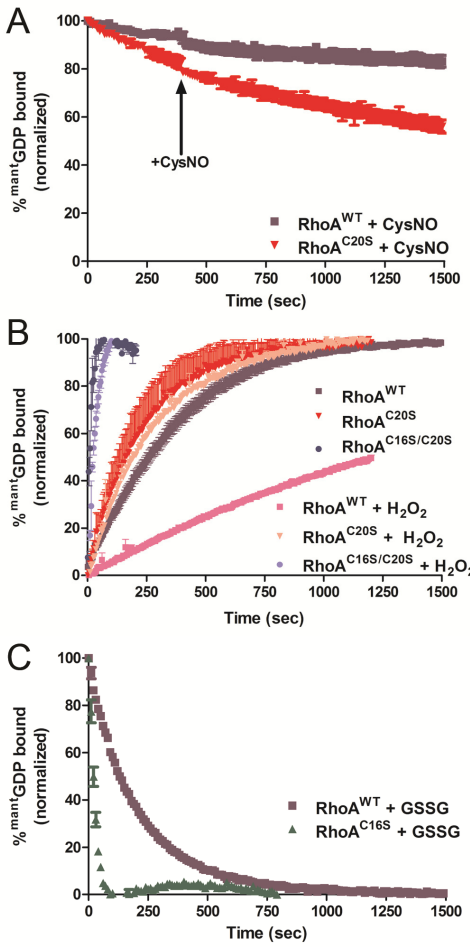

Figure 14. Nucleotide binding assays of oxidized RhoA.

(A) RhoA^{WT} and RhoA^{C20S} preloaded with ^{mant}GDP and exposed to CysNO. RhoA (1 μM) was exposed to 100 μM CysNO in the reaction cuvette at the indicated time point and dissociation was monitored. (B) RhoA and the redox-insensitive variants were exposed to H_2O_2 as described in the methods and ^{mant}GDP association assays were performed. (C) Nucleotide dissociation assays of glutathiolated RhoA and RhoA^{C16S}. The site of oxidation was determined by mass spectrometry. All reactions were performed in triplicate and were fit to a single exponential dissociation curve (where applicable) using GraphPad Prism, and the error is reported as the standard deviation of the replicates.

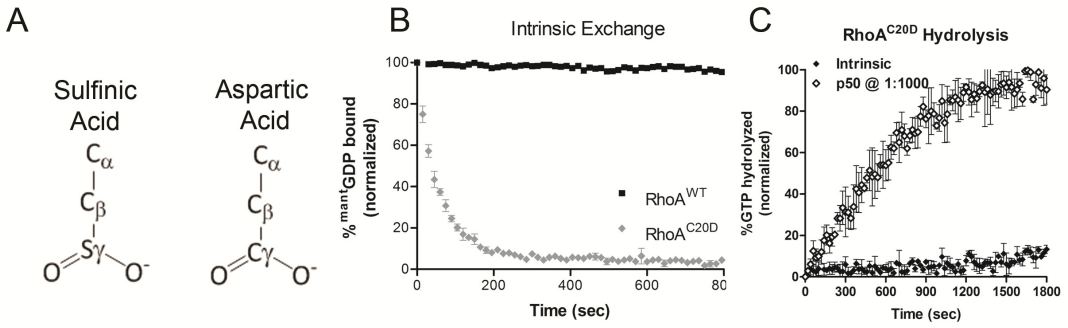

Figure 15. Oxidation mimetic RhoA^{C20D} shows the critical role of Cys^{20} in nucleotide binding.

(A) Graphical depiction of cysteine oxidized to sulfinic acid and aspartic acid for comparison. (B) Intrinsic nucleotide dissociation of RhoA^{C20D} that was loaded with ^{mant}GDP and performed as described previously. (C) Nucleotide hydrolysis of RhoA^{C20D} with and without GAP present. RhoA^{C20D} was preloaded with GTP and hydrolysis was measured as described previously.

Nucleotide exchange and hydrolysis kinetics of RhoA variants

We generated a series of mutations at both Cys^{20} and Cys^{16} and analyzed the effects of these mutations on RhoA nucleotide binding kinetics to evaluate which redox insensitive variant(s) best mimic the biochemical, stability, and structural properties of $RhoA^{WT}$.

As the $RhoA^{C16A/C20A}$ variant was previously used as a redox-insensitive variant in a cellular context (*81*), we initially compared the intrinsic rates of nucleotide exchange of $RhoA^{WT}$ and $RhoA^{C16A/C20A}$ using the ^{mant}GDP dissociation assay. In this assay, the rate of nucleotide dissociation can be determined by monitoring the loss of ^{mant}GDP fluorescence in the presence of unlabeled nucleotide. As shown in **Figure 17** (and in **Table 3**), the $RhoA^{C16A/C20A}$ variant shows a greatly increased rate of intrinsic dissociation of ~150-fold. This result indicates that this variant impairs nucleotide binding in RhoA; therefore, we characterized additional variants to identify a redox-insensitive variant that did not significantly alter RhoA activity. As the serine side chain is the closest mimetic to cysteine, we next compared Cys>Ser variants in effort to obtain a redox-insensitive variant with similar biochemical properties to $RhoA^{WT}$.

While introducing double mutations at Cys^{20} and Cys^{16} ($RhoA^{C16S/C20S}$) significantly enhanced the rate of nucleotide dissociation relative to $RhoA^{WT}$ by ~40-fold, this is 4-fold less than that observed for the $RhoA^{C16A/C20A}$ variant. However, single mutations at these positions better retain the intrinsic rates of nucleotide dissociation relative to $RhoA^{WT}$ as $RhoA^{C16S}$ and $RhoA^{C20S}$ enhanced intrinsic rates GDP dissociation by ~3-fold and ~5-fold, respectively. As the nucleotide binding constant in RhoA is so high, increased nucleotide dissociation is an indirect readout of nucleotide affinity. Taken together, these data indicate that single mutations at Cys^{16} and Cys^{20} retain nucleotide binding most similar to that of $RhoA^{WT}$ (**Figure 17A**).

In the cellular context, the intrinsic rate exchange is too slow to respond to stimuli and GEP-mediated nucleotide exchange better mimics the ability to become activated. Therefore,

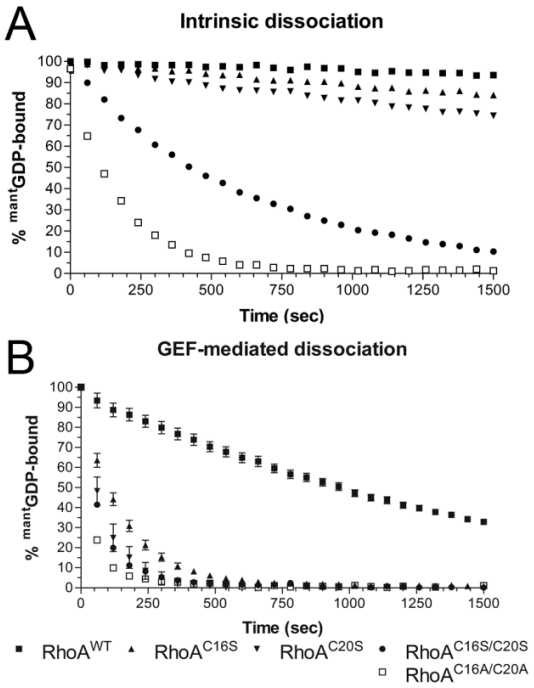

Figure 16. Biochemical characterization of RhoA redox-insensitive mutants.

A) Intrinsic nucleotide dissociation measured in RhoA and RhoA variants lacking the p-loop cysteine residues using ^{mant}GDP. B) GEF-mediated nucleotide dissociation performed in RhoA and RhoA variants in the presence of the minimum catalytic fragment of DBS. All reactions contained the GEF at a 1:10 ratio to RhoA. All reactions were performed in triplicate and were fit to a single exponential dissociation curve using GraphPad Prism, and the error is reported as the standard deviation of the replicates. Normalized results are presented for graphical comparison of the experiments. The experimental conditions and data analyses for these assays are described in the Materials and Methods.

we exposed RhoA to the minimal catalytic domain (DH/PH domains) of the Rho-specific GEF Dbs at a GEF:RhoA ratio of 1:10 (**Figure 17B**). Under these conditions, the Rho Cys>Ser variants all showed increased sensitivity to the RhoGEF, Dbs. Thus, $RhoA^{C16S}$ and $RhoA^{C20S}$ showed increased rates of 8- and 18-fold, respectively, compared to their GEF-mediated $RhoA^{WT}$ rates (all rates are presented in **Table 3**).

In addition to GEFs, GAPs regulate the activation state of GTPases by promoting GTP hydrolysis and inactivating the GTPase. To examine whether the redox-insensitivevariants were sensitive to GAP-mediated hydrolysis, we measured intrinsic and GAP-mediated GTP hydrolysis. Using the FlipPi GTP-hydrolysis assay that has been previously described (*15, 131*), the rate of nucleotide hydrolysis for each variant was determined (**Figure 18**). While $RhoA^{C20S}$ and $RhoA^{C16S/C20S}$ showed faster intrinsic hydrolysis rates, the increases were marginal and unlikely to play a major role in the cellular regulation of these variants. In the presence of the catalytic domain of p50 RhoGAP, all variants showed sensitivity to GAP-mediated hydrolysis with only the $RhoA^{C20S}$ and $RhoA^{C16S/C20S}$ variants showing slightly faster rates with the same concentration of GAP.

RhoA Cys>Ser stability by Circular Dichroism

Circular Dichroism (CD) thermal melts were performed on the RhoA variants to study the stability of the variants generated. The thermal denaturation curves were performed at pH 6.5 with 500 μM $MgCl_2$ and 10 μM GDP and were collected at 221 nm (**Figure 19**). These results indicate that none of the redox-insensitive variants significantly destabilize RhoA. However, the sulfenic acid oxidation mimetic $RhoA^{C20D}$ showed decreased thermal stability by ~7°C compared to $RhoA^{WT}$.

2D NMR of RhoA variants

As the $RhoA^{C16A/C20A}$ variant showed a high rate of nucleotide dissociation in our assays, we performed 2D NMR analyses of this variant and compared the spectra to $RhoA^{WT}$

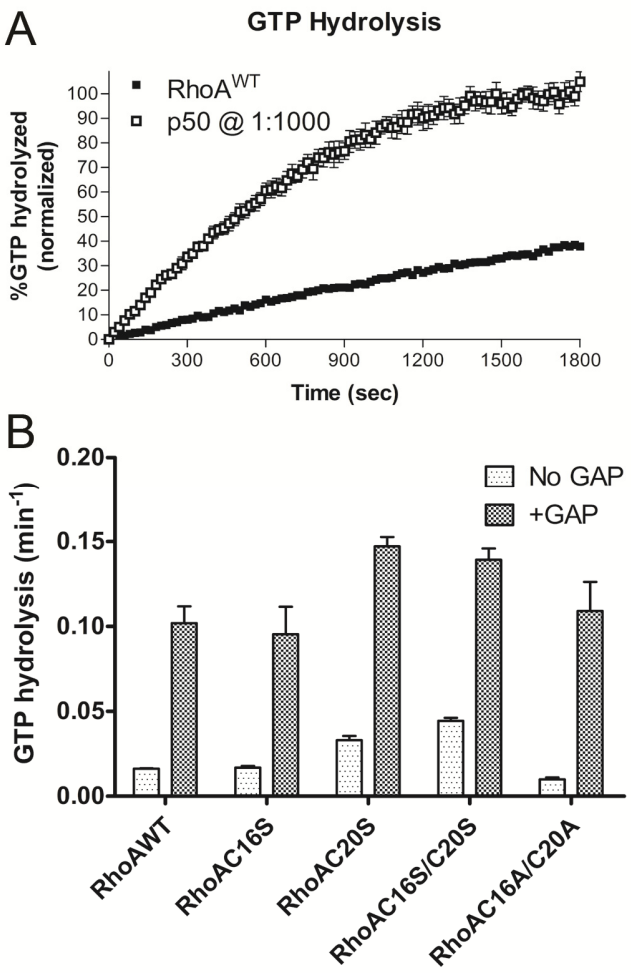

Figure 17. GTP hydrolysis of RhoA and RhoA redox-insensitive mutants.

(A) RhoA GTP hydrolysis kinetic traces in the absence and presence of the minimal catalytic domain of p50 RhoGAP. (B) The relative rates of hydrolysis in the absence and presence of GAP at 1:1000 GAP:RhoA are presented for all redox insensitive variants. All reactions were performed in triplicate and were fit to a single exponential dissociation curve using GraphPad Prism, and the error is reported as the standard deviation of the replicates. The experimental conditions and data analyses for these assays are described in the Materials and Methods.

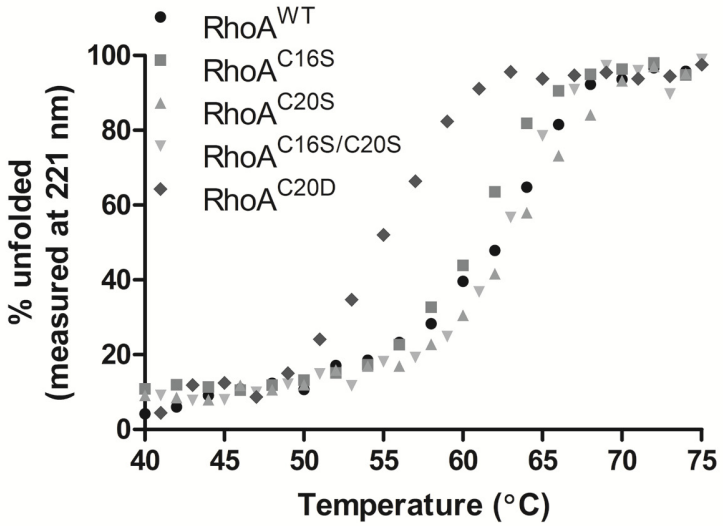

Figure 18. Thermal denaturation of RhoA and RhoA variants.

The thermal stability of RhoA was measured using circular dichroism at 221 nm. T_m values were as follows: $RhoA^{WT}$, 61.2 ± 0.6; $RhoA^{C16S}$, 60.7 ± 1.8; $RhoA^{C20S}$, 63.8 ± 1.9; $RhoA^{C16S/C20S}$, 62.0 ± 0.5; and $RhoA^{C20D}$, 54.67 ± 0.05. All denaturation curves were performed in duplicate and normalized to represent the relative unfolding over the selected temperature range.

Table 3. Nucleotide dissociation and hydrolysis rates in the presence and absence of GEFs and GAPs

Nucleotide release	Intrinsic k_{off} (e-5 s^{-1})	Fold Increase x/$RhoA^{WT}$	$DBS^{DH/PH}$ k_{off} (e-5 s^{-1})	Fold Increase x/$RhoA^{WT}$
$RhoA^{WT}$	3.6 ± 0.1	1	71.8 ± 0.6	1
$RhoA^{C16S}$	11.56 ± 0.1	3.2	604 ± 7	8.4
$RhoA^{C20S}$	18.17 ± 0.1	5.0	1098 ± 28	15.25
$RhoA^{C20D}$	1738 ± 39	482	N/A	--
$RhoA^{C16S/C20S}$	150.8 ± 0.6	41.9	1270 ± 14	17.6
$RhoA^{C16A/C20A}$	536.3 ± 4.65	149	2220 ± 36	30.8
Nucleotide hydrolysis	Intrinsic k_{off} (e-5 min^{-1})	Fold Increase x/$RhoA^{WT}$	P50 RhoGAP k_{off} (e-5 s^{-1})	Fold Increase x/$RhoA^{WT}$
$RhoA^{WT}$	27.1 ± 0.8	1	169.8 ± 37	1
$RhoA^{C16S}$	28.1 ± 2.8	1.0	159.1 ± 46	0.9
$RhoA^{C20S}$	54.9 ± 8.4	2.0	245.3 ± 13	1.4
$RhoA^{C20D}$	6.3 ± 1.8	0.23	154.1 ± 41	0.9
$RhoA^{C16S/C20S}$	74.1 ± 4.8	2.7	232.2 ± 25	1.4
$RhoA^{C16A/C20A}$	16.6 ± 1.8	0.6	154.1 ± 42	0.9

(**Figure 18A**). Backbone NH resonances of GDP-bound RhoA have been previously assigned (*172*) and were used in our NMR analyses. A 2D ^{1}H-^{15}N NMR HSQC allows for observation of backbone and side chain N-H groups and provides a site-specific probe for every residue in a protein aside from proline. In **Figure 18B**, $RhoA^{C16A/C20A}$ is overlayed with $RhoA^{WT}$. We determined that the $RhoA^{C16A/C20A}$ variant had 29 detected peaks with altered chemical shifts (peaks with chemical shift differences greater than one linewidth, 0.05 ppm in the ^{1}H dimension or 0.4 ppm in the ^{15}N dimension) compared to $RhoA^{WT}$. The $RhoA^{C20S}$ redox-insensitive variant (**Figure 18C**) had an NMR spectra that was more similar to $RhoA^{WT}$ with only 16 peaks showing altered chemical shifts compared to $RhoA^{WT}$. Lastly, $RhoA^{C20D}$ (**Figure 18D**) showed 43 peaks with chemical shifts, indicating that the structure of this variant had the largest degree of variation. All residues that showed chemical shifts are plotted on the RhoAWT structure to indicate where on the structure was effected by the tested variants (**Figure 19)**.

Cys^{20} is sensitive to oxidation in SDS-PAGE

SDS-PAGE of RhoA purified from *E. coli* has always shown a diffuse band for $RhoA^{WT}$. While the SDS-PAGE loading buffer contains 100 mM DTT, this does not remove the smear observed on the gel. This effect appears to depend on Cys^{20} in RhoA. When running $RhoA^{C20S}$ and $RhoA^{C16S/C20S}$, RhoA appears as a clean band (**Figure 20**). However, $RhoA^{C16S}$, which still contains Cys^{20}, retains the smeared band. This indicates that the observed banding pattern is due to the reactivity of Cys^{20}. If the reducing agent in the loading buffer is replaced with iodoacetamide (IAA), then clear bands are observed with $RhoA^{WT}$ and $RhoA^{C16S}$. However, this result does not eliminate the possibility that Cys^{20} is oxidized, which would generate a reactive thiol during the denaturation step that could create a mixture of oxidized species during gel preparation. To verify that no oxidation was present on RhoA prior to SDS-PAGE analysis, we performed mass spectrometry of trypsin-digested peptides in the presence of IAA. In these samples, oxidation of Cys^{20} was not detected.

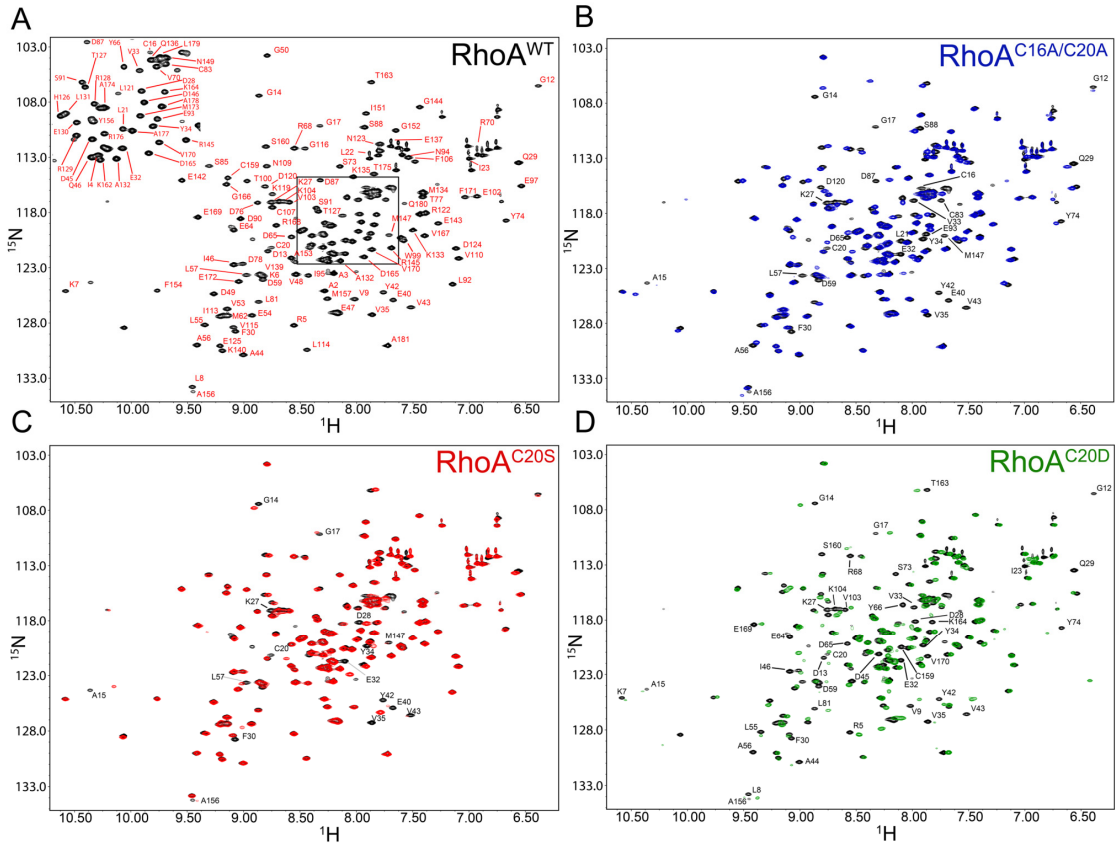

Figure 19. 2D NMR analyses of RhoA and RhoA variants.

(A) HSQC of RhoA^{WT} with the assigned residues highlighted. Assignments have been previously performed and the same conditions used previously were used herein. (B) Overlay of HSQC spectra of RhoA^{WT} (black) and RhoA$^{C16A/C20A}$ (blue). Residues that showed chemical shifts are labeled in black based on the RhoA assignments. (C) Overlay of HSQC spectra of RhoA^{WT} and RhoA^{C20S} (red). (D) Overlay of HSQC spectra of RhoA^{WT} and RhoA^{C20D} (green).

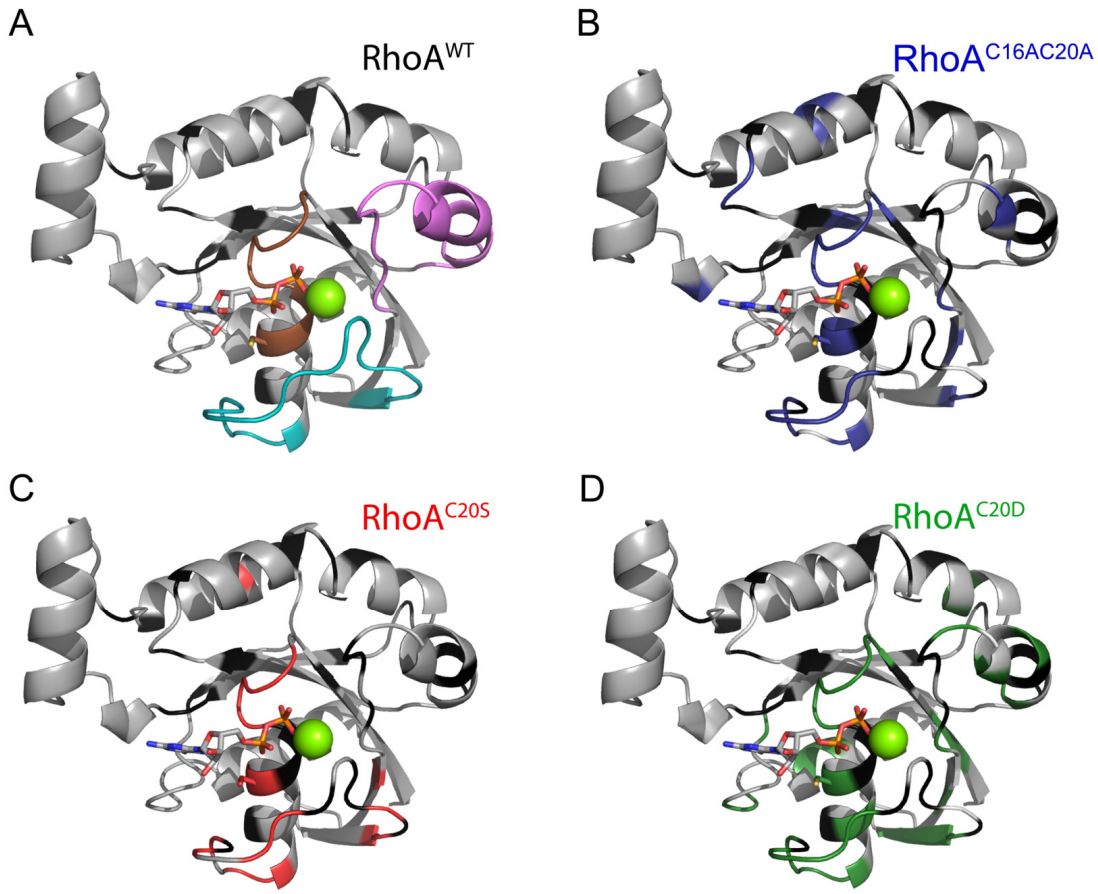

Figure 20. Residues with chemical shifts plotted on pymol-generated structures.

Residues that showed chemical shifts due to mutation are plotted on the structure of RhoA (pymol id 1FTN). (A) RhoA^{WT} plotted with the p-loop in orange, switch I in cyan, and switch II in magenta for comparison of the structures. (B) All residues that showed a chemical shift by HSQC in RhoA$^{C16A/C20A}$ are plotted in blue. (C) Residues with a chemical shift in RhoA^{C20S} are plotted in red. (D) Residues with a chemical shift in RhoA^{C20D} are plotted in green. In black are all residues that are undefined in the NMR data. All residues showing no change are in grey.

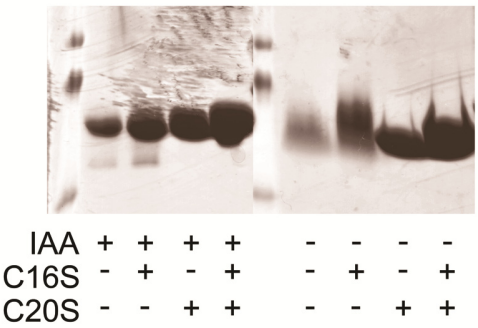

Figure 21. SDS-PAGE of RhoA variants.

The reactivity of Cys^{20} causes poor resolution by SDS-PAGE. On the left half of the gel, RhoA variants were denatured in the presence of iodoacetamide. In the right half of the gel, RhoA variants from the same sample were denatured in the presence of reducing agent. $RhoA^{WT}$ and $RhoA^{C16S}$, which both contain Cys^{20}, both showed poor resolution on the reducing gel.

In cell activation of RhoA variants

It has previously been shown that RhoA is activated by peroxide in cells (*81*). However, this study used the $RhoA^{C16A/C20A}$ variant that displays altered nucleotide binding kinetics. The ABD-F modification study and the use of the $RhoA^{C20S}$ variant presented within suggest that mutation of $RhoA^{C20S}$ is sufficient to prevent RhoA oxidation. Thus, we generated a $RhoA^{C20S}$ variant and transfected this variant into Swiss3T3 cells (**Figure 21**). This variantshowed similar levels of activation compared to $RhoA^{WT}$ by the Rhotekin-RBD pull down assay, which suggests that this variant is a more reliable redox-insensitive variant than $RhoA^{C16A/C20A}$.

To mimic the effect of oxidation of RhoA in cells, we employed the $RhoA^{C20D}$ variant to determine the effect on GTP binding in cells. While the $RhoA^{C20D}$ variant cannot form the disulfide bond that has been previously observed between Cys^{16} and Cys^{20}, it does mimic the primary oxidation step at Cys^{20}. The $RhoA^{C20D}$ variant, like the $RhoA^{C16A/C20A}$ variant, showed significantly increased activation in the RBD-pull down experiments in Swiss3T3 cells (**Figure 21**).

Discussion

While numerous reports support modulation of RhoA activity by ROS and RNS, few have determined whether RhoA undergoes direct oxidation, and if so, the site(s) and type(s) of modification as well as the consequences on RhoA activity. Previously, RhoA has been shown to be form a disulfide between Cys^{16} and Cys^{20} after exposure to $NO_2^{\cdot}$ (*173*). In a separate study, $NO^{\cdot}$, which was generated using PAPA-NONOate, was shown to prevent nucleotide binding in RhoA in vitro and inactivate RhoA in aortic smooth muscle cells (*167*). Further, RhoA has been shown to be activated by peroxide in REF52 cells (*81*). In this study, a $RhoA^{C16AC20A}$ redox-insensitive variant was used to determine whether the effect of peroxide was due to direct thiol oxidation of RhoA. While this variant is insensitive to oxidation, we find that it possesses greatly enhanced rates of GDP dissociation relative to

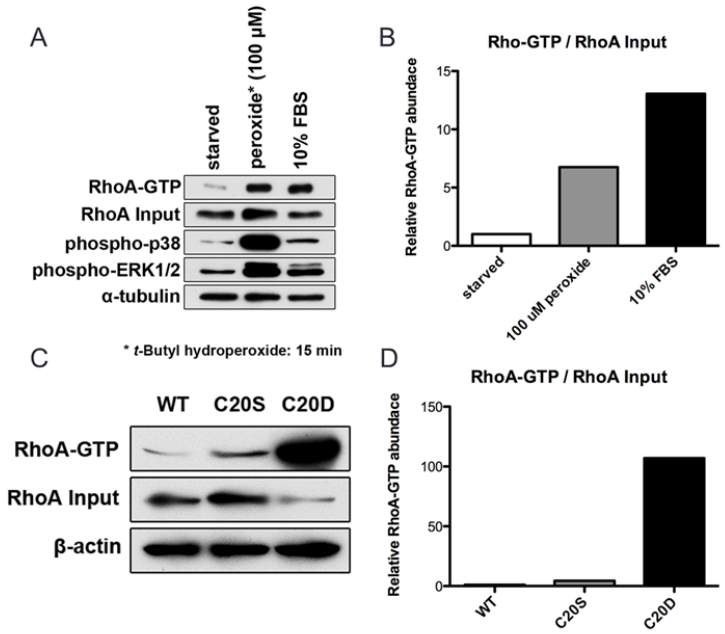

Figure 22. RhoA regulation by peroxide and activation state of redox variants.

(A) Endogenous RhoA was shown to be activated by peroxide in Swiss3T3 cells. Cells were serum starved and treated with 100 μM t-butyl peroxide for 15 min. Levels of GTP-bound RhoA and activated p38 and pErk1/2 were probed for. (B) Quantitation of GTP-bound RhoA from (A). (C) Endogenous RhoA was knocked down and RhoAWT, RhoAC20S, and RhoAC20D were exogenously expressed in Swiss3T3 cells. After stable transfection, the cells were probed for GTP-bound RhoA. (D) Quantitation of GTP-bound RhoA from (C). Data in figure collected by Bingying Zhou.

RhoA^{WT}. This observation is consistent with the increased activation observed in REF52 cells in the absence of oxidant.

However, several studies have shown regulation of RhoA by activation of Rho effector proteins. In Chang et al, RhoA downregulation was observed after treatment with DETANO-NONOate in vascular smooth muscle cells. However, in this study, NO$^{\cdot}$ was found to upregulate SHP-2, which caused downregulation of RhoA (*168*). Further, in Chandraet al, both NO$^{\cdot}$ from SIN-1 as well as H_2O_2 were shown to activate Protein Kinase C, which in turn activated p115-Rho-GEF and RhoA in bovine aortic endothelial cells (*162*). In yet another study of RhoA and NO$^{\cdot}$, RhoA/Rho Kinase activity was shown to be downregulated by endogenously generated NO$^{\cdot}$ and exogenously added sodium nitroprusside in rat aortic cells (*174*). However, in this study, the authors surmised that NO$^{\cdot}$ led to the activation of cGK, which has been shown to inactivate RhoA (*175, 176*). Common to all of these studies, however, was the use of NO$^{\cdot}$ donors, which have been shown to oxidize RhoA in vitro and directly regulate RhoA in cells, and these cellular-based studies did not look at direct RhoA oxidation. As RhoA has been shown to be directly regulated by these oxidants, we sought to biochemically characterize the oxidation events in RhoA and generate a redox-insensitive variant of RhoA, which would aid in studying the role of oxidants and RhoA function.

Given the number of cellular studies that implicate functional alteration of RhoA activity by RNS and ROS, we sought to identify a redox inactive variant that retains the ability to bind and hydrolyze GTP similar to RhoA^{WT}. Therefore, several Cys>Ser variants were generated and characterized to determine whether any retain RhoA^{WT} properties. Redox inactive variants also served as controls for determining the sites of oxidation in response to thiol oxidizing agents in our in vitro studies. Further, we looked at the activation state of the redox-insensitive variants in cells as well as the oxidation mimetic RhoA^{C20D}, which shows increased activation in Swiss3T3 cells and is agreement with our biochemical data.

Running SDS-PAGE of $RhoA^{WT}$ indicated that RhoA may be selectively oxidized at lower pH (<7.0). We verified RhoA cysteine reactivity by studying the modification of RhoA with ABD-F, which is a compound that selectively reacts with thiolates. The ABD-F data indicate that RhoA is oxidized primarily at Cys^{20} and Cys^{16} (**Figure 12**). Thus, the $RhoA^{C16S}$ variant shows greater reactivity to ABD-F than $RhoA^{C16S/C20S}$. This indicates that Cys^{20}, which is still present in the $RhoA^{C16S}$ variant, is being modified; however, in $RhoA^{C20S}$, ABD-F reactivity was similar to the $RhoA^{C16S/C20S}$ variant, which suggests that Cys^{16} was not modified in $RhoA^{C20S}$. The ABD-F reactivity observed in $RhoA^{C16S/C20S}$ was attributed to partial modification of Cys^{159}, which is exposed when the protein undergoes nucleotide exchange, and partial modification of Cys^{105}, which is on a face of RhoA that does not interact with effectors or interact with the nucleotide and is not expected to alter GTPase function. These data suggest that Cys^{20} is the central residue in RhoA regulation by oxidation.

Due to the ABD-F results, we revisited the effects of oxidants on RhoA structure, stability and biochemical properties (+/- response to regulators), specifically oxidation at Cys^{20}. Initially, we exposed RhoA to CysNO to determine the effect of S-nitrosation. Previously, RhoA was shown to have a significant increase in nucleotide dissociation after exposure to $NO_2^{\cdot}$ (*79*). While a subsequent study showed that a disulfide bond is generated between Cys^{16} and Cys^{20} (*83*), this study did not explore other potential oxidative modifications that could result. We selected CysNO to oxidize RhoA as this oxidant modifies exposed thiols with an NO group without radical formation. After exposing RhoA to CysNO, the rate of nucleotide dissociation of ^{mant}GDP-loaded RhoA was unaffected. This result is surprising as it suggests that nitrosation does not effect nucleotide binding and indicates that radical formation regulates RhoA nucleotide binding by nitric oxide oxidation.

Oxidation by peroxide has been previously suggested to increase the rate of nucleotide dissociation by approximately 10-fold (*79*). However, RhoA was not oxidized by peroxide treatment before nucleotide dissociation was measured in this study, but rather peroxide

was added at the start of the assay. Results from this in vitro study indicate that peroxide addition to RhoA can increase nucleotide dissociation, but the sites and type of oxidation were not determined. The rate of thiol oxidation by peroxide can vary significantly as it is dependent on the accessibility and pK_a of the cysteine (*177*). Further, the rate of cysteine oxidation on free cysteine has been shown to be approximately 20 $M^{-1}s^{-1}$. Therefore, we pretreated RhoA and RhoA variants with peroxide and observed nucleotide association. As $RhoA^{WT}$ showed a decrease in nucleotide binding after peroxide treatment, whereas $RhoA^{C20S}$ did not, this data indicates that oxidation is mediated through Cys^{20}. Further, as a disulfide bond between Cys^{16} and Cys^{20} has been shown to inhibit nucleotide binding due to oxidation, it is likely that a disulfide bond between Cys^{16} and Cys^{20} has been formed, which explains the loss of binding that was observed.

Another common $2e^-$ modification common in cells is glutathiolation, which has been observed for Ras (*77*). As glutathiolation has been shown to be a possible outcome of activation by $NO_2^{\cdot}$ (*120*), which has been shown to generate a thiol radical in Ras (*178*), we tested the effect of glutathiolation on RhoA activity as this pathway of glutathiolation is likely for RhoA in cells. While we observed that glutathiolation of RhoA at Cys^{20} showed an increased nucleotide dissociation rate, we predict that oxidation at Cys^{20} can promote disulfide bond formation between Cys^{16} and Cys^{20} similar to peroxide. Therefore, we glutathiolated $RhoA^{C16S}$ to prevent intramolecular disulfides. This variant showed an increased nucleotide dissociation rate, indicating further destabilization of the nucleotide binding site.

While we did not perform any experiments to explicitly determine the structure of the RhoA variants, we used CD spectroscopy and 2D NMR to indirectly observe the stability and structure of $RhoA^{WT}$, $RhoA^{C20S}$, $RhoA^{C16A/C20A}$, and $RhoA^{C20D}$. Thermal denaturation scans using CD (**Figure 19**) revealed that all of the redox-insensitive variants had similar thermal stability. However, the oxidation mimetic, $RhoA^{C20D}$, showed decreased thermal stability.

The HSQC spectra show that the RhoA^{C20S} variant is more similar to RhoA^{WT} than RhoA$^{C16S/C20S}$ (**Figure 20**). While the RhoA^{C20S} variant most closely resembled RhoA^{WT}, the oxidation mimetic RhoA^{C20D} had the largest number of chemical shifts. When the residues that showed a chemical shift are plotted on the crystal structure of RhoA, all variants at position 20 affected switch I and p-loop chemical shifts. However, RhoA^{C16AC20A} and to a further degree, RhoA^{C20D}, more altered chemical shifts in residues that are in switch I and p-loop as well as in switch II. Thus, the NMR spectra suggest that RhoA^{C20S} is a better redox-insensitive variant than RhoA$^{C16A/C20A}$ as there are less chemical shift differences between RhoA^{C20S} and RhoA^{WT}.

RhoA is initially oxidized at Cys^{20}, which results in increasing the rate of nucleotide dissociation and was observed in glutathiolated RhoA and the RhoA^{C20D} sulfinic acid mimic. However, as 2e$^-$ mediated oxidation is slow, it is likely that oxidants capable of generating a thiol radical play a bigger role in regulating RhoA activity. While the CysNO data suggests that nitrosation does not effect nucleotide dissociation, nitrosation is generally a free radical-mediated process in cells. Thus, $NO_2^{\cdot}$ has been shown to cause nucleotide degradation and dissociation (*169*) and likely leaves Cys^{20} as a thiol radical. This radical can react with Cys^{16}, which results in RhoA inactivation due to the disulfide bond, or with other types of oxidants, such as glutathione or nitric oxide. Therefore, future studies that examine the oxidation properties of RhoA in cells should consider using the RhoA^{C20S} variant to verify whether RhoA is being directly regulated by oxidants in cells. Taken together, our in vitro characterization of RhoA redox-insensitive variants shows that the RhoA^{C20S} variant has the most similar kinetic rates, structure, and stability compared to RhoA^{WT}, and importantly, is insensitive to thiol oxidation. As cellular based studies regarding oxidants have provided conflicting results in terms of RhoA regulation, the RhoA^{C20S} variant will provide a new tool to determine whether RhoA is being directly oxidized and regulated, or whether the Rho effector proteins are being differentially regulated.

Chapter 5: Site-specific monoubiquitination activates Ras by impeding GTPase-activating protein function

Introduction

KRas has recently been shown to be activated by monoubiquitination (mUb). Similar to oncogenic mutations, mUb of Ras at position 147 activates Ras by causing a defect in GTPase activating protein (GAP) function. To characterize the mechanism by which mUb impairs GAP-mediated downregulation of Ras, we made various modifications at position 147 of Ras and examined the impact on Ras sensitivity to GAP function. Whereas small modifications (iodoacetamide and glutathione) at position 147 of Ras do not affect GAP-mediated hydrolysis, ligation of Ras to Ub^{G76C} (native linker), Ub^{X77C} (one residue longer), and PDZ2 (with a native ubiquitin linker) was defective in GAP-mediated GTP hydrolysis. However, restoration of GAP activity was observed for Ras modified with the similarly sized PDZ2 domain containing a shorter and stiffer linker region than ubiquitin. Therefore, the properties of the linker region dictate whether modification affects GAP-mediated hydrolysis, and our data indicate that the GAP defect requires a minimum linker length of 7 to 8 residues.

Commentary

Ras GTPases regulate a variety of cellular functions, including gene expression, cell growth, and differentiation (*179*). Although Ras proteins are part of a larger superfamily of small guanine nucleotide binding proteins, Ras is the only family member that is frequently mutated in human cancer. Approximately 30% of all tumors contain Ras mutations. There are three isoforms of Ras (HRas, NRas, and KRas), which differ by their subcellular location. KRas is the most commonly mutated isoform of Ras in tumors (*128*). Ras GTPases cycle

between the GDP-bound 'off' state and GTP-bound 'on' state to regulate a plethora of signaling pathways that control cellular growth. As the intrinsic rates of nucleotide dissociation and GTP hydrolysis are too slow to function on the time scale of most cellular events, Ras activity is dictated by regulatory proteins. These regulatory proteins include guanine exchange factors (GEFs), which activate Ras by facilitating nucleotide exchange, and GTPase-activating proteins (GAPs), which downregulate Ras activity by increasing the rate of GTP hydrolysis. Oncogenic mutations lead to constitutive activation of Ras most commonly by causing a GAP defect. Recent work by Sasaki et al (*16*) demonstrated that post-translational modification of KRas at position 147 by monoubiquitination (mUb) is another, yet novel, mechanism of Ras activation. While mUb has been shown to regulate a number of cell functions, including DNA repair, gene expression, endocytosis, and nuclear export (*180*), the regulation of protein activity by mUb is emerging as another functional role (*181*). Furthermore, mUb is highly regulated and can be reversed by deubiquitinating enzymes (*182*). KRas is predominately monoubiquitinated at Lys^{147}. Sasaki et al showed that mUb of KRas (mUbRas) resulted in an increased fraction of GTP-bound Ras, altered effector specificity, and increased tumorigenicity. $Lysine^{147}$ is part of the highly conserved motif (SAx) in Ras superfamily GTPases and forms critical interactions with the guanine nucleotide base. Within the SAx motif in the Ras subfamily, Lys^{147} is less conserved (67%) relative to Ser^{145} (97%) and Ala^{146} (89%) (*183*). Mutation of Ala^{146} to valine results in oncogenic transformation of Ras due to increased nucleotide exchange, which populates Ras in the GTP-bound form (*184*). Thus, Sasaki et al hypothesized that mUb of Ras at Lys^{147} activates Ras by enhancing nucleotide exchange and populating Ras in its active GTP-bound state.

While mutation of the site of KRas mUb (K147L) reduced tumorigenesis in 3T3 cells injected into mice (*16*), it is unclear whether altered levels of Ras mUb occur in primary tumors as most studies probe for Ras mutations and not upregulation of Ras activity.

Moreover, the levels of mUb Ras are controlled by enzymes responsible for ubiquitination and deubiquitination, which can become altered in many cancers (*185*). Aside from elucidating how ubiquitin alters Ras properties, determining the enzymes necessary for Ras-mediated ubiquitination is a critical future direction in understanding the role of this modification in healthy and diseased states. Sasaki et al found that mUbRas^{G12V} was more oncogenic than Ras^{G12V} (*16*). This is an interesting result as KRas mUb may contribute to tumorigenicity in the context of a GAP-defective oncogenic mutation (G12V), possibly because of enhanced association with select effectors (*16*). Thus, more studies probing Ras oncogenicity should be performed in cell lines with and without Ras mutation-driven tumors. In addition, the role of mUbRas in regulating effector specificity should be investigated. Understanding the functional consequences underlying this post-translational modification will be critical to understanding the role of mUbRas under normal and oncogenic conditions.

Towards this goal, Baker et al recently elucidated how mUb of KRas at 147 upregulates Ras activity *in vitro*. Moreover, they were able to verify the GAP-deficient defect of mUb KRas immunoprecipitated from HEK293T cells (*15*). First, it was shown that mutating Lys^{147} to less conservative substitutions, such as K147A and K147L, had only a modest effect on intrinsic and regulator (GEF/GAP)-mediated GTP hydrolysis and nucleotide exchange. This finding indicates that Lys^{147} does not play a critical role in nucleotide binding, but rather, Lys^{147} may be conserved in Ras GTPases for regulation by ubiquitin modification. Baker et al developed a method to chemically modify Ras *in vitro* with ubiquitin using variants containing a cysteine substituted at the site of ubiquitination (Ras^{K147C} and ubiquitin^{G76C}) (*15*). The studies were conducted in the context of the Ras^{C118S} substitution, which does not alter Ras structure or biochemical properties (*66, 131*), so that position 147 was specifically modified. The intrinsic and regulator-mediated rates of nucleotide dissociation and GTP hydrolysis on Ras$^{C118S/K147C}$ (hereafter called Ras^{CSKC}) were measured. While mUb of Ras did

not alter the intrinsic rates of nucleotide dissociation or GTP hydrolysis, mUbRas impaired GAP-mediated GTP hydrolysis. This finding explains the observed increase in active GTP-loaded Ras observed for the mUbRas pool *in vivo* (*16*). Baker et al verified these *in vitro* findings in HEK293T cells as immunoprecipitated mUbRas, but not unmodified KRas, was GAP defective. Thus, increased Ras activation upon mUb results from the loss of GAP activity and not an increase in intrinsic nucleotide exchange (*15*). Monoubiquitination of Ras may be activated in a similar manner to common GAP-defective oncogenic Ras mutations at positions 12, 13, and 61 (*128*).

It is unclear how mUb of Ras impairs GAP-mediated hydrolysis while retaining the intrinsic rate of GTP hydrolysis. One possibility is that mUbRas is not responsive to GAP-mediated hydrolysis because GAPs cannot bind to the transition state of mUbRas, similar to many oncogenic mutations at position 12 and 13 (*186*). Using the transition state analog that consists of AlF_3 and GDP, Baker et al determined that mUbRas could still bind GAPs while in the transition state, albeit with decreased binding (*15*). However, binding to the transition state is not necessarily indicative of GAP sensitivity because the Ras^{G12A} mutant is unresponsive to GAP-mediated hydrolysis but can still bind to GAPs in the presence of the transition-state analogs (*186*). It is currently postulated that GAPs enhance the rate of GTP hydrolysis by stabilizing the switch regions around position Gln^{61} for in-line nucleophilic attack on the γ phosphate as well as to move Tyr^{32} to an open position, which provides space for the GAP arginine 'finger' to insert into the binding pocket and catalyze phosphate hydrolysis (*187*). The data from Baker et al indicate that ubiquitin ligation to Ras impairs GAP-mediated hydrolysis without forming a high-affinity interaction with a particular surface of Ras. Using nuclear magnetic resonance (NMR) spectroscopy and Rosetta-based computer simulations, Baker et al demonstrated that ubiquitin does not specifically interact with Ras but that ubiquitin ligation to Ras affects the dynamics of the switch regions and

phosphoryl-binding loop (p-loop) (*15*). This finding suggests that mUbRas may alter the conformational dynamics of regions critical for GAP-mediated GTP hydrolysis.

While Ras has not been shown to directly interact with ubiquitin, it is unclear if there are transient or low affinity interactions between Ras and ubiquitin that alter the ability of GAP proteins to facilitate the rate of GTP hydrolysis. To simplify this post-translational modification, mUb may be viewed as two components: a ball, which consists of the core ubiquitin domain, and a chain (tether), which consists of the 7-residue linker from the core ubiquitin domain to the carboxy-terminus. To confirm that the deficiency in GAP-mediated GTP hydrolysis was not due to specific interactions formed between Ras and ubiquitin, we ligated Ras^{CSKC} to a modified PDZ2 domain ($PDZ2^{UL}$; with the same carboxy-terminal linker as ubiquitin), which is a protein with a similar size and fold as ubiquitin. We found that Ras ligated to $PDZ2^{UL}$ was also defective in GAP-mediated GTP hydrolysis, which supports earlier NMR and modeling studies (*15*) that indicate that ubiquitin does not specifically interact with Ras but samples a range of conformations on the surface of Ras to render Ras insensitive to GAP-mediated GTP hydrolysis. To address whether the size of the modification (ball) or length of the tether (chain) at position 147 significantly contributes to the loss of GAP-mediated hydrolysis, we expanded on our earlier work by modifying Ras with various modifications. These modifications include iodoacetamide (IAA), glutathione, PDZ2 with a shortened linker region ($PDZ2^{SL}$; the chain was truncated to 6 residues), and ubiquitin with a slightly longer linker Ub^{X77C} (chain length was increased to 8 amino acids) and measured the intrinsic and GAP-mediated rates of GTP hydrolysis.

Although mutation of Ras at Lys^{147} does not significantly alter nucleotide hydrolysis (*15*), it is possible that small modifications of Ras at Lys^{147} could affect GAP-mediated GTP hydrolysis. Thus, we first modified purified $KRas^{CSKC}$ with IAA. This modification was selected because IAA is small, uncharged, and the chemistry of cysteine oxidation has been sufficiently documented (*188, 189*). Using a fluorescence-based GTP hydrolysis assay (*15,*

131), we found that iodoacetylation of KRas^{CSKC} did not affect either the intrinsic or GAP-mediated rates of GTP hydrolysis when using the p120 RasGAP catalytic domain (GAP^{334}) compared to unmodified KRas^{CSKC} (**Figure 24A**). We also modified KRas^{CSKC} with glutathione. Glutathione was selected because it is larger than IAA (305 Daltons compared to 58, respectively) and has a negative charge. Furthermore, the cysteine in glutathione allows for disulfide bond formation between KRas^{CSKC} and glutathione, which is similar to the ubiquitin ligation technique presented in Baker et al (*15*). We verified that KRas^{CSKC} was 100% glutathiolated at position 147 using mass spectrometry (**Figure 24B, C**), and similar to our findings with iodoacetylated Ras^{CSKC}, we find that glutathiolated Ras^{CSKC} possesses similar rates of intrinsic and GAP-mediated GTP hydrolysis compared to unmodified KRas^{CSKC}. These *in vitro* results indicate that perturbations at position 147 of Ras, by mutation or small molecule modifications (up to ~300 Da), do not affect GAP-mediated hydrolysis.

We next asked whether the linker length associated with either PDZ2 or ubiquitin ligation to Ras was important for GAP-mediated GTP hydrolysis. We have previously shown that a ~2 kDa larger ball (PDZ2^{UL} instead of ubiquitin) ligated to position 147 of Ras retained the GAP defect observed with mUb (*15*); however, it was unclear how different chain lengths associated with the ligation affect GAP-mediated GTP hydrolysis. Toward this end, we altered the properties of the linker between Ras to either ubiquitin or PDZ2. We first increased the linker length by 1 residue by ligating Ras to a ubiquitin variant (Ub^{X77C}; **Figure 25C**) and observed a similar GAP defect to that of mUbRas. However, when we shortened the chain length by 1 residue, by modifying Ras with PDZ2 with the native PDZ2 carboxy-terminus (PDZ2^{SL}; 6 residue linker), we observed that ligation of PDZ2^{SL} to Ras restored sensitivity to GAP-mediated GTP hydrolysis. While the linker length for this ligation is 1 residue shorter, the composition of the linker differs from that found in ubiquitin and is predicted to be less flexible by FlexServ (*190*). Taken together, these data indicate that the

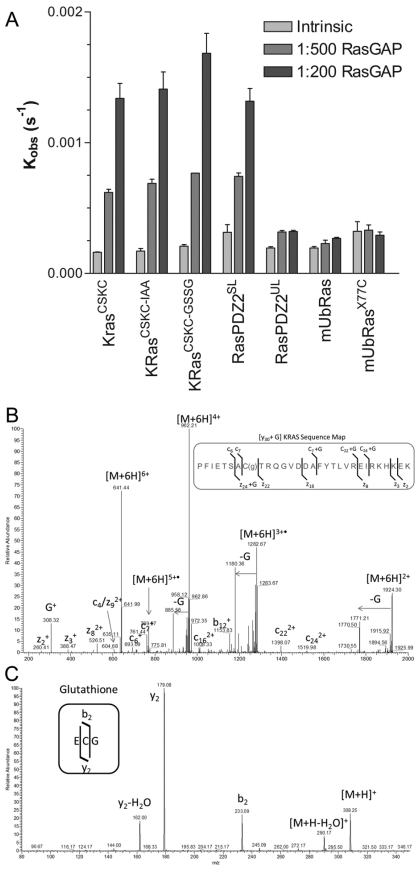

Figure 23. Characterization of GTP hydrolysis of oxidized Ras^{CSKC}.

(A) Rates of intrinsic and GAP-mediated hydrolysis of KRas with various modifications. The minimal catalytic domain of p120 Ras^{GAP}, residues 1-334, was used. The relative rates of hydrolysis are presented using the phosphate detection protein FlipPi, as previously reported (10, 11). All reactions were performed in triplicate and fit to a single exponential dissociation curve using GraphPad Prism. The error is reported as the standard deviation of the replicates. (B) MS3 product ion showing c- and z-type product ions resulting from the dissociation of the N-C (alpha) bonds due to electron transfer dissociation (ETD) of a 6^+ charge of collision-induced dissociation (CID)-derived [Y30+G] product ions. The [Y30+G] product ions were generated by CID-MS/MS, which generated b- and y-type fragment ions from the dissociation of the backbone amide bonds of a 20^+ product ion from intact KRas^{CSKC} modified with a single glutathione. (C) MS4 product ion spectrum derived from CID-MS3 of the singly charged glutathione product ion (G+). Note that the glutathione moiety was confidently localized to cysteine 147 of KRas^{CSKC} by tandem mass spectrometry. Mass spectrometry data collected in collaboration with Harsha Gunawardena.

linker length and/or flexibility are critical for the GAP defect upon ligation to position 147 of Ras and suggest that conformational sampling or accessibility to a particular surface(s) of Ras may play an important role in the ability of mUb at position 147 of Ras to impede GAP-mediated GTP hydrolysis.

By comparing the findings in Baker et al to the present results, the composition and length of the linker (chain) associated with either PDZ2 or ubiquitin ligation to position 147 of Ras appear critical for inhibition of GAP-mediated GTP hydrolysis. Although we find that a ball size between 8-10 kDa attached to a ubiquitin linker of at least 7 residues can impede GAP-mediated hydrolysis, we have not determined whether there is a minimum ball or maximum chain size associated with the inhibition of GAP function. However, we have shown that there is a minimal chain length for effective inhibition. We modified Ras at position 147 with Ub^{X77C}, which is 1 C-C bond length longer than the native ubiquitin modification as well as Ub^{G76C}, which is 2 C-C bond lengths shorter than the native modification, and both of these modifications fully inhibit GAP-mediated GTP hydrolysis in our assays. Further, when using the $PDZ2^{SL}$ modification, which is 5 C-C bond lengths shorter than the native modification, Ras was responsive to GAP-mediated GTP hydrolysis (see **Figure 25** for chain length depictions and **Figure 26** for a structural representation of the modifications). These results suggest that there is a minimum chain length for the ubiquitin modification to inhibit GAP-mediated GTP hydrolysis of Ras. However, as ubiquitin does not appear to specifically interact with Ras, we reviewed proposed mechanisms of GAP-mediated hydrolysis to generate a hypothesis as to why mUbRas displays a GAP defect.

GAP proteins interact with Ras and greatly facilitate GTP hydrolysis rates via three primary steps, according to a report by Kötting et al (*191, 192*). Using Fourier-transformed infrared (FTIR) spectroscopy and photo-caged GTP-bound Ras complexed with p120 RasGAP, the authors first observed movement of switch I from an ordered 'off' state to an

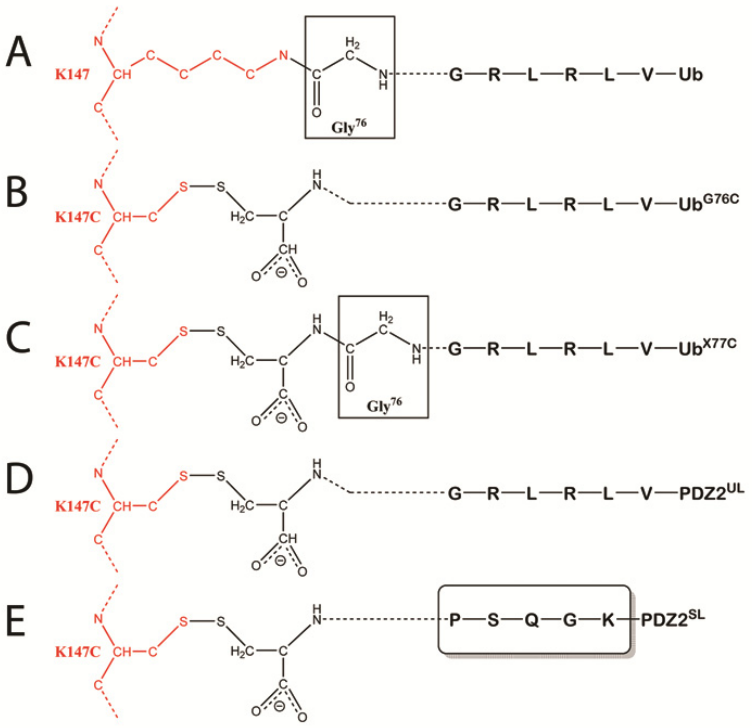

Figure 24. Depiction of the protein:protein ligations in this study.

Ras is indicated in red and the attached modifications are in black. The single letter amino acid code associated with the tether of ubiquitin and PDZ2 are highlighted in bold font. (A) The native ubiquitin modification of Lys^{147} of Ras. (B) The chemical ubiquitination by disulfide formation between Ras^{K147C} and Ub^{G76C}. (C) The chemical ubiquitination of Ras^{K147C} by Ub^{X77C}. Gly^{76} is highlighted by a black box to show the increased size of the Ub^{X77C} modification compared to the native modification. (D) The chemical ubiquitination of Ras^{K147C} to $PDZ2^{UL}$. (E) The chemical ubiquitination of Ras^{K147C} to $PDZ2^{SL}$. The linker region of $PDZ2^{SL}$ is outlined to highlight the differences within the linker region. The core domain of each ligated protein is also shown.

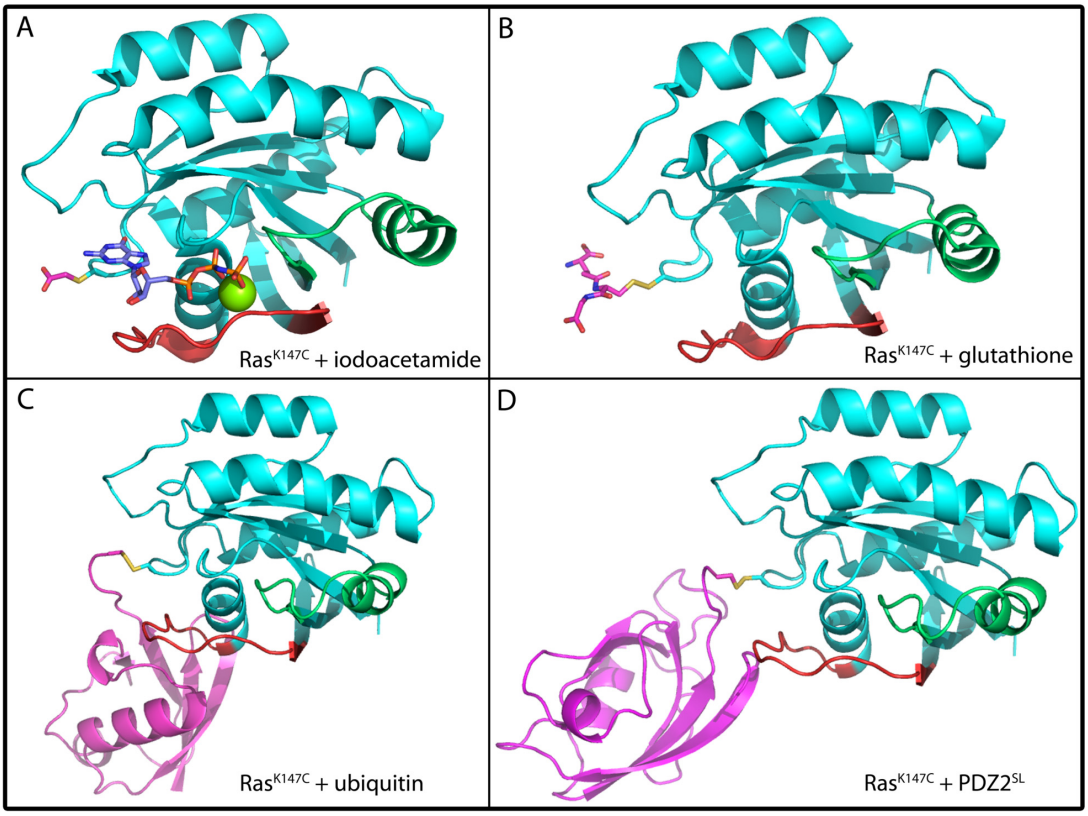

Figure 25. Pymol-generated images of the small molecule modifications as well as PDZ2 and mUb.

(A) KRas (PDB 3GFT) with the K147C mutation modified with iodoacetamide. (B) KRas (PDB 3GFT) with the K147C mutation modified with glutathione. (C) HRas (PDB 1CRR) with the K147C mutation ligated to ubiquitin, which is ligated to Ras by a disulfide bond through a cysteine at K147C and a C-terminal cysteine in ubiquitin (G76C). (D) HRas (1CRR) with the K147C mutation ligated to PDZ2^{SL} with a C-terminal cysteine by a disulfide bond. Structural depictions on (A) and (B) were generated in pymol and are presented for comparison of size. Depictions in (C) and (D) were generated using Rosetta and are depictions of low-energy models of the complex. Ras is shown in teal in all images, switch I (residues 25-40) is in red, switch II (residues 57-75) is in green, and each modification is in magenta. The nucleotide has been removed from (B), (C), and (D) for clarity.

ordered 'on' state. The second step of GAP-mediated hydrolysis involves the movement of the arginine finger of the GAP into the catalytically active position, and the third step is cleavage of the γ phosphate. Recently, Rudack et al used FTIR and biomolecular simulations to study the mechanism of GAP-mediated GTP hydrolysis in Ras in more detail (*193*). In this study, the authors suggest that GTP hydrolysis is a result of the α, β, and γ phosphates being pulled into an eclipsed conformation by GAP binding, which results in the γ phosphate becoming more electro-positive; this allows the catalytic water to hydrogen bond with the γ phosphate and accelerate hydrolysis by nucleophilic attack. Further, Rudack et al used FTIR to show that the GAP-arginine finger forms hydrogen bonds with the α and γ phosphates of GTP (*193, 194*). Molecular dynamics simulations performed by Kötting et al (*191, 192*) indicate that when the arginine finger inserts into the active site of Ras, it displaces 5 water molecules and increases the negative charge on the β phosphate and imparts partial positive charge to the γ phosphate of GTP. The removal of the water molecules has been theorized to provide the thermodynamic (entropic) energy necessary for GAP-mediated hydrolysis (*191*). Furthermore, Grigorenko et al (*195*) suggested that the placement of the arginine finger locks a conformation of the GTP binding pocket that decreases the free energy necessary for γ phosphate cleavage. In the GAP-bound state, Grigorenko et al determined that Gln^{61} of Ras and Arg^{789} of p120 RasGAP, as well as Thr^{35} (switch I), Mg^{2+}, Gly^{60} (switch II) and Lys^{16} (p-loop), provide further orientation of the phosphates of GTP and facilitates hydrolysis. However, in intrinsic Ras-mediated GTP hydrolysis, only Thr^{35}, Mg^{2+}, Gly^{60}, Lys^{16}, and water molecules are directly involved in GTP hydrolysis, which results in an increased activation energy (*195*). The primary factors proposed for driving increased nucleotide hydrolysis of Ras by GAPs include reorientation of the γ phosphate, Gln^{61}, and catalytic water of Ras as well as the placement of the arginine finger from the GAP.

These mechanistic studies of GAP-mediated hydrolysis can be used to generate a hypothesis for the results observed by Baker et al (*15*). Although Baker et al showed that

GAPs still bind to the transition state of mUbRas, the binding affinity and whether the GAP favors the proper conformation of Ras for GTPase activity was not determined. The data by Kötting et al imply a structural rearrangement by insertion of the arginine finger by the GAP after binding to Ras, and it is unclear whether this structural rearrangement by the GAP is impeded in mUbRas. NMR and Rosetta simulations indicate that when Ras^{147} is ligated to ubiquitin, ubiquitin samples a large surface area of Ras, including parts of the p-loop and switch regions. As GAP binding has been shown to restrict the motions of the phosphate moieties of GTP and switch regions (*193*), these regions in mUbRas may not conducive for GAP-mediated hydrolysis (*15*). Specifically, the NMR data suggest that conformational dynamics of the p-loop and switch regions are altered by ubiquitin ligation at position 147, which could change either the rates or population of the conformers associated with these regions. However, it will be important to better characterize the conformational dynamics associated with GTP-bound mUbRas as only the GDP-bound form of mUbRas was studied by NMR (*15*). The inability to populate the correct orientation of the active site, specifically the region near the p-loop, could prevent stabilization of the switch regions in Ras as well as the eclipsed conformation of GTP, which would likely prevent GAP-mediated hydrolysis. This hypothesis is consistent with the simulations performed by Rudack et al, who proposed that the eclipsed phosphate conformation is necessary for hydrolysis. Thus, modification alone at position 147 is not enough to prevent hydrolysis-competent conformations; however, the ability of tethered ubiquitin to sample regions associated with the catalytic site (p-loop and switch regions) is necessary to interfere with GAP function. In this case, other modifications of Ras, such as $PDZ2^{SL}$, that possess a shorter tether may not alter the conformational dynamics of the Ras switch regions and p-loop, and thus retain the ability to be downregulated by GAPs, which is likely why the smaller modifications (IAA and glutathione) and $PDZ2^{SL}$ do not affect GAP-mediated hydrolysis.

In summary, we present additional data that provide further insight into how ligation of ubiquitin to Ras^{147} results in a GAP-deficient phenotype. Using the KRas^{CSKC} variant, we were able to build on the recent publication by Baker et al and show that smaller modifications of Ras at position 147 (IAA and glutathione) do not affect GAP-mediated hydrolysis. However, as both the PDZ and ubiquitin modifications result in a GAP defect, the minimum size of the modification necessary to generate the GAP defect is not known. Rather, by changing the tether length of the PDZ2 domain, we were able to show that there is a critical tether length needed to produce a GAP defect. Thus, with the PDZ2^{SL} modification, no loss of GAP function was observed; however, with the longer tether, PDZ2^{UL}, a complete loss of GAP function was observed. The ability of ubiquitin ligation to Ras at position 147 to impede GAP-mediated GTP hydrolysis appears to be dependent on the length and composition of the linker, which we speculate to be important for the conformational sampling of a surface(s) on Ras that prevents GAPs from catalyzing GTP hydrolysis, and downregulation of Ras activity. As mUbRas appears to mediate Ras-induced tumorigenesis in HEK293T cells, understanding how this modification alters Ras function could aid in providing a new direction for inhibiting Ras-driven tumors.

Chapter 6: Biophysical and Proteomic Characterization Strategies for Cysteine Modifications in Ras GTPases

Introduction

One of the most reactive amino acids in proteins is cysteine, which can undergo a variety of different post-translational modifications and several different types of oxidative reactions (*196*). In fact, thiol oxidation plays a key role in regulating redox homeostasis and protecting the cell during oxidative stress (*197-199*). Moreover, many genes that respond to redox stress show altered regulation by reactive oxygen and nitrogen species (ROS and RNS) (*200*). Some of the common end products of cysteine oxidation are disulfide bond formation, mixed disulfide bond formation with glutathione (glutathiolation), and nitrosation as well as sulfenic, sulfinic, and sulfonic acid (*201*). Many redox-sensitive proteins contain cysteine residue(s) that have an altered pK_a. The microenvironment surrounding the cysteine determines the pK_a of the thiol side chain. However, cysteine pK_a values are difficult to reliably predict as several factors influence pK_a, including solvent exposure, hydrogen bond formation, and charge-charge interactions (*202*). The pK_a of L-cysteine in water has been measured to be ~8.5-9, and the thiolate form (RS^-) is approximately tenfold more reactive than the thiol form (RSH) (*203*). Thus, redox-regulated proteins often contain reactive cysteines with altered pK_a values that are close to or lower than physiological pH.

Critical cellular enzymes that regulate redox homeostasis include peroxiredoxins (reduce peroxide), thioredoxins (reduce oxidized peroxiredoxin), and glutathione peroxidases (reduce peroxide using the cellular glutathione pool), which act through mechanisms involving cysteine oxidation. The pK_a of the active-site cysteines have been

shown to be markedly reduced in each of these classes of enzymes; for example, the active-site cysteine pK_a has been shown to be approximately 5-6 in 2-Cys peroxiredoxins (*204*), the active-site cysteine in Escherichia coli thioredoxin was measured to be between 7.1 (*205*) and 7.5 (*206*), and the pK_a of the active-site cysteine in glutathione peroxidase has been estimated to be 7.2 (*207*).

The work in our lab is centered on the redox regulation of Ras superfamily GTPases. We have shown that the activity of a subset of Ras and Rho GTPases can be regulated through redox-sensitive cysteines (*21, 57, 164*). Ras GTPases, in particular, have received a great deal of interest in the field of redox biology. There are four distinct Ras genes in the human genome, H-, K- (1A and 1B) and N-Ras, which differ primarily in their carboxyl-terminal regions. They encode small, 21-kDa guanine nucleotide binding proteins that function as molecular switches to modulate signaling pathways that control cell growth, differentiation, and apoptosis (*86*). This is achieved by cycling between the inactive ('off') GDP-bound and active ('on') GTP-bound states. Given the high affinity interaction between Ras and its nucleotide ligands (GDP and GTP) as well as the slow intrinsic rate of GDP dissociation and GTP hydrolysis, two classes of modulatory proteins regulate the activation state of Ras proteins. One class of proteins that activate Ras is guanine nucleotide exchange factors (GEFs), which promote exchange of GDP for GTP. Analogous to guanine nucleotide exchange factors, redox agents have been shown to stimulate nucleotide exchange and alter the activity of Ras proteins through reaction with cysteine 118 (Cys^{118}), which is located in a conserved guanine nucleotide-binding motif (*94*). We have found that only redox agents capable of thiyl radical formation, such as $NO_2^{\bullet}$, can modulate Ras activity (*69*). Thiyl radical formation at Cys^{118} facilitates guanine nucleotide exchange in Ras by promoting oxidation and the subsequent dissociation of the bound guanine base (*62*). In cells, where the GTP/GDP ratio is in excess, this can lead to exchange of GDP for GTP and result in Ras

activation. Importantly, this mechanism of Ras regulation has been shown to play a role in Ras-mediated tumorigenesis and tumor maintenance (*63*).

Rho GTPases are members of the Ras superfamily, and like Ras GTPases, function as molecular switches to regulate cellular growth. However, they also regulate cell motility and oxidant regulation (*4*). We have previously shown that a subset of Rho GTPases can be regulated through redox modification (*80*). These GTPases contain a distinct, reactive cysteine that is conserved in ~40% of Rho GTPases and renders them sensitive to oxidation and oxidative modification in cells (*81*).

Although several methods to determine cysteine pK_a values have been employed in the field (*202*), we have recently developed a fluorescence-based method to measure cysteine pK_a values (*208*). Using 4-fluoro-7-aminosulfonylbenzofurazan (ABD-F), a compound that specifically reacts with the thiolate form of the cysteine side chain, we have been able to measure the pK_a of reactive thiols in Ras and Rho family GTPases. In Ras, Cys^{118} is the only solvent accessible cysteine in the core catalytic domain (Ras residues 1-166). Thus, Ras provides an excellent system to demonstrate the use of the ABD-F strategy for measuring pK_a values of cysteine thiol side chains.

When coupled with mass spectrometry (MS), this method provides an analytical platform for the detection and quantification of redox modifications in Ras family GTPases and other proteins. The bottom-up MS method we've employed (*209*) requires proteolytic digestion with trypsin followed by LC-MS analysis by electrospray ionization (ESI). The accurate identification of peptides has become a routine practice with the availability of a vast number of programs and search engines that assist in assigning peptide sequences to mass spectra using probabilistic prediction algorithms (*210*). In addition, the intensity, or spectral count information, can be used for the relative or absolute quantification of peptides associated with site-specific protein modifications.

Herein, we describe in detail a new method for determining the pK_a of cysteine thiols in proteins as well as the use of MS approaches to quantify the level of modification, including (1.1: Cysteine pK_a determination using 4-fluoro-7-aminosulfonylbenzofurazan), the preparation and handling of several ROS and RNS (1.2: Generation of cysteine-modifying redox-active compounds and 1.3: $NO_2^{\cdot}$ generation and NONOates), and mass spectrometry-based methods for determining the type and site of cysteine oxidation (1.4: Quantitative mass spectrometry), including 1.4.1: Isotope-coded affinity tag-labeling for relative cysteine quantification, 1.4.2: Quantification of the cysteine oxidation, 1.4.3: Differential quantification of cysteine oxidation, 1.4.4 Differential thiol trapping to determine reversible oxidation of cysteine residues, and 1.4.5 Filter-aided sample preparation.

Materials

2.1 ABD-F buffers and reagents

1. Components: 4-fluoro-7-aminosulfonylbenzofurazan (ABD-F), black, flat-bottom, non-coated plates, and protein spin concentrators.
2. Reducing Buffer: 15 mM 4-(2-hydroxyethyl)-1-piperazineethanesulfonic acid (Hepes), pH 8.0, 5 mM $MgCl_2$, 30 mM NaCl, 200 μM diethylene triamine pentaacetic acid (DTPA), 5 mM dithiothreitol (DTT; added day of use).
3. ABD-F modification buffer: 15 mM 2-(N-morpholino)ethanesulfonic acid (MES), pH 6.5; see note 1), 5 mM $MgCl_2$, 30 mM NaCl, 200 μM DTPA.
4. pH screen buffer (for a pH range between 5.5 to 8.5): 100 mM MES, 100 mM Hepes, 5 mM $MgCl_2$, 200 μM DTPA (titrate each pH value individually).

2.2 Nitrosation reagent (CysNO/GSNO) generation

1. Solution I: 50 mM L-cysteine (or reduced glutathione) in 120 mM HCl
2. Solution II: 50 mM $NaNO_2$

3. Solution III: 40 mM Ammonium Sulfamate
4. CysNO dilution buffer: 100 mM Hepes, pH 7.5, 5 mM $MgCl_2$, 1 mM DTPA

2.3 Nitric oxide releasing agents (NONOates)

1. All NONOate compounds (available from Cayman Chemicals)
2. 4,5-diaminofluorescein (DAF-2)

2.4 Mass Spectrometry techniques

2.4.1. Isotope-coded affinity tag (ICAT)-labeling for relative cysteine quantification

1. Strong cation-exchange (SCX) PolySulfoethyl A column; Isotope-coded affinity tag (ICAT) reagents (AB Sciex; Framingham, Ma), kit includes a cation-exchange cartridge and Avidin affinity cartridge; micro-concentrator/spin filter device; C18 spin column.

2.4.2 Quantification of the cysteine oxidation

1. Ammonium Bicarbonate (ABC) Buffer: 200 mM NH_4HCO_3
2. ABC + Iodoacetamide (IAM): 200 mM NH_4HCO_3, 5 mM IAM
3. Phosphate buffer: 100 mM Na_2HPO_4, pH 7.4, 50 mM NaCl, 5 mM $MgCl_2$
4. Phosphate-buffered saline (PBS): 10 mM Na_2HPO_4, 2 mM KH_2PO_4, 137 mM NaCl, 2.7 mM KCl
5. BIAM-elution buffer: 50 Na_2HPO_4, pH 7.2, 2 mM D-biotin, 150 mM sodium chloride

2.4.3 Differential quantification of cysteine oxidation

1. Tris Buffer: 50 mM Tris, pH 8.5, 25 mM NaCl, 5 mM $MgCl_2$
2. SCX Buffer A: 10 mM KH_2PO_4, pH 3.0, 20% (vol/vol) acetonitrile (ACN)
3. SCX Buffer A: 10 mM KH_2PO_4, pH 3.0, 350 mM KCl, 20% (vol/vol) ACN

2.4.4 Differential thiol trapping to determine reversible oxidation of cysteine residues

1. Denaturing alkylation buffer (DAB): 200 mM Tris, pH 8.5, 8 M urea, 0.5% (wt/vol) SDS, 10 mM EDTA

2.4.5 Filter-aided sample preparation (FASP)

1. Denaturing buffer: 0.1 M Tris, pH 8.5, 8 M Urea
2. Iodoacetamide (IAM) buffer (should be made day of use): 0.1 M Tris, pH 8.5, 50 mM IAM, 8 M urea

Methods

3.1: Cysteine pK_a determination using 4-fluoro-7-aminosulfonylbenzofurazan (ABD-F)

1: Determine the amount (in moles) of protein that will be required to perform the assay. The assay as described is performed in a 96-well plate and requires fluorescence detection at 513 nm (excitation at 389 nm). Each well should contain approximately 5 or 10 μM protein and be performed in triplicate at each pH value (technical repeats). To determine the pK_a accurately, a pH range must be performed with adequate coverage. As ABD-F fluorescence intensity is sensitive to the site of modification, it is important to ensure similar buffer conditions across the pH range selected.

2: Calculate the quantity of protein required; for example, 12 pH values performed in triplicate requires approximately 72 nmol of protein to perform the assay (200 μl/well; 10 μM/well * (36 wells * 200 μl) = 72 nmol required).

3: Reduce the protein with dithiothreitol (DTT) or dithiobutylamine (DTBA) (see note 2) to increase the yield of protein that can react with ABD-F. For adequate reduction, exchange the protein into a buffer containing 5 mM (or greater) DTT. Prepare the reducing buffer (minimum pH of 8.0) and exchange the protein into the buffer. As a subset of oxidative reactions (sulfenic and sulfonic acid) will not be reversed by DTT (see note 3), this

step serves to increase the percentage of protein that can be modified by ABD-F and enhances the signal-to-noise ratio of the assay.

4: While the protein is being buffer exchanged, prepare the ABD-F modification buffer. To remove dissolved oxygen (see note 4), sparge the ABD-F modification buffer with an inert gas, such as N_2, for 30 minutes.

5: Incubate the protein in reducing buffer for at least 60 minutes on ice for complete reduction.

6: Buffer exchange the protein into the sparged ABD-F modification buffer using spin concentrators (use appropriately sized membrane pores). This step removes reducing agents from the sample. It is critical that at least three rounds of exchange are performed to efficiently remove the reducing agent from the sample (see note 5).

7: Determine the protein concentration.

8: Set up the 96-well plates. The excitation wavelength for ABD-F is 389 nm and emission wavelength is 513 nm. Set up a 'dummy tray' that contains half of the volume of the final reaction (100 µl). In the 'dummy tray', add ABD-F to a final concentration that is double the intended concentration (add 2 mM ABD-F in 100 µl). As the reaction proceeds through second-order kinetics, it is critical that all wells contain exactly the same amount of protein and ABD-F; therefore, the rate of modification is related to the thiol/thiolate state of the cysteine. In a separate 96-well plate, replicate the pH screen of the 'dummy tray', but add 20 µM protein in 100 µl to each well (see note 6).

9: Using a multi-channel pipette, quickly remove the solution from the 'dummy tray' and place the solution into the respective wells of the test plate to initiate the ABD-F reaction. Quickly start the plate reader for data collection.

10: Data analysis (see note 7). Use the linear portion of the initial slopes to calculate the rate of fluorescence generation over time (**Figure 27 A, B**). Plot the determined rates of fluorescence generation vs. pH and fit the resulting sigmoidal curve to a Boltzman sigmoidal

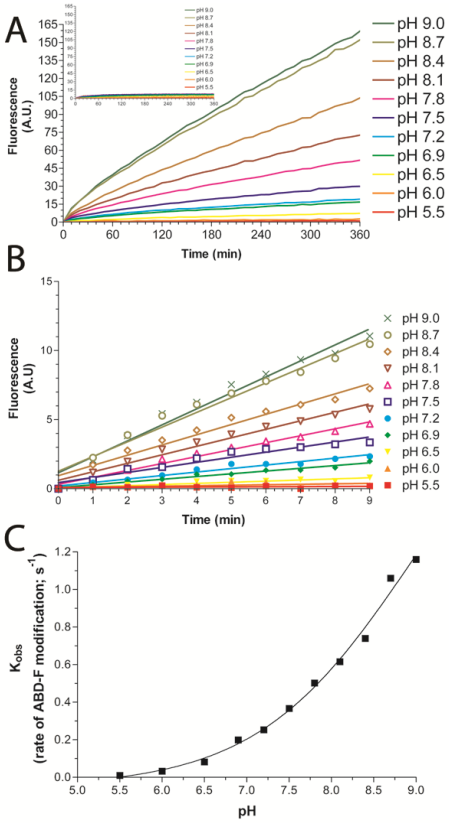

Figure 26. ABD-F modification of H-Ras^{WT} over a selected pH range.

(A) H-Ras^{WT} (10 μM) was reacted with ABD-F (1 mM) over 6 h at the indicated pH values. Each reaction was performed in triplicate (error bars removed for clarity). Absolute fluorescence values are presented. In systems containing one modifiable cysteine, the total fluorescence values will plateau at a similar value if given sufficient time. The inset shows the relative reactivity of H-Ras^{C118S}, which was performed under identical conditions as H-Ras^{WT}. (B) The initial rates of ABD-F modification are used for pK_a determination. Here, the initial data are presented (zoomed in from Fig 1A), and the initial rate was determined using GraphPad Prism; linear curve fitting was performed. Error bars are removed for clarity. (C) The observed rates of modification are plotted against pH. Each data point represents the rate of modification determined from the curve fitting in (B). The data were fit to a Boltzmann Sigmoidal distribution to determine the pK_a. Control data (see inset in figure 27A) show that only Ras Cys^{118} is modified by ABD-F as the Ras^{C118S} control shows no reactivity. However, RasCys^{118} does not have an altered pK_a. Hence, the maximal rate of modification could not be obtained as Ras becomes unstable at high pH values. Therefore, the pK_a is an estimate.

equation. This equation is used to calculate the pK_a for a single site-specific modification (see note 8; **Figure 27C**).

11: After the fluorescence data has been collected, determine the site(s) modified by ABD-F (see note 9). A straightforward method is to employ liquid chromatography-mass spectrometry (LC-MS) on trypsin-digested samples. We have also found that cysteine-to-serine mutants can be used to confirm modification sites if the mutation does not alter the protein structure and/or ABD-F reactivity.

3.2: Generation of cysteine-modifying redox-active compounds (CysNO/GSNO generation)

As the reactions of ROS and RNS with proteins are diverse and often complex, this section will focus on the generation and quantification of various redox-active compounds. Chapter 3.4 describes mass spectrometry (MS) approaches to quantify and determine the sites of modification.

1: Prepare solution I and solution II on the day of use (see note 10), as detailed in Section 2.2 (see note 11).

2: Mix 100 µl of solution I with 100 µl of solution II and place into a foil-covered 1.5-ml eppendorf tube. Allow the reaction mixture to sit in the dark for 10 min. These reactions are highly light sensitive; therefore, care should be maintained to keep all reactions in the dark.

3: Add 20 uL of 40 mM ammonium sulfamate to remove unreacted nitrate and allow the reaction to proceed in the dark for an additional 2 min. This protocol assumes an ~85% efficiency of the reaction (although published reports suggest an efficiency as high as ~90% (*211*)) and adds a sufficient concentration of sulfamate to remove all remaining NO_2.

4: Dilute the thiol-NO (i.e., CysNO or GSNO) with 880 µl (4-fold) of a CysNO dilution buffer (see Materials). While this buffer can be altered to fit the needs of the individual

researcher, the high concentration of the buffer component prevents changes in pH, reduces metal contaminants, and increases the half-life of the thiol-NO in solution (*132, 212*).

5: Concentration determination. The easiest way to measure the concentration of the generated thiol-NO is to measure absorbance at 336 nm. The molar absorptivity for CysNO and GSNO is 900 $M^{-1}cm^{-1}$. Alternatively, the molar absorptivity of 16.8 $M^{-1}cm^{-1}$ at 543 nm can be used for concentration determination (see note 12).

3.3 $NO_2^{\cdot}$ generation and NONOates

While CysNO represents a good nitrosation agent that can modify protein thiols through non-radical oxidative (two-electron) chemistry, the activity of Ras GTPases are uniquely sensitive to free radical oxidation. Free radical agents, such as $NO_2^{\cdot}$, can react with a solvent accessible thiol in Ras to produce a thiyl radical. Through electron transfer, the bound guanine nucleotide becomes oxidized, which results in enhanced guanine nucleotide dissociation and exchange (activation) (*57*). Thus, Ras activity is modulated by free radical agents capable of thiyl radical formation but not through non-radical oxidation. However, this radical-mediated mechanism may not be unique to Ras GTPases. Increasing evidence suggests that in many cases, non-radical-mediated thiol oxidation reactions may be too slow to be biologically relevant (*213*). Thus, in this section, we describe the preparation and handling of $NO_2^{\cdot}$ for use in radical-mediated protein modification.

3.3.1 $NO_2^{\cdot}$ gas generation

1: $NO_2^{\cdot}$ gas can be purchased from various companies; however, it can just as easily be generated. Obtain a small reaction vial and add a small piece of copper wire (~100 mg or less) and cover the vial with a rubber stopper that is airtight.

2: Deplete the oxygen from the vial using an inert gas, such as N_2.

3: Inject in a small volume of nitric acid. Allow the reaction to proceed for 5 to 10 min. Nitrogen dioxide radicals are formed by the following equation:

$Cu + 4HNO_3 \rightarrow Cu(NO_3)_2 + 2NO_2^{\cdot} + 2H_2O$ Reaction 1

The reaction proceeds by the above reaction pathway if a brown gas is generated. This reaction should be performed in a hood as $NO_2^{\cdot}$ gas is highly toxic.

4: Estimate the concentration of $NO_2^{\cdot}$ gas that will dissolve in solution using Henry's Law. Henry's Law states that the amount of a gas that will dissolve in solution is directly proportional to the partial pressure of the gas in equilibrium with the liquid. The coefficient (k) for $NO_2^{\cdot}$ is needed for these calculations. From a table containing these coefficients, a range of 1800-2500 mol/L/atm can be obtained (*214*). As the density for $NO_2^{\cdot}$ gas (2.62 g/cm^3) is heavier than N_2 gas (0.808 g/cm^3), one can assume that the relative gas concentration is 100% $NO_2^{\cdot}$ at the bottom of the vial. The coefficient needs to be converted to units of atm/mol/L by taking the reciprocal of the coefficient. Thus, a range of $1.2\text{-}3.4\times10^{-2}$ atm/mol/L is obtained.

5: Prepare a reaction vial with the protein. Seal the reaction vial and deplete the oxygen using N_2 or another inert gas. The headspace remaining will be critical; thus, the volume remaining in the reaction vial after the addition of the protein sample needs to be determined.

6: Add $NO_2^{\cdot}$ gas to the reaction vial. The amount of gas added to the sealed reaction vial will not likely affect the pressure in the reaction vial significantly; therefore, the pressure is estimated to be 1 atm. However, the percent of $NO_2^{\cdot}$ added to the vial relative to the remaining headspace must be calculated to determine the percent of $NO_2^{\cdot}$ gas in the gas mixture. Thus, if 100 µl of pure $NO_2^{\cdot}$ gas is added to a reaction vial with 1 ml headspace (inert N_2 gas), then the total concentration of $NO_2^{\cdot}$ gas will be 10% (thus, 0.10*1.00 atm = 0.10 atm $NO_2^{\cdot}$ gas in this example).

7: Using the equation c = p/k, where c is the concentration, p is the partial pressure (from Step 8, 0.10 atm), and k is the inverse of Henry's Law coefficient (from Step 4, using an average of 2.3×10-2 atm/mol/L), approximately 4.35 mol/L $NO_2^{\cdot}$ gas will dissolve in liquid in a sealed reaction vial, according to the example presented.

3.3.2 NONOates

NONOates, such as the compounds listed in **Table 4**, are compounds that release $NO^{\cdot}$ in solution in a pH and time-dependent manner over seconds, minutes, or hours. There are 8 NONOate compounds available. All NONOates are relatively stable at alkaline pH (approximately 24 hours at 0°C) and are water-soluble. However, at pH 5, the release of $NO^{\cdot}$ is nearly instantaneous. In addition, each NONOate has a characteristic UV absorbance value. Relevant information on NONOates is listed in **Table 4**.

1: Suspend the desired amount of NONOate in 10 mM NaOH to minimize $NO^{\cdot}$ release (see note 13 and **Figure 28**).

2: To measure $NO^{\cdot}$ release in the selected buffer, 4,5-diaminofluorescein (DAF-2) can be used. DAF-2 specifically binds to $NO^{\cdot}$ and undergoes a change in fluorescence upon reaction. DAF-2 has excitation and emission wavelengths of 485 and 538 nM, respectively. Approximately 10 μM DAF-2 is recommended. DAF-2 has a detection limit of 5 nM at neutral pH (see note 14).

3.4 Quantitative mass spectrometry

The cysteine labeling procedure known as isotope-coded affinity tag (ICAT) (*215*) was the first stable isotope labeling method used in quantitative proteomics. The ICAT approach was designed primarily for the semi-quantitation of proteins expressed in two cellular states by labeling proteins with heavy and light cysteine-reactive tags. The trypsin-digested peptides that correspond to the differential labels are identified using MS, and the relative signal intensities are used for quantitative comparison (see **Figure 29**).

Table 4. Specifications and use of NONOate compounds

Name	Cas#	Efficiency (mol NO per NONOate)	Half-life at 37˚C; 22-25˚C	λmax (nm)	ε ($M^{-1}cm$
DETA NONOate	146724-94-9	2	20 h; 56 h	252	7640
Spermine NONOate	136587-13-8	2	39 min; 230 min	252	8500
Proli NONOate	N/A	2	1.8 sec; N/A	252	8400
DPTA NONOate	146724-95-0	2	3 h; 5 h	252	7860
DEA NONOate	372965-00-9	1.5	2 min; 16 min	250	6500
PAPA NONOate	146672-58-4	2	15 min; 77 min	252	8100
MAHMA NONOate	146724-86-9	2	1 min; 2.7 min	250	7250
Sulpho NONOate	61142-90-3	0	7 min; 77 min	252	8100

(*1-3*)

All NONOate compounds currently available and the CAS# (Proli NONOate currently has no CAS#) are listed. The efficiency represents the number of moles NO released per mol of NONOate compound. The half-life information is provided at both temperatures. The λmax is the wavelength where concentration of the compounds can be taken using a UV spectrophotometer and ε is the corresponding extinction coefficient.

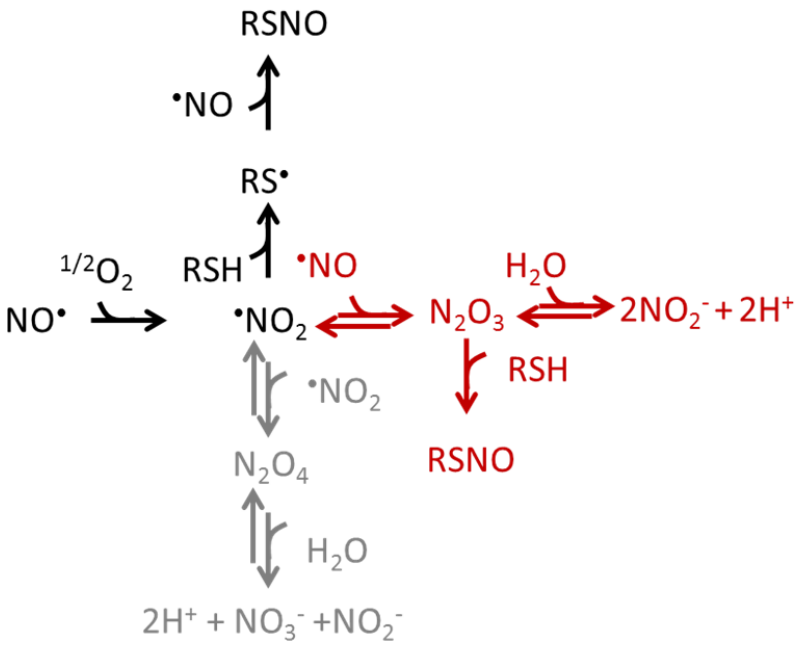

Figure 27. The reaction profile of NO· generated from NONOates.

The two most important reactions with NO_2· are with free thiols (black pathway) and free NO· (red pathway). The rate for NO_2· with free thiol (RSH) is ≥2×107 $M^{-1}s^{-1}$ [50,51]. For the reaction of NO_2· with NO· to form N_2O_3, the rate is 1.1×109 $M^{-1}s^{-1}$ [52,50]. While this reaction is readily reversible, the reaction kinetics *in vitro* will favor the nitrosation of thiols through the reaction N_2O_3 + RSH → RSNO (in red, rate of 1.2×107 $M^{-1}s^{-1}$, and an autohydrolysis rate with water of 4.75×107 s^{-1}). However, in an *in vivo* system, the pathway in black will likely be the major route of protein oxidation [13]. While the product of the pathway in red is identical to the pathway in black (free radical-mediated), the reactions involving thiyl radical species result in unique regulation in Ras family GTPase activity. The gray reaction pathway is less likely to occur because it relies on three bimolecular reactions (2(NO· + NO· → NO_2·) and NO_2· + NO_2 →N_2O_4), whereas the red and black pathways require only two bimolecular reactions.

Proteomics-based methodologies have recently been developed to study redox regulation in proteins, also known as the redoxome (*216, 217*). A number of stable isotope-labeling methods exist for measuring cysteine oxidation by MS. The majority of these methods fall into two main categories: 1) cysteine oxidation measured directly by comparing the loss of oxidized peptide as a function of oxidants by the relative signal intensities of cysteine-containing peptides labeled with light and heavy stable isotope reagents, such as ICAT, biotinylated-ICAT (*96, 218*), or biotinylated iodoactamide (BIAM) (*217*); 2) cysteine oxidation measured indirectly by thiol-blocking, selective reduction, and reversible modification using thiol probes that detect a gain in signal due to thiol oxidation (defined as oxICAT; see F**igure 30**) (*219*). In the context of measuring redox modifications, ICAT and other types of cysteine-reactive tags allow for the accurate quantification of cysteine-containing peptides (*220*). Here, we describe new techniques for detecting and quantifying cysteine oxidation using mass spectrometry-based methods, including 3.4.1: Isotope-coded affinity tag-labeling for relative cysteine quantification, 3.4.2: Quantification of the cysteine oxidation, 3.4.3: Differential quantification of cysteine oxidation, 3.4.4 Differential thiol trapping to
determine reversible oxidation of cysteine residues, and 3.4.5 Filter-aided sample preparation (see note 15).

3.4.1. Isotope-coded affinity tag (ICAT)-labeling for relative cysteine quantification

1: Generate proteins from cellular extracts and measure total protein using the bicinchoninic acid (BCA) assay.

2: Supplement the buffer with 0.1% sodium dodecyl sulfate (SDS) before modification with the ICAT reagents (see note 16).

3: Incubate the modified and unmodified samples at 37°C with the acid-cleavable ^{12}C (light) or ^{13}C (heavy) ICAT reagents in the absence of reducing agent using the protocol supplied by the manufacturer.

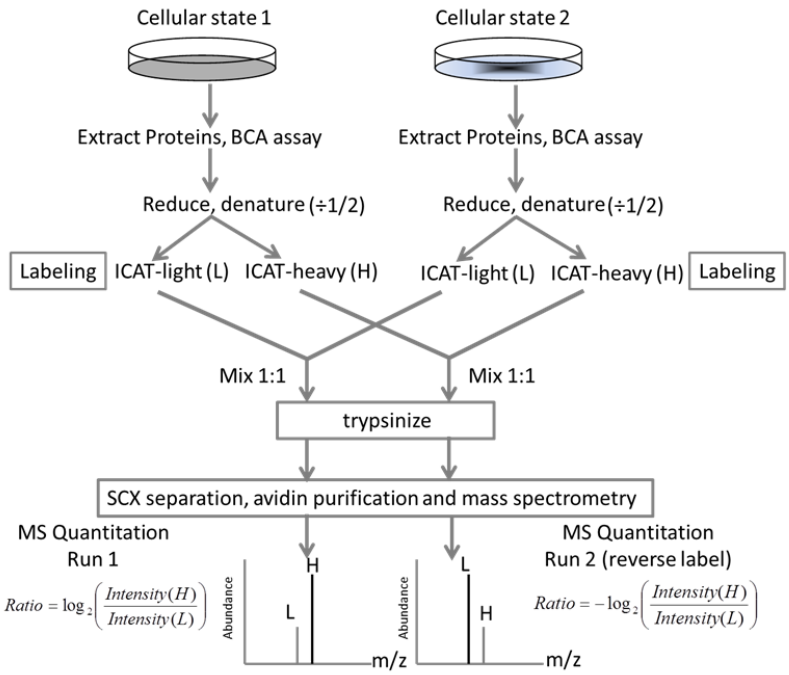

Figure 28. Generalized ICAT-based relative quantification schematic for measuring cysteine peptides.

ICAT allows for the relative quantification of samples from two separate conditions, such as quantification of protein expression levels under different cellular conditions. However, if one omits the reducing steps and adds an oxidation step to one of the conditions, then this approach can be adapted to study oxidation of proteins in cellular tissue (described in detail in the acid-cleavable ICAT with H_2O_2 approach). Each sample can be subjected to a technical replicate by reverse labeling to ensure reproducibility. Furthermore, ICAT reagents can be swapped out for other stable isotope labeled tags, such as BIAM or Cys-tandem mass tag reagents. Figure generated by Harsha Gunawardena.

4: After 2 h of incubation, mix the light and heavy ICAT-labeled protein samples at a stoichiometric ratio of 1:1, and trypsin digest the mixture by incubating at 37°C overnight in ABC buffer.

5: Purify the trypsin-digested peptides using a cation-exchange cartridge to remove excess labeling reagent. The desalted peptides are affinity purified using the avidin affinity cartridge. Dry the peptides and suspend in the cleavage reagent to release the peptides from the acid-cleavable linker by incubating at 37°C for 2 h. Dry the acid-cleaved peptides and suspend in 0.1% formic acid for LC-MS analysis (see note 17, see note 18 for data analysis, see notes 19 and 20 for alternative approaches).

3.4.2 Quantification of the cysteine oxidation

The biotinylated iodoacetamide (BIAM) approach can be used to study oxidation of exposed cysteines under controlled redox conditions by quantifying differential BIAM labeling. The redox chemistry includes the reversible oxidation of cysteine residues by the addition of H_2O_2 or other oxidants as well as reduction with reducing agents to reduce oxidized cysteines.

1: Generate oxidized proteins.

2: Dissolve the proteins in ABC buffer containing 5 mM iodoacetamide (IAM) and incubate at room temperature in the dark for 30 min to complete the modification of accessible Cys residues with IAM.

3: Centrifuge the samples at 15,000×g for 1 h, dialyze the supernatant against phosphate buffer and divide the sample into two equal parts.

4: Dilute the two equal samples to 5 ml with phosphate buffer.

5: Add 250 μl of 100 mM DTT. Similarly, incubate the second control sample with 250 μl phosphate buffer.

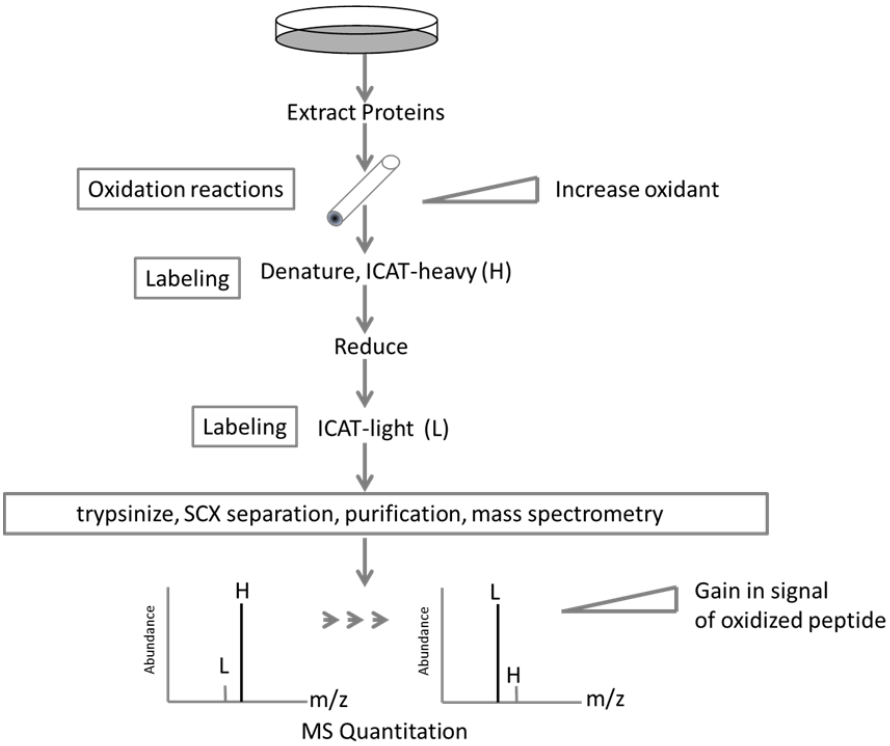

Figure 29. The oxICAT schematic for measuring cysteine oxidation.

This method measures reversible cysteine oxidation. Here, the protein is denatured and labeled in one step, which labels all non-oxidized and buried cysteines with the heavy label, and is completed by reducing the oxidized species and labeling with the light isotope. Thus, if several experiments are performed by varying levels of oxidant exposure, one can estimate the level of oxidation (relative reactivity) of cysteines in a protein. A gain in signal intensity of the light-isotope labeled signal is an indirect measure of reversible thiol oxidation. Note that a technical or biological replicate analysis can be performed by reversing the order of the ICAT labels with the heavy isotope representing the oxidized species. Figure generated by Harsha Gunwardena.

6: Incubate both samples at room temperature for 30 min and treat with 275 µl of 10 mM BIAM for 30 min in the dark at room temperature. Remove excess BIAM by overnight dialysis against ABC buffer.

7: Load the sample on an avidin affinity cartridge followed by incubation for 20 min at room temperature.

8: Wash the column with 1-4 volumes of PBS, collect the flow-through, and wash the column further with PBS until the absorbance at 280 nm returns to baseline.

9: Elute the BIAM-modified proteins with four bed volumes of BIAM-elution buffer.

10: Trypsin-digest the proteins overnight at 37°C. Purify peptides using a PepClean desalting column according to the manufacturer's protocol and analyze the peptides by LC-MS analysis.

3.4.3 Differential quantification of cysteine oxidation

1: Incubate oxidized and reduced protein samples (200 µg) in 100 µL of Tris buffer with light and heavy acid-cleavable ICAT reagents, respectively, at 37°C for 3 h in the absence of reducing agents.

2: Volumetrically mix the light and heavy labeled proteins at a 1:1 ratio and buffer exchange the samples against ABC buffer.

3: Digest the samples with trypsin by overnight incubation at 37°C.

4: Lyophilize the digested peptides and suspend in either affinity loading buffer for direct avidin affinity purification or fractionate by reconstituting the dried peptides in SCX Buffer A.

5: Fractionate the peptides using HPLC and a strong cation-exchange (SCX) PolySulfoethyl A column with a step gradient of SCX Buffer A to SCX Buffer B.

6: Mix the individual fractions from SCX with equivalent amounts of affinity loading buffer and load onto an avidin affinity cartridge. Dry the avidin-affinity purified peptides

using a lyophilizer and suspend in the cleavage reagent to release the ICAT-labeled peptides from the acid-cleavable linker by incubating at 37°C for 2 h.

7: Dry the peptides obtained by acid cleavage and suspend in 0.1% formic acid for LC-MS/MS analyses.

3.4.4 Differential thiol trapping to determine reversible oxidation of cysteine residues

1: After purifying the oxidized protein sample, precipitate the protein with 10% trichloroacetic acid (TCA).

2: Centrifuge the TCA precipitates (13,000×g, 4°C, 30 min) and wash the pellet with 500 µL of ice-cold 10% TCA and 200 µL of ice-cold 5% TCA.

3: Dissolve the pellet in 80 µL of denaturing alkylation buffer (DAB) and the contents of one vial of cleavable heavy ICAT reagent dissolved in 20 ul of ACN.

4: Incubate the sample at 900 rpm for 1 h at 37°C in the dark. To remove the light ICAT reagent, precipitate the proteins with 400 µL of chilled (20°C) acetone for 4 h at 20°C. After centrifugation (13,000×g, 4°C, 30 min), wash the pellet twice with 500 µL of chilled acetone.

5: Dissolve the protein pellet in a mixture of 80 µL of DAB, 1 µL of 100 mM DTT, or other selected reducing agents.

6: Add the contents of one vial of cleavable light ICAT reagent dissolved in 20 µL of ACN.

7: Incubate the sample at 900 rpm for 1 h at 37°C in the dark.

8: Perform trypsin-digestion of the ICAT-labeled peptides, enrichment on streptavidin columns, and cleavage of the biotin tag according to the description in Sections 3.4.1 and 3.4.2.

9: Subject the sample to LC-MS/MS analysis.

3.4.5 Filter-aided sample preparation (FASP)

There are two major strategies for converting proteins extracted from biological material to generating peptides suitable for MS-based proteome analysis: SDS-PAGE separation and in-gel digestion, or in-solution digestion. The SDS-PAGE separation method reduces sample complexity by removing sample contaminants, such as detergents, salts, DNA, and other non-protein compounds. The in-gel digestion approach is generally less efficient compared to in-solution digestion; however, when sample amounts are not limiting, this technique has shown wider usage amongst biologists for generating peptides. More recently, the filter-aided sample preparation (FASP) method, has been introduced as it removes high levels of salts, SDS, and other contaminants prior to in-solution digestion (*221-224*). In the FASP protocol, all protein clean-up steps, enrichment, and tryptic digestions are performed in a single micro-concentrator/spin-filter device. The technique can be quite useful for performing fast sample clean-up of *in vitro*-purified proteins where no further separation is required.

1: Mix 30 µl of sample with 200 µl of denaturing buffer in a YM10 or YM30 (depending on protein size) spin column and centrifuge for 15 min at 14,000×g.

2: Add an additional 200 µl of denaturing buffer to a YM10 or YM30 spin column and centrifuge for 15 min at 14,000×g (see note 21).

3: Discard the flow-through.

4: Add 100 µl of IAM buffer and mix on a shaker at 600 rpm for 1 min.

5: Incubate for 20 min at 25°C (see note 22).

6: Centrifuge for 10 min at 14,000×g.

7: Add 100 µl of denaturing buffer to the spin column and spin for 15 min at 14,000×g. Repeat this step two additional times.

8: Add 100 µl of ABC buffer and spin as in step 7. Repeat this step two additional times.

9: Add 16 µl of 0.1 µg/µl trypsin solution (trypsin should be diluted with ABC buffer) to the micro-concentrator/spin-filter device (see note 23 for an alternative approach).

10: Remove old collection tubes from the spin column and replace with fresh collection tubes before centrifuging for 10 min at 14,000×g.

11: Add 40 µl of ABC buffer and centrifuge for 10 min at 14,000×g to collect peptides.

Notes

Note 1: pH 6.5 was selected because low pH values help maintain cysteine residues in the thiol (RSH) state. Higher pH buffers (> 8.0) allow cysteines to populate the thiolate (RS^-) state, which makes them more susceptible to air oxidation.

Note 2: To modify proteins with redox-active reagents, it is important that the thiol moieties of the protein be in the reduced state. ABD-F will not react with oxidized cysteines and will result in reduced fluorescence yield. Further, oxidation of a thiol to sulfenic acid (RSOH) can result in disulfide bond formation. Thus, disulfide bonds and further oxidation states can readily occur when the protein is in the sulfenic acid state regardless of the thiol pK_a. If the protein is in the sulfinic (RSO_2H) or sulfonic (RSO_3H) state, the protein cannot be reduced and will be less reactive to ROS and RNS. By maintaining the protein in a reduced state, the reactivity will be dependent on the thiol/thiolate state of the protein.

Note 3: DTT works most efficiently at pH values greater than 8.0. This is because the reducing agent is effective when one of the thiol moieties is in the thiolate form. The pK_a of the DTT thiols are ~9.2 and 10.1 (*225*). Mercaptoethanol (β-ME) is not optimal as it can stably modify thiols, which will reduce reactivity with ABD-F. Tris(2-carboxyethyl)phosphine (TCEP), which is a phosphine reducing agent, appears to be efficient at reducing disulfides; however, other oxidation states, such as sulfenic acid (RSOH), are not efficiently reduced by TCEP according to our observations. A new reducing agent, dithiobutylamine (DTBA), functions similarly to DTT and has a thiol pK_a that is approximately one unit lower (*226*), which increases the reactivity of DTBA at physiological

pH values. However, this reducing agent needs to be generated in house and is currently unavailable for purchase.

Note 4: The buffer should have all oxygen removed as this will aid in preventing air oxidation over time, especially when studying thiols with altered pK_a values, as the thiolate (RS^-) is more reactive than a thiol (RSH).

Note 5: ABD-F reacts with free thiols in solution. Thus, reducing agents that act through a free thiol (e.g., DTT, β-ME, and DTBA) will generate fluorescence signal (false reactivity) and interfere with pK_a measurements. Therefore, these reagents cannot be present during data collection.

Note 6: A final concentration of 10 μM protein is sufficient to give a good signal-to-noise ratio for most proteins. In general, a 100:1 ABD-F:protein ratio is sufficient.

Note 7: Although the curve fitting approach outlined quantifies the initial linear slopes, collecting data at longer times will aid in verifying whether equivalent amounts of protein and ABD-F were added to each well. **See Figure 27A**.

Note 8: This method is most effective when using a protein that only has one solvent accessible cysteine because the reactivity of other cysteines will complicate data analysis.

Note 9: If the protein of interest contains multiple solvent accessible cysteines, the assay can be modified to determine whether the protein has a cysteine with an altered pK_a. Using a substitution mutant of the suspected redox-sensitive cysteine (Cys-to-Ser (or Ala) mutation), perform the assay essentially as described but at one pH value (pH 6.5 is recommended such that non-redox-sensitive cysteines that do not have altered pK_a values do not result in high background signal). Thus, the cysteine mutant serves as a control and provides the background level of ABD-F modification in the protein.

Note 10: As reported in Grossi et al (*211*), the pH of the reaction is critical for generating optimum nitroso-thiol content; therefore, after solution I and II are mixed, the solution pH should be approximately 1.7 to 2.0.

Note 11: In general, any volume and concentration of nitroso-thiol is possible. The protocol explained in detail here is scaled to meet the needs of our experiments. Thus, this protocol will yield approximately 1100 µl of 8 mM thiol-NO.

Note 12: An alternative is to use the Saville Assay (*227*) to measure thiol-NO concentration. However, this assay detects NO_2^- as well as the thiol-NO, which could lead to error if the free NO_2^- in solution has not been reacted with the thiol or sulfamate. In our experience, the absorbance at 336 nm is reliable.

Note 13: An inherent disadvantage to using NONOates is that they generate NO·. In the case of Ras, NO_2· is required for thiyl radical production. However, NO· can react with O_2 to form NO_2· as well as other reaction products. A further disadvantage is that once NO_2· is generated, it can react with NO· released by the NONOate to produce other reaction products. A common reaction product is N_2O_3, which can nitrosate cysteines at an approximate rate of 1.2×10^7 $M^{-1}s^{-1}$ (**Figure 28**) (*228*). In Ras reactions with DEA NONOate, we observed that only a fraction of Ras reacts with NO_2· to induce nucleotide dissociation, and a sizable fraction of Ras can be nitrostated by N_2O_3. However, nitrosation of Ras through a non-radical pathway does not alter Ras activity (*66, 229*). Modification by N_2O_3 is only likely under the reaction conditions used *in vitro* with purified proteins; however, in cells, this oxidation pathway is not favored.

Note 14: One can verify the dependence of the NO· species generated on protein activity when using NONOates by adding in PTIO (2-Phenyl-4,4,5,5-tetramethylimidazoline-1-oxyl 3-oxide), which is a selective NO· scavenger. This control will allow the user to verify whether free radical byproducts cause the observed effects, as opposed to a competing reaction with the NONOate breakdown products.

Note 15: All of the strategies described in 3.4 rely on the loss of the analytical signal upon cysteine modification (oxidation). Most cysteine residues are maintained in their

reduced state in cells, measuring glutathiolation directly using chemical labeling significantly impacts the sensitivity and dynamic range of (oxidation) detection.

Note 16: Buffers with low concentrations of SDS or urea allow for more complete labeling of the unfolded protein by the ICAT reagents.

Note 17: All buffers should be prepared in HPLC grade water for optimum performance. All reversed-phase LC-MS buffers should be prepared in LC-MS grade water.

Note 18: All peptides containing cysteine residues will contain heavy and light pairs of ICAT labels, and their relative intensities are measured using a full MS scan. The relative intensity, ratio = [Lint/Hint], is used to determine the relative levels of modification.

Note 19: A similar strategy to ICAT has been demonstrated to measure cysteine oxidation due to $NO^{\cdot}$ through the use of light and heavy n-ethyldmaleimide (NEM) reagents that are generally used to protect sulfhydryls. We believe that this strategy could be adapted to study glutathiolation as well because the ICAT reagents can be easily replaced by NEM and d5-NEM. More recently, other stable isotope labeling reagents have become available, such as Cys-TMT. The use of Cys-TMT allows for an analytical workflow to quantitatively assay free cysteine residues and determine the extent of modification using six biologically distinct conditions in a single mass spectrometry experiment. The multiplexing is particularly useful for studies involving time-course measurements.

Note 20: An alternative strategy compared to the methods described in Section 3.4 is to introduce a reduction step to remove reversible cysteine modifications. Protein modifications can be measured indirectly by the following steps: 1) Alkylation of free sulfhydryl groups on cysteine residues. 2) Reduction of glutathione adducts by glutaredoxin (Grx), which does not affect other cysteine modifications. 3) Blocking all nascent sulfhydryl groups with an irreversible labeling reagent, such as IAM or NEM. The advantage of this method is that glutathione-specific cysteines will be quantitatively assayed. This methodology is more sensitive due to a net increase in the analytical signal for measuring

glutathiolation, which is advantageous because most cysteine residues have low levels of glutathiolation in cells.

Note 21: A YM30 filter (MW cut-off of 30 kDa) is used to improve filtration speeds, whereas denaturants assist on-filter retention of proteins less than 30 kDa. However, the use of YM10 filters would be a conservative approach for ensuring the retention of lower molecular weight proteins/polypeptides (approximately 5-8 kDa range).

Note 22: As we are studying cysteine oxidation in the sample prior to alkylation, the reducing step is omitted. Alkylation is performed to prevent disulfide exchange from scrambling the oxidative modifications to other cysteine residues that are exposed upon trypsin digest.

Note 23: Incubate overnight at 37°C or incubate for 1-5 minutes using microwave irradiation as described in the GOFAST method (*230*). An alternative approach uses endoprotease Lys-C (1:100 enzyme:protein ratio) for 4 h at 37°C prior to trypsin digestion to improve the overall peptide digestion efficiency.

Chapter 7: Magnesium coordination of RhoG

Introduction

The Ras superfamily of GTPases consists of over 200 members and are categorized into five subclasses on the basis of sequence: Ras, Rho, Rab, Sar1/Arf, and Ran (*86, 145-147, 150*). These GTPases are present in all eukaryotes and possess 30-55% sequence homology within the family (*84*). Ras superfamily GTPases serve as molecular switches that regulate cellular processes by cycling between the inactive GDP-bound and active GTP-bound conformers (*65, 89, 145, 149, 150*). The structural changes that result from GDP/GTP cycling are localized within two regions, switch I (residues 30-38) and switch II (residues 59-67), with the GTP-bound conformer binding to its downstream effectors with higher affinity (*231, 232*). The rate limiting step in guanine nucleotide cycling is nucleotide hydrolysis.

Rho GTPases regulate pathways involved in cell growth, differentiation, cell death, cell morphology, and cell motility (*145, 147, 158, 161, 233, 234*). Most studies to date have focused on Rac1, RhoA, and Cdc42. Protein modulatory factors regulate the activity of GTPases, including guanine nucleotide exchange factors (GEFs) that induce nucleotide dissociation by disrupting Mg^{2+} and guanine nucleotide coordination (*87, 235, 236*) and GTPase activating proteins (GAPs) that inactivate the GTPases by catalyzing the hydrolysis of the γ-phosphate of GTP.

Rho GTPase activity has been shown to be deregulated in human cancer. However, unlike Ras, which is frequently mutated in human cancers, deregulation of Rho GTPases occurs through changes in the expression levels of the GTPases, GEFs, GAPs, and guanine dissociation inhibitors (GDIs). Furthermore, overexpression of RhoG and Rac1 has been observed in malignant breast cancers (*237*). GEFs, which activate Rho GTPases, are often

upregulated, whereas GAPs, which negatively regulate GTPase activity, are often downregulated in invasive tumors. In addition, GDIs, which sequester Rho GTPases and prevent their activation, have been shown to be deregulated in many cancers, which leads to GTPase upregulation (*238*).

Magnesium levels have also been shown to regulate cell proliferation and apoptosis. Mg^{2+} serves two important roles in GTPases, it is a cofactor with guanine nucleotides that helps to stabilize the negative charge of the phosphates of GTP/GDP in the binding pocket and plays a role in GTP hydrolysis. Notably, Mg^{2+} depletion has been linked to carcinogenesis and increased metastasis in cancer (*239*).

Interestingly, RhoG has been shown to signal both in a series or in parallel (*240, 241*) with Rac1. Thus, these studies have shown that RhoG activates Rac1 (in series) or can activate Rac1-specific pathways in the absence of Rac1 (in parallel). Our data suggest that Lys^{30} of RhoG (Gly^{30} in Rac1) may play a critical role in determining how RhoG signals. Depending on the orientation of Lys^{30} in RhoG, it may be possible for RhoG to 'switch' between its known effectors and Rac1 effectors simply by burying the lysine in the absence of bound Mg^{2+}.

This hypothesis is supported by in-cell data where the constitutively active Rac1 mutant, $Rac1^{Q61L}$, induced transformation in NIH3T3 cells (*242*); however, the constitutively active $RhoG^{Q61L}$ mutant did not lead to transformation. Furthermore, $Rac1^{G30K}$ in NIH3T3 cells reduced the transforming ability of Rac1 by 15-fold, and the $RhoG^{K30G/Q61L}$ variant increased the transforming potential of RhoG in NIH3T3 cells to similar levels as $Rac1^{Q61L}$ (*242*). These data indicate that residue 30 plays a key role in the recognition of regulatory factors and/or effectors. Thus, we have preliminary data that examines the role of Lys^{30} in RhoG in nucleotide exchange and have compared our data to $Rac1^{WT}$. Here, we have shown that Lys^{30} plays a unique role in nucleotide binding in RhoG and may stabilize nucleotide binding in the absence of Mg^{2+}.

Methods

Protein purification of RhoG

The truncated form of the human RhoG gene ($RhoG^{1-177}$) was cloned into the pQlinkH vector. The hyper-variable region of RhoG, including the C-terminal CAAX box, was removed as this region does not undergo post-translational lipid modification in bacteria, is unstructured, and its removal does not affect nucleotide binding or GTP hydrolysis (*243*). All proteins were expressed in BL21 Rosetta 2 cells and purified following the Qiagen Nickel NTA purification protocol (Germantown, MD). RhoG was further purified by size exclusion chromatography (Superdex-75 10/300 GL column; GE Life Sciences; Piscataway, NJ) and judged greater than 95% pure by SDS-PAGE analysis.

Nucleotide exchange assays

The rate of GDP dissociation from Ras was measured using 2'-/3'-O-(N'-methylanthraniloyl)guanosine-5'-O-diphosphate (^{mant}GDP) as previously reported (*108, 109*). One micromolar RhoG or RhoG variant loaded with ^{mant}GDP (BioLog; San Diego, CA) was added to 1 mL of degassed assay buffer (50 mM Tris pH 7.4, 50 mM NaCl, 5 mM $MgCl_2$, 2 mM GDP, and 100 μM diethylenetriaminepentaacetic dianhydride; DTPA), and the rate of guanine nucleotide dissociation was measured by monitoring the change in fluorescence (excitation: 365 nm; emission: 435 nm; 25˚C) over time using a Perkin Elmer LS50B fluorimeter (Waltham, MA). All experiments were performed in triplicate. Fluorescent nucleotide dissociation curves were fit to a one-phase exponential decay equation using GraphPad Prism version 3.03 (GraphPad Software; San Diego, CA). For GEF-induced RhoG-GDP dissociation assays, the minimal catalytic domain of Vav2 was used at a 1:1 ratio (*244*). This concentration of Vav2 was selected as the rate enhancement of nucleotide exchange was easy to measure using fluorimetric assays and other labs have published using the GEF at

this concentration. EDTA-induced nucleotide dissociation was performed by adding 25 mM EDTA to the reaction cuvette at the indicated time point.

Results

We have conducted fluorescence-based nucleotide dissociation assays with Rac1, RhoG, and RhoG variants. Our preliminary data, shown in **Figure 31,** reveals that the $RhoG^{WT}$ (red curve) nucleotide dissociation rate is much slower compared to the rate of Rac1 (blue curve) nucleotide exchange.

To determine the role of Lys^{30} in guanine nucleotide exchange and GEF specificity, we have employed nucleotide exchange assays for the direct measurement of nucleotide dissociation in the presence and absence of a catalytic fragment from the GEF Vav2, which is shown in **Figure 31B**. We observed that by making a single mutation in RhoG, $RhoG^{K30G}$ (green curve), we were able to increase the activation of RhoG by Vav2 (**Figure 31B)**.

The $RhoG^{K30G}$ mutation, which makes RhoG more Rac1-like, was constructed and nucleotide exchange was measured. The results (**Figure 31B** and **C)** indicated that $RhoG^{K30G}$ reacted nearly identically to Rac1 GEF-mediated nucleotide exchange with Vav2, a Rac1-specific GEF, and in EDTA-mediated nucleotide exchange. This data suggests that residue 30 in Rho family GTPases plays a role in modulating Vav2 specificity and activity.

EDTA was used to remove Mg^{2+} from RhoG. Most GTPases show nucleotide dissociation on the addition of EDTA, which reflects a reduction in the nucleotide binding affinity. However, on the addition of EDTA to RhoG, we observed a transient increase in fluorescence, followed by slow nucleotide dissociation. The results, shown in **Figure 31C,** suggest that there was a change in the chemical environment around the MANT moiety on nucleotide binding, which was indicated by the transient fluorescence increase, and that RhoG binds nucleotide even in Mg^{2+}-null situations. However, this effect was ablated when

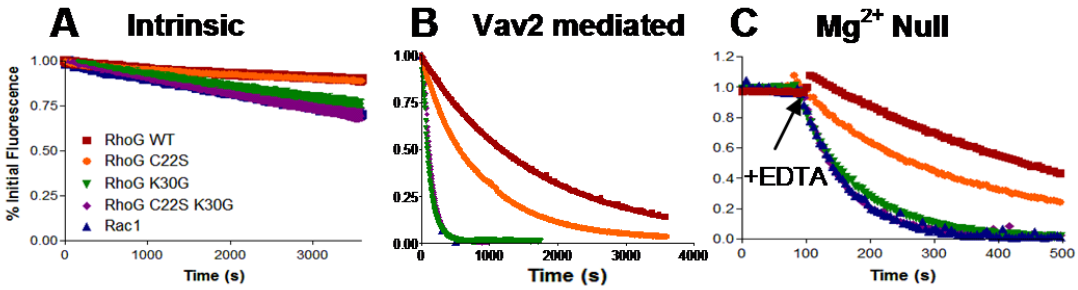

Figure 30. Nucleotide dissociation of RhoG and Rac1.

The nucleotide dissociation studies were performed by preloading the GTPase with the fluorescent GDP analog, ^{mant}GDP, which has a greater fluorescence when bound to a protein than when free in solution, and the rate of dissociation was measured by detecting the loss of signal intensity as ^{mant}GDP dissociates. Fluorescent nucleotide dissociation studies were performed on RhoG, RhoG variants, and Rac1 as shown by the figure legend. (A) Intrinsic nucleotide dissociation was determined in a buffer containing 5 mM $MgCl_2$, 2 mM non-labeled GDP, and 1 µM protein. (B) Vav2 mediated dissociation was performed similarly to intrinsic, but with 1 µM Vav2 present. (C) EDTA data was collected in the same manner as (A), but with 25 mM EDTA present. All data was normalized to the maximal value and performed in quadruplicate. Note the change in time scale for (C).

we used the RhoG^{K30G} variant, suggesting that Lys^{30} plays a role in nucleotide binding under specific situations.

Discussion

RhoG shares the closest sequence homology (72% identity) with Rac1. However, while Rac1 induces the formation of lamellopodia, RhoG has been shown to promote dorsal ruffles (*240, 245*). In addition, Ellerbroek et al has observed that RhoG is activated by the GEF, SGEF, whereas Rac1 is not (*246*). In addition, RhoG has been shown to activate Rac1 through interaction with the GEF Dock/ELMO (*245*). In contrast to these studies that have suggested independent pathways for RhoG and Rac1, RhoG has also been shown to activate Rac1-specific pathways in cells where Rac1 expression has been silenced. Our data suggest that RhoG may be able to perform these functions by regulating Mg^{2+} coordination and the position of Lys^{30}.

Recent studies have indicated that RhoG recognizes its unique modulatory proteins in part through Lys^{30} of switch I (*242, 247*). Sequence alignments of RhoG and Rac1 show that there are two residues in the p-loop and switch I regions of RhoG and Rac1 that are different, Cys^{22} and Lys^{30} (RhoG numbering). Therefore, we mutated these two residues to match the Rac1 sequence (RhoG^{C22S} and RhoG^{K30G}) individually and together and observed that the response to Vav2 of RhoG increased to match the rates observed for Rac1. By preloading RhoG and RhoG variants with ^{MANT}GDP, we observed that RhoG had a slower nucleotide dissociation rate compared to Rac1 (**Figure 31A**). Further, we noticed differential reactivity to the Rho GEF Vav2 (**Figure 31B**). In addition, the observed effects were primarily mediated through Lys^{30}. Thus, as lysine has a positive charge, we postulated that Mg^{2+} binding may be altered. To determine the role of Mg^{2+} binding and nucleotide dissociation, we preloaded RhoG with ^{MANT}GDP and measured nucleotide dissociation in the presence of EDTA (**Figure 31C**). We observed that Lys^{30} altered the effect of sequestering Mg^{2+} with EDTA. Thus, with RhoG, we observed a transient increase in fluorescence before a slow rate

of nucleotide dissociation; however, in the RhoG^{K30G} variant, we observed no increase in fluorescence and a rate of nucleotide dissociation that mirrored Rac1. Therefore, this data suggests that Lys^{30} of RhoG plays a unique role in nucleotide binding, and the altered position of this residue upon loss of Mg^{2+} binding may result in RhoG interacting with Rac1-specific effectors.

A structural comparison of Rac1^{GTP} and Rac1^{GDP} is presented in **Figure 32A**. Differences between active GTP-bound and inactive GDP-bound Rac1 are primarily located within switch I and II. These structural changes underlie differences in recognition of downstream effectors and GAPs, which bind with preferential affinity to the GTP-bound form. RhoG is the only Rho family GTPase that contains a lysine in switch I (*248*). The homologous residue in Rac1, Gly^{30}, is important for binding to the Rac1-specific effector, p67 of NADPH oxidase, through a backbone hydrogen bond (**Figure 32B**) (*249*). Glycine^{30} interacts with p67 through a backbone amide. As RhoG contains a lysine at this position, RhoG likely has a reduced affinity for p67 oxidase. However, in the absence of bound Mg^{2+}, the lysine side chain may reorient towards the p-loop and promote an interaction between RhoG and p67. Therefore, Lys^{30} may contribute to the different specificity of GEFs, GAPs, and effectors that interact with RhoG and Rac1.

In addition, reactive oxygen species (ROS) are also involved in oncogenesis (*250*). Intriguingly, a subset of Ras superfamily GTPases have been shown to be activated by ROS and RNS (*69, 80*). RhoG has been connected to the production of ROS through the activation of Rac1 (*240, 246, 247, 251*), which regulates NADPH oxidase activity (*252, 253*). RhoG has also been shown to regulate NADPH oxidase activation in neutrophils (*254*). Thus, RhoG activity may be affected by both Mg^{2+} levels and ROS levels, two things that are known to be altered in the tumor environment. Thus, another question that remains unanswered in RhoG function is its sensitivity towards oxidants.

Based on our nucleotide dissociation results (**Figure 31**), we hypothesize that Lys^{30} in

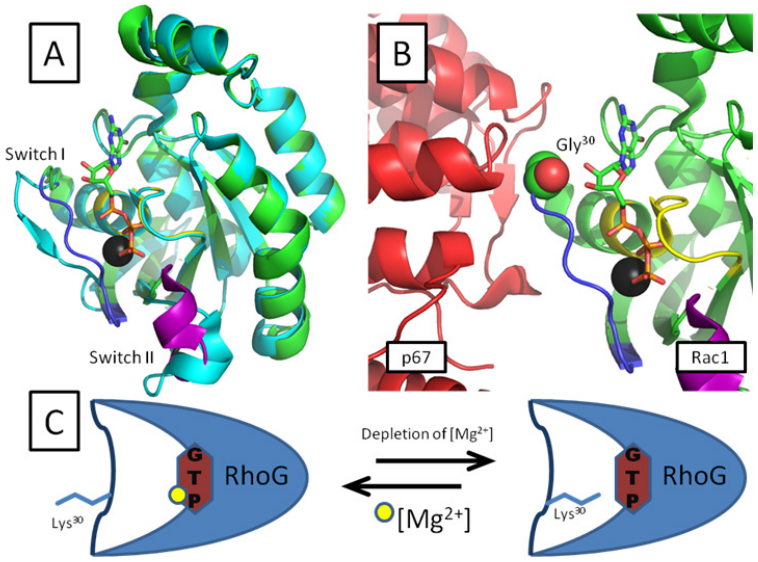

Figure 31. A model of the RhoG lysine switch hypothesis.

(A) Overlay of $Rac1^{GTP}$ (green; PDB ID: 1E96) and $Rac1^{GDP}$ (cyan; PDB ID: 2P2L) structures with Mg^{2+} shown in black, and GTP shown as a stick representation and color coded by atom (O-red, N-blue, C-green, and P-orange). Switch I of Rac1GTP is colored blue, switch II is colored purple, and the p-loop is colored yellow to highlight these regions. The major changes within the two structures are located within switch I and switch II. (B) The tetratrico-peptide repeat (TPR) domain of p67, a subunit of NADPH oxidase (red), bound to Rac1 (green) with Gly30 shown as spheres. Switch I is colored blue, switch II is purple, and the p-loop is shown in yellow. Activated GTP-bound Rac1 binds to effectors with higher affinity than the GDP-bound state. Rac1 residues important for effector recognition are Ser^{22}, Asn^{26}, Gly^{30}, and Gln^{162}. In RhoG, two of these residues are substituted, S22C and G30K, and only the latter comprises a non-conservative substitution. Gly^{30} plays a significant role in effector recognition for Rac1. (C) We propose that Lys^{30} is normally solvent accessible and plays a role in RhoG-specific effector recognition. However, Lys^{30} may be able to replace Mg^{2+} and simulate a GTP-like conformation. As the rest of this binding interface is virtually unchanged, we hypothesize that RhoG may be able to bind to and activate Rac1 effectors under certain cellular conditions.

RhoG reorientates upon dissociation of Mg^{2+}. Moreover, as highlighted in **Figure 32C**, we further propose that this interaction may stabilize nucleotide binding in the absence of Mg^{2+}. Future studies to determine the structure of RhoG should aid in understanding the role of Lys^{30} in RhoG. In addition, effector binding studies in the presence and absence of Mg^{2+} should be performed. If effector binding in the absence of bound Mg^{2+} but not in the presence of Mg^{2+} is observed, then these results would provide an explanation for previously published reports where RhoG was able to independently activate Rac1-specific pathways. As Mg^{2+} depletion is tied to reactive oxygen species (ROS) production in the cell, and both of these cellular agents have been connected to deregulated growth, understanding the connections between RhoG and the expression of its regulatory proteins, Mg^{2+}, and ROS will provide new direction and drug targets in cancer research.

Chapter 8: Conclusions and future directions

While our studies on Ras GTPases has answered some pertinent questions in the field, questions remain regarding the role of the thiol in RasG12C-driven cancers. In this study, we have shown that role of glutathiolation in Ras is merely a consequence of free radical-mediated oxidation at Cys^{118}. This project was needed in the Ras oxidation field as many papers had stated that glutathiolation activated Ras (*71, 77, 94, 100, 101*). Thus, by generating glutathiolated Ras, we were able to show definitively that glutathiolation has no effect on exchange, hydrolysis, or the structure. Thus, our data suggested that the activation of glutathiolated Ras that has been previously detected was due to the presence of free radicals in their assays.

Furthermore, we were also able to build on previous studies of Ras ubiquitination. After a study by Baker et al (*15*), which showed that loss of GAP responsiveness in mUbRas was due to ubiquitin modification at position 147, it was unclear as to whether ubiquitin itself was important for GAP function or whether any modification would suffice. Thus, using a Ras^{K147C} variant, we oxidized Ras and modified the protein specifically at position 147. We showed that small molecule modifications, such as acetylation and glutathiolation, do not impair GAP activity on Ras. Taking the study a step further, we showed that there appears to be a minimal linker length (between ubiquitin and Ras) that is critical for inhibiting Ras sensitivity to GAPs. While this study made strides toward understanding how this modification regulates Ras, it left unanswered whether the linker length could be longer than the minimal size that was determined and whether the size of the modification was

required to be approximately 8 kDa. Thus, moving forward, these will be key questions to answer.

In yet another study involving thiols in Ras, the Ras^{G12C} oncogenic mutant has shown that part of its unique phenotype may be due to the presence of a thiol in the p-loop. The Ras^{G12C} mutant has been shown to be a common mutation in lung cancer. Our objective is to determine how this residue participates in Ras activity and use the resulting data to determine whether Ras^{G12C}, or other position 12 mutants, can be selectively inhibited. Thus, we are currently working in collaboration with Chris Counter to determine how oxidation of Ras^{G12C} can alternatively regulate Ras activity. Toward this end, we have characterized the mutant Ras^{G12C} and shown that this thiol is redox sensitive in addition to being GAP insensitive. As the Counter laboratory has shown Ras regulation by eNOS through Cys^{118}, his lab is perfectly equipped to aid in answering how similar pathways might regulate Ras^{G12C} in oncogenic settings.

While Rho family GTPases have been shown to be regulated by redox agents in *in vitro* systems, there is less evidence for direct modification of these GTPases in cell and animal models. However, Rho GTPases regulate pathways that have been shown to be directly regulated by the cellular redox state. Future studies need to determine the effects of direct oxidation of Rho GTPases in an *in vitro* context to allow for a clearer understanding of the cellular effects. Further, future cellular studies that observe redox-mediated regulation of these GTPases need to use redox-inactive variants to confirm the effects in cells. In addition, many of the current in cell studies have focused on exogenous oxidants, and more studies with endogenously produced oxidants are necessary to better characterize the how the Rho GTPases are regulated by oxidation in vivo. While the study by Aghajanian et al (*81*) was one of the first such studies to show in-cell activation of RhoA due to exogenously and endogenously applied oxidants, these studies are scarce on other Rho family GTPases, and this remains the only study on RhoA to determine the effects of direct oxidation on RhoA in

cells where the redox-sensitive cysteine residues were mutated to a redox-insensitive variant.

However, increasing numbers of studies are showing that the Rho signaling pathways are involved in redox signaling, and it has been shown that Rac1 directly interacts with SOD and NADPH oxidase; therefore, it is likely that a majority of the Rho family GTPases can also be regulated by the redox signaling enzymes. As we have generated and characterized a new redox sensitive variant of RhoA, $RhoA^{C20S}$, that has similar nucleotide binding kinetics, nucleotide hydrolysis, and stability as $RhoA^{WT}$, future studies probing the role of the Rho signaling pathway will be greatly benefited by use of the $RhoA^{C20S}$ variant. In conclusion, in the cell, it is likely that activation of these GTPases occurs when they are modified by a free radical at Cys^{20} (or Cys^{18} in other Rho GTPases), which will result in nucleotide dissociation and GTP loading. However, this will result in the formation of a thiolate (RS^-) at the site of oxidation, which will have an increased sensitivity towards further oxidation to both one-electron and two-electron oxidation events, and the type of oxidation, such as nitrosation, glutathiolation, sulfenic, sulfinic, sulfonic acid, or disulfide formation in RhoA, will have differing effects on the level of activation observed.

Concluding thoughts

Herein, we discussed the importance of ROS/RNS in modulating the activity of select Ras and Rho GTPases and the role of these GTPases in controlling the expression and activity of ROS/RNS-regulating enzymes. In addition, our data and a growing body of literature suggest that Rho GTPases are particularly susceptible to redox control given their unique redox-sensitive cysteine-containing p-loop motif. This redox-sensitive cysteine interacts with the bound nucleotide, and $1e^-$ and $2e^-$ redox modifications at this cysteine enhance nucleotide exchange, likely by disrupting interactions with the bound nucleotide. Under physiological conditions, ROS/RNS likely activate Ras and Rho GTPases, whereas oxidative stress may promote their inactivation. To aid in discerning whether oxidative

regulation of Rho GTPases is direct or indirect, we have identified redox-insensitive variants that mimic the wild-type proteins. Moreover, future cell-based studies should be performed with endogenous ROS/RNS sources, redox state characterization, and absent GTPase overexpression. Further, Rho and Ras subclasses also regulate expression and activity of key redox regulating enzymes. RhoA and Ras regulate NOS expression and activity, Rap1A has been implicated in Nox regulation. Rac controls NOS and Nox, and Rac1 has recently been shown to directly interact with SOD1. Given that Rac1 and SOD1 are ubiquitously expressed proteins involved in numerous cell functions, future experiments should be directed to discerning the mechanism of and effects from this interaction. Further, as the literature is increasingly dedicated to redox-based signaling, perhaps future studies will better define how ROS/RNS regulate Ras and Rho GTPase activity and whether these GTPases are regulated by or control additional redox-modulating enzymes.

REFERENCES

1. Keefer, L. K., Nims, R. W., Davies, K. M., and Wink, D. A. (1996) "NONOates" (1-substituted diazen-1-ium-1,2-diolates) as nitric oxide donors: convenient nitric oxide dosage forms, *Methods Enzymol 268*, 281-293.

2. Maragos, C. M., Morley, D., Wink, D. A., Dunams, T. M., Saavedra, J. E., Hoffman, A., Bove, A. A., Isaac, L., Hrabie, J. A., and Keefer, L. K. (1991) Complexes of .NO with nucleophiles as agents for the controlled biological release of nitric oxide. Vasorelaxant effects, *J Med Chem 34*, 3242-3247.

3. Maragos, C. M., Wang, J. M., Hrabie, J. A., Oppenheim, J. J., and Keefer, L. K. (1993) Nitric oxide/nucleophile complexes inhibit the in vitro proliferation of A375 melanoma cells via nitric oxide release, *Cancer Res 53*, 564-568.

4. Jaffe, A. B., and Hall, A. (2005) Rho GTPases: biochemistry and biology, *Annu Rev Cell Dev Biol 21*, 247-269.

5. Visvikis, O., Maddugoda, M. P., and Lemichez, E. (2010) Direct modifications of Rho proteins: deconstructing GTPase regulation, *Biol Cell 102*, 377-389.

6. Adamson, P., Marshall, C. J., Hall, A., and Tilbrook, P. A. (1992) Post-translational modifications of p21rho proteins, *J Biol Chem 267*, 20033-20038.

7. Adamson, P., Paterson, H. F., and Hall, A. (1992) Intracellular localization of the P21rho proteins, *J Cell Biol 119*, 617-627.

8. Bokoch, G. M., Bohl, B. P., and Chuang, T. H. (1994) Guanine nucleotide exchange regulates membrane translocation of Rac/Rho GTP-binding proteins, *J Biol Chem 269*, 31674-31679.

9. Johnson, J. L., Erickson, J. W., and Cerione, R. A. (2009) New insights into how the Rho guanine nucleotide dissociation inhibitor regulates the interaction of Cdc42 with membranes, *J Biol Chem 284*, 23860-23871.

10. Navarro-Lerida, I., Sanchez-Perales, S., Calvo, M., Rentero, C., Zheng, Y., Enrich, C., and Del Pozo, M. A. (2012) A palmitoylation switch mechanism regulates Rac1 function and membrane organization, *Embo J 31*, 534-551.

11. Ellerbroek, S. M., Wennerberg, K., and Burridge, K. (2003) Serine phosphorylation negatively regulates RhoA in vivo, *J Biol Chem 278*, 19023-19031.

12. Forget, M. A., Desrosiers, R. R., Gingras, D., and Beliveau, R. (2002) Phosphorylation states of Cdc42 and RhoA regulate their interactions with Rho GDP dissociation inhibitor and their extraction from biological membranes, *Biochem J 361*, 243-254.

13. de la Vega, M., Burrows, J. F., and Johnston, J. A. (2011) Ubiquitination: Added complexity in Ras and Rho family GTPase function, *Small GTPases 2*, 192-201.

14. Sadowski, M., Suryadinata, R., Tan, A. R., Roesley, S. N., and Sarcevic, B. (2012) Protein monoubiquitination and polyubiquitination generate structural diversity to control distinct biological processes, *IUBMB Life 64*, 136-142.

15. Baker, R., Lewis, S. M., Sasaki, A. T., Wilkerson, E. M., Locasale, J. W., Cantley, L. C., Kuhlman,B., Dohlman, H. G., and Campbell, S. L. (2013) Site-specific monoubiquitination activates Ras by impeding GTPase-activating protein function, *Nat Struct Mol Biol 20*, 46-52.

16. Sasaki, A. T., Carracedo, A., Locasale, J. W., Anastasiou, D., Takeuchi, K., Kahoud, E. R., Haviv, S., Asara, J. M., Pandolfi, P. P., and Cantley, L. C. (2011) Ubiquitination of K-Ras enhances activation and facilitates binding to select downstream effectors, *Sci Signal 4*, ra13.

17. Nethe, M., and Hordijk, P. L. (2010) The role of ubiquitylation and degradation in RhoGTPase signalling, *J Cell Sci 123*, 4011-4018.

18. Nethe, M., Anthony, E. C., Fernandez-Borja, M., Dee, R., Geerts, D., Hensbergen, P. J., Deelder, A. M., Schmidt, G., and Hordijk, P. L. (2010) Focal-adhesion targeting links caveolin-1 to a Rac1-degradation pathway, *J Cell Sci 123*, 1948-1958.

19. Wei, J., Mialki, R. K., Dong, S., Khoo, A., Mallampalli, R. K., Zhao, Y., and Zhao, J. (2013) A new mechanism of RhoA ubiquitination and degradation: Roles of SCF E3 ligase and Erk2, *Biochim Biophys Acta*.

20. Visvikis, O., Lores, P., Boyer, L., Chardin, P., Lemichez, E., and Gacon, G. (2008) Activated Rac1, but not the tumorigenic variant Rac1b, is ubiquitinated on Lys 147 through a JNK-regulated process, *Febs J 275*, 386-396.

21. Lander, H. M., Hajjar, D. P., Hempstead, B. L., Mirza, U. A., Chait, B. T., Campbell, S., and Quilliam, L. A. (1997) A molecular redox switch on p21(ras). Structural basis for the nitric oxide-p21(ras) interaction, *J Biol Chem 272*, 4323-4326.

22. Thannickal, V. J., and Fanburg, B. L. (2000) Reactive oxygen species in cell signaling, *Am J Physiol Lung Cell Mol Physiol 279*, L1005-1028.

23. Ray, P. D., Huang, B. W., and Tsuji, Y. (2012) Reactive oxygen species (ROS) homeostasis and redox regulation in cellular signaling, *Cell Signal 24*, 981-990.

24. Forman, H. J., Fukuto, J. M., and Torres, M. (2004) Redox signaling: thiol chemistry defines which reactive oxygen and nitrogen species can act as second messengers, *Am J Physiol Cell Physiol 287*, C246-256.

25. Spadaro, D., Yun, B. W., Spoel, S. H., Chu, C., Wang, Y. Q., and Loake, G. J. (2010) The redox switch: dynamic regulation of protein function by cysteine modifications, *Physiol Plant 138*, 360-371.

26. Poole, L. B., Karplus, P. A., and Claiborne, A. (2004) Protein sulfenic acids in redox signaling, *Annu Rev Pharmacol Toxicol 44*, 325-347.

27. Winterbourn, C. C., and Hampton, M. B. (2008) Thiol chemistry and specificity in redox signaling, *Free Radic Biol Med 45*, 549-561.

28. Sanchez, R., Riddle, M., Woo, J., and Momand, J. (2008) Prediction of reversibly oxidized protein cysteine thiols using protein structure properties, *Protein Sci 17*, 473-481.

29. Trujillo, M., and Radi, R. (2002) Peroxynitrite reaction with the reduced and the oxidized forms of lipoic acid: new insights into the reaction of peroxynitrite with thiols, *Arch Biochem Biophys 397*, 91-98.

30. Barton, J. P., Packer, J. E., and Sims, R. J. (1973) Kinetics of Reaction of Hydrogen-Peroxide with Cysteine and Cysteamine, *J Chem Soc Perk T 2*, 1547-1549.

31. Folkes, L. K., and Wardman, P. (2004) Kinetics of the reaction between nitric oxide and glutathione: implications for thiol depletion in cells, *Free Radic Biol Med 37*, 549-556.

32. Florence, T. M. (1995) The Role of Free-Radicals in Disease, *Aust Nz J Ophthalmol 23*, 3-7.

33. Seet, R. C. S., Lee, C. Y. J., Lim, E. C. H., Tan, J. J. H., Quek, A. M. L., Chong, W. L., Looi, W. F., Huang, S. H., Wang, H. S., Chan, Y. H., and Halliwell, B. (2010) Oxidative damage in Parkinson disease: Measurement using accurate biomarkers, *Free Radical Bio Med 48*, 560-566.

34. Gruber, J., Schaffer, S., and Halliwell, B. (2008) The mitochondrial free radical theory of ageing--where do we stand?, *Front Biosci 13*, 6554-6579.

35. Wardman, P., and Vonsonntag, C. (1995) Kinetic Factors That Control the Fate of Thiyl Radicals in Cells, *Method Enzymol 251*, 31-45.

36. Ross, D., Norbeck, K., and Moldeus, P. (1985) The Generation and Subsequent Fate of Glutathionyl Radicals in Biological-Systems, *Journal of Biological Chemistry 260*, 5028-5032.

37. Apel, K., and Hirt, H. (2004) Reactive oxygen species: metabolism, oxidative stress, and signal transduction, *Annu Rev Plant Biol 55*, 373-399.

38. Antunes, F., and Cadenas, E. (2000) Estimation of H2O2 gradients across biomembranes, *Febs Lett 475*, 121-126.

39. Touyz, R. M., Briones, A. M., Sedeek, M., Burger, D., and Montezano, A. C. (2011) NOX isoforms and reactive oxygen species in vascular health, *Mol Interv 11*, 27-35.

40. Dang, P. M., Cross, A. R., Quinn, M. T., and Babior, B. M. (2002) Assembly of the neutrophil respiratory burst oxidase: a direct interaction between p67PHOX and cytochrome b558 II, *Proc Natl Acad Sci U S A 99*, 4262-4265.

41. Cuzzocrea, S., Mazzon, E., Dugo, L., Di Paola, R., Caputi, A. P., and Salvemini, D. (2004) Superoxide: a key player in hypertension, *Faseb J 18*, 94-101.

42. Fransen, M., Nordgren, M., Wang, B., and Apanasets, O. (2012) Role of peroxisomes in ROS/RNS-metabolism: implications for human disease, *Biochim Biophys Acta 1822*, 1363-1373.

43. Forstermann, U., and Sessa, W. C. (2012) Nitric oxide synthases: regulation and function, *Eur Heart J 33*, 829-837, 837a-837d.

44. Zhou, L., and Zhu, D. Y. (2009) Neuronal nitric oxide synthase: structure, subcellular localization, regulation, and clinical implications, *Nitric Oxide 20*, 223-230.

45. Hemmens, B., and Mayer, B. (1998) Enzymology of nitric oxide synthases, *Methods Mol Biol 100*, 1-32.

46. Garcia-Cardena, G., Fan, R., Shah, V., Sorrentino, R., Cirino, G., Papapetropoulos, A., and Sessa, W. C. (1998) Dynamic activation of endothelial nitric oxide synthase by Hsp90, *Nature 392*, 821-824.

47. Fleming, I., and Busse, R. (2003) Molecular mechanisms involved in the regulation of the endothelial nitric oxide synthase, *Am J Physiol Regul Integr Comp Physiol 284*, R1-12.

48. Beck, K. F., Eberhardt, W., Frank, S., Huwiler, A., Messmer, U. K., Muhl, H., and Pfeilschifter, J. (1999) Inducible NO synthase: role in cellular signalling, *J Exp Biol 202*, 645-653.

49. Birben, E., Sahiner, U. M., Sackesen, C., Erzurum, S., and Kalayci, O. (2012) Oxidative stress and antioxidant defense, *World Allergy Organ J 5*, 9-19.

50. Anderson, M. E. (1998) Glutathione: an overview of biosynthesis and modulation, *Chem Biol Interact 111-112*, 1-14.

51. Buettner, G. R. (1993) The pecking order of free radicals and antioxidants: lipid peroxidation, alpha-tocopherol, and ascorbate, *Arch Biochem Biophys 300*, 535-543.

52. Maritim, A. C., Sanders, R. A., and Watkins, J. B., 3rd. (2003) Diabetes, oxidative stress, and antioxidants: a review, *J Biochem Mol Toxicol 17*, 24-38.

53. Gaston, B. (1999) Nitric oxide and thiol groups, *Biochim Biophys Acta 1411*, 323-333.

54. Biswas, S., Chida, A. S., and Rahman, I. (2006) Redox modifications of protein-thiols: emerging roles in cell signaling, *Biochem Pharmacol 71*, 551-564.

55. Findlay, V. J., Tapiero, H., and Townsend, D. M. (2005) Sulfiredoxin: a potential therapeutic agent?, *Biomed Pharmacother 59*, 374-379.

56. Ying, J., Clavreul, N., Sethuraman, M., Adachi, T., and Cohen, R. A. (2007) Thiol oxidation in signaling and response to stress: detection and quantification of physiological and pathophysiological thiol modifications, *Free Radic Biol Med 43*, 1099-1108.

57. Davis, M. F., Vigil, D., and Campbell, S. L. (2011) Regulation of Ras proteins by reactive nitrogen species, *Free Radic Biol Med 51*, 565-575.

58. Lander, H. M., Ogiste, J. S., Teng, K. K., and Novogrodsky, A. (1995) p21ras as a common signaling target of reactive free radicals and cellular redox stress, *J Biol Chem 270*, 21195-21198.

59. Lander, H. M., Milbank, A. J., Tauras, J. M., Hajjar, D. P., Hempstead, B. L., Schwartz, G. D., Kraemer, R. T., Mirza, U. A., Chait, B. T., Burk, S. C., and Quilliam, L. A. (1996) Redox regulation of cell signalling, *Nature 381*, 380-381.

60. Mott, H. R., Carpenter, J. W., and Campbell, S. L. (1997) Structural and functional analysis of a mutant Ras protein that is insensitive to nitric oxide activation, *Biochemistry 36*, 3640-3644.

61. Tsujita, M., Batista, W. L., Ogata, F. T., Stern, A., Monteiro, H. P., and Arai, R. J. (2008) The nitric oxide-sensitive p21Ras-ERK pathway mediates S-nitrosoglutathione-induced apoptosis, *Biochem Biophys Res Commun 369*, 1001-1006.

62. Heo, J., and Campbell, S. L. (2004) Mechanism of p21Ras S-nitrosylation and kinetics of nitric oxide-mediated guanine nucleotide exchange, *Biochemistry 43*, 2314-2322.

63. Lim, K. H., Ancrile, B. B., Kashatus, D. F., and Counter, C. M. (2008) Tumour maintenance is mediated by eNOS, *Nature 452*, 646-649.

64. Ibiza, S., Perez-Rodriguez, A., Ortega, A., Martinez-Ruiz, A., Barreiro, O., Garcia-Dominguez, C. A., Victor, V. M., Esplugues, J. V., Rojas, J. M., Sanchez-Madrid, F., and Serrador, J. M. (2008) Endothelial nitric oxide synthase regulates N-Ras activation on the Golgi complex of antigen-stimulated T cells, *Proc Natl Acad Sci U S A 105*, 10507-10512.

65. Kjeldgaard, M., Nyborg, J., and Clark, B. F. (1996) The GTP binding motif: variations on a theme, *Faseb J 10*, 1347-1368.

66. Williams, J. G., Pappu, K., and Campbell, S. L. (2003) Structural and biochemical studies of p21Ras S-nitrosylation and nitric oxide-mediated guanine nucleotide exchange, *Proc Natl Acad Sci U S A 100*, 6376-6381.

67. Davis, M. F., Zhou, L., Ehrenshaft, M., Ranguelova, K., Gunawardena, H. P., Chen, X., Bonini, M., Mason, R. P., and Campbell, S. L. (2012) Detection of Ras GTPase protein radicals through immuno-spin trapping, *Free Radic Biol Med*.

68. Heo, J., Prutzman, K. C., Mocanu, V., and Campbell, S. L. (2005) Mechanism of free radical nitric oxide-mediated Ras guanine nucleotide dissociation, *J Mol Biol 346*, 1423-1440.

69. Heo, J., and Campbell, S. L. (2006) Ras regulation by reactive oxygen and nitrogen species, *Biochemistry 45*, 2200-2210.

70. Heo, J. (2011) Redox control of GTPases: from molecular mechanisms to functional significance in health and disease, *Antioxid Redox Signal 14*, 689-724.

71. Clavreul, N., Adachi, T., Pimental, D. R., Ido, Y., Schoneich, C., and Cohen, R. A. (2006) S-glutathiolation by peroxynitrite of p21ras at cysteine-118 mediates its direct activation and downstream signaling in endothelial cells, *The FASEB journal : official publication of the Federation of American Societies for Experimental Biology 20*, 518-520.

72. Clavreul, N., Bachschmid, M. M., Hou, X., Shi, C., Idrizovic, A., Ido, Y., Pimentel, D., and Cohen, R. A. (2006) S-glutathiolation of p21ras by peroxynitrite mediates endothelial insulin resistance caused by oxidized low-density lipoprotein, *Arterioscler Thromb Vasc Biol 26*, 2454-2461.

73. Clavreul, N., Adachi, T., Pimental, D. R., Ido, Y., Schoneich, C., and Cohen, R. A. (2006) S-glutathiolation by peroxynitrite of p21ras at cysteine-118 mediates its direct activation and downstream signaling in endothelial cells, *Faseb J 20*, 518-520.

74. Merenyi, G., Lind, J., Goldstein, S., and Czapski, G. (1998) Peroxynitrous acid homolyzes into *OH and *NO2 radicals, *Chem Res Toxicol 11*, 712-713.

75. Kissner, R., and Koppenol, W. H. (2002) Product distribution of peroxynitrite decay as a function of pH, temperature, and concentration, *J Am Chem Soc 124*, 234-239.

76. Szabo, C., Ischiropoulos, H., and Radi, R. (2007) Peroxynitrite: biochemistry, pathophysiology and development of therapeutics, *Nat Rev Drug Discov 6*, 662-680.

77. Adachi, T., Pimentel, D. R., Heibeck, T., Hou, X., Lee, Y. J., Jiang, B., Ido, Y., and Cohen, R. A. (2004) S-glutathiolation of Ras mediates redox-sensitive signaling by angiotensin II in vascular smooth muscle cells, *J Biol Chem 279*, 29857-29862.

78. Heo, J., and Campbell, S. L. (2005) Mechanism of redox-mediated guanine nucleotide exchange on redox-active Rho GTPases, *J Biol Chem 280*, 31003-31010.

79. Heo, J., and Campbell, S. L. (2005) Mechanism of redox-mediated guanine nucleotide exchange on redox-active Rho GTPases, *J Biol Chem 280*, 31003-31010.

80. Heo, J., Raines, K. W., Mocanu, V., and Campbell, S. L. (2006) Redox regulation of RhoA, *Biochemistry 45*, 14481-14489.

81. Aghajanian, A., Wittchen, E. S., Campbell, S. L., and Burridge, K. (2009) Direct activation of RhoA by reactive oxygen species requires a redox-sensitive motif, *PLoS One 4*, e8045.

82. Raines, K. W., Bonini, M. G., and Campbell, S. L. (2007) Nitric oxide cell signaling: S-nitrosation of Ras superfamily GTPases, *Cardiovasc Res 75*, 229-239.

83. Gerhard, R., John, H., Aktories, K., and Just, I. (2003) Thiol-modifying phenylarsine oxide inhibits guanine nucleotide binding of Rho but not of Rac GTPases, *Mol Pharmacol 63*, 1349-1355.

84. Oxford, G., and Theodorescu, D. (2003) Ras superfamily monomeric G proteins in carcinoma cell motility, *Cancer Lett 189*, 117-128.

85. Paduch, M., Jelen, F., and Otlewski, J. (2001) Structure of small G proteins and their regulators, *Acta Biochim Pol 48*, 829-850.

86. Takai, Y., Sasaki, T., and Matozaki, T. (2001) Small GTP-binding proteins, *Physiol Rev 81*, 153-208.

87. John, J., Rensland, H., Schlichting, I., Vetter, I., Borasio, G. D., Goody, R. S., and Wittinghofer, A. (1993) Kinetic and structural analysis of the Mg(2+)-binding site of the guanine nucleotide-binding protein p21H-ras, *J Biol Chem 268*, 923-929.

88. Sprang, S. (2001) GEFs: master regulators of G-protein activation, *Trends Biochem Sci 26*, 266-267.

89. Geyer, M., and Wittinghofer, A. (1997) GEFs, GAPs, GDIs and effectors: taking a closer (3D) look at the regulation of Ras-related GTP-binding proteins, *Curr Opin Struct Biol 7*, 786-792.

90. Sprang, S. R. (1997) G proteins, effectors and GAPs: structure and mechanism, *Curr Opin Struct Biol 7*, 849-856.

91. Barbacid, M. (1987) ras genes, *Annu Rev Biochem 56*, 779-827.

92. Bos, J. L. (1989) ras oncogenes in human cancer: a review, *Cancer Res 49*, 4682-4689.

93. Lowy, D. R., and Willumsen, B. M. (1993) Function and regulation of ras, *Annu Rev Biochem 62*, 851-891.

94. Lancaster, J. R., Jr. (2008) Protein cysteine thiol nitrosation: maker or marker of reactive nitrogen species-induced nonerythroid cellular signaling?, *Nitric Oxide 19*, 68-72.

95. Mitchell, L., Hobbs, G. A., Aghajanian, A., and Campbell, S. L. (2012) Redox Regulation of Ras and Rho GTPases: Mechanism and Function, *Antioxid Redox Signal*.

96. Sethuraman, M., Clavreul, N., Huang, H., McComb, M. E., Costello, C. E., and Cohen, R. A. (2007) Quantification of oxidative posttranslational modifications of cysteine thiols of p21ras associated with redox modulation of activity using isotope-coded affinity tags and mass spectrometry, *Free Radic Biol Med 42*, 823-829.

97. Kuster, G. M., Pimentel, D. R., Adachi, T., Ido, Y., Brenner, D. A., Cohen, R. A., Liao, R., Siwik, D. A., and Colucci, W. S. (2005) Alpha-adrenergic receptor-stimulated hypertrophy in adult rat ventricular myocytes is mediated via thioredoxin-1-sensitive oxidative modification of thiols on Ras, *Circulation 111*, 1192-1198.

98. Kuster, G. M., Siwik, D. A., Pimentel, D. R., and Colucci, W. S. (2006) Role of reversible, thioredoxin-sensitive oxidative protein modifications in cardiac myocytes, *Antioxid Redox Signal 8*, 2153-2159.

99. Pimentel, D. R., Adachi, T., Ido, Y., Heibeck, T., Jiang, B., Lee, Y., Melendez, J. A., Cohen, R. A., and Colucci, W. S. (2006) Strain-stimulated hypertrophy in cardiac myocytes is mediated by reactive oxygen species-dependent Ras S-glutathiolation, *J Mol Cell Cardiol 41*, 613-622.

100. Clavreul, N., Bachschmid, M. M., Hou, X., Shi, C., Idrizovic, A., Ido, Y., Pimentel, D., and Cohen, R. A. (2006) S-glutathiolation of p21ras by peroxynitrite mediates endothelial insulin resistance caused by oxidized low-density lipoprotein, *Arterioscler Thromb Vasc Biol 26*, 2454-2461.

101. Adachi, T., Weisbrod, R. M., Pimentel, D. R., Ying, J., Sharov, V. S., Schoneich, C., and Cohen, R. A. (2004) S-Glutathiolation by peroxynitrite activates SERCA during arterial relaxation by nitric oxide, *Nat Med 10*, 1200-1207.

102. Bonini, M. G., and Augusto, O. (2001) Carbon dioxide stimulates the production of thiyl, sulfinyl, and disulfide radical anion from thiol oxidation by peroxynitrite, *J Biol Chem 276*, 9749-9754.

103. Liaudet, L., Vassalli, G., and Pacher, P. (2009) Role of peroxynitrite in the redox regulation of cell signal transduction pathways, *Front Biosci 14*, 4809-4814.

104. Ushio-Fukai, M., Alexander, R. W., Akers, M., Yin, Q., Fujio, Y., Walsh, K., and Griendling, K. K. (1999) Reactive oxygen species mediate the activation of Akt/protein kinase B by angiotensin II in vascular smooth muscle cells, *J Biol Chem 274*, 22699-22704.

105. Lee, C., Miura, K., Liu, X., and Zweier, J. L. (2000) Biphasic regulation of leukocyte superoxide generation by nitric oxide and peroxynitrite, *J Biol Chem 275*, 38965-38972.

106. John, J., Schlichting, I., Schiltz, E., Rosch, P., and Wittinghofer, A. (1989) C-terminal truncation of p21H preserves crucial kinetic and structural properties, *J Biol Chem 264*, 13086-13092.

107. Gunawardena, H. P., Huang, Y., Kenjale, R., Wang, H., Xie, L., and Chen, X. (2011) Unambiguous characterization of site-specific phosphorylation of leucine-rich repeat

Fli-I-interacting protein 2 (LRRFIP2) in Toll-like receptor 4 (TLR4)-mediated signaling, *J Biol Chem 286*, 10897-10910.

108. Lenzen, C., Cool, R. H., Prinz, H., Kuhlmann, J., and Wittinghofer, A. (1998) Kinetic analysis by fluorescence of the interaction between Ras and the catalytic domain of the guanine nucleotide exchange factor Cdc25Mm, *Biochemistry 37*, 7420-7430.

109. Lenzen, C., Cool, R. H., and Wittinghofer, A. (1995) Analysis of intrinsic and CDC25-stimulated guanine nucleotide exchange of p21ras-nucleotide complexes by fluorescence measurements, *Methods Enzymol 255*, 95-109.

110. Sondermann, H., Soisson, S. M., Boykevisch, S., Yang, S. S., Bar-Sagi, D., and Kuriyan, J. (2004) Structural analysis of autoinhibition in the Ras activator Son of sevenless, *Cell 119*, 393-405.

111. Shutes, A., and Der, C. J. (2006) Real-time in vitro measurement of intrinsic and Ras GAP-mediated GTP hydrolysis, *Methods Enzymol 407*, 9-22.

112. Scheffzek, K., Ahmadian, M. R., Kabsch, W., Wiesmuller, L., Lautwein, A., Schmitz, F., and Wittinghofer, A. (1997) The Ras-RasGAP complex: structural basis for GTPase activation and its loss in oncogenic Ras mutants, *Science 277*, 333-338.

113. Gu, H., Lalonde, S., Okumoto, S., Looger, L. L., Scharff-Poulsen, A. M., Grossman, A. R., Kossmann, J., Jakobsen, I., and Frommer, W. B. (2006) A novel analytical method for in vivo phosphate tracking, *Febs Lett 580*, 5885-5893.

114. Brune, M., Hunter, J. L., Corrie, J. E., and Webb, M. R. (1994) Direct, real-time measurement of rapid inorganic phosphate release using a novel fluorescent probe and its application to actomyosin subfragment 1 ATPase, *Biochemistry 33*, 8262-8271.

115. Grzesiek, S., and Bax, A. (1993) Measurement of amide proton exchange rates and NOEs with water in 13C/15N-enriched calcineurin B, *J Biomol NMR 3*, 627-638.

116. Bax, A., Ikura, M., Kay, L. E., Barbato, G., and Spera, S. (1991) Multidimensional triple resonance NMR spectroscopy of isotopically uniformly enriched proteins: a powerful new strategy for structure determination, *Ciba Found Symp 161*, 108-119; discussion 119-135.

117. Delaglio, F., Grzesiek, S., Vuister, G. W., Zhu, G., Pfeifer, J., and Bax, A. (1995) NMRPipe: a multidimensional spectral processing system based on UNIX pipes, *Journal of biomolecular NMR 6*, 277-293.

118. John, J., Rensland, H., Schlichting, I., Vetter, I., Borasio, G. D., Goody, R. S., and Wittinghofer, A. (1993) Kinetic and structural analysis of the Mg(2+)-binding site of the guanine nucleotide-binding protein p21H-ras, *J Biol Chem 268*, 923-929.

119. Beckman, J. S., and Koppenol, W. H. (1996) Nitric oxide, superoxide, and peroxynitrite: the good, the bad, and ugly, *Am J Physiol 271*, C1424-1437.

120. Jourd'heuil, D., Jourd'heuil, F. L., and Feelisch, M. (2003) Oxidation and nitrosation of thiols at low micromolar exposure to nitric oxide. Evidence for a free radical mechanism, *J Biol Chem 278*, 15720-15726.

121. Ushio-Fukai, M., Alexander, R. W., Akers, M., and Griendling, K. K. (1998) p38 Mitogen-activated protein kinase is a critical component of the redox-sensitive signaling pathways activated by angiotensin II. Role in vascular smooth muscle cell hypertrophy, *J Biol Chem 273*, 15022-15029.

122. Han, D., Hanawa, N., Saberi, B., and Kaplowitz, N. (2006) Mechanisms of liver injury. III. Role of glutathione redox status in liver injury, *Am J Physiol Gastrointest Liver Physiol 291*, G1-7.

123. Lofgren, S., Fernando, M. R., Xing, K. Y., Wang, Y., Kuszynski, C. A., Ho, Y. S., and Lou, M. F. (2008) Effect of thioltransferase (glutaredoxin) deletion on cellular sensitivity to oxidative stress and cell proliferation in lens epithelial cells of thioltransferase knockout mouse, *Invest Ophthalmol Vis Sci 49*, 4497-4505.

124. Franco, R., and Cidlowski, J. A. (2009) Apoptosis and glutathione: beyond an antioxidant, *Cell Death Differ 16*, 1303-1314.

125. Meyer, E. B., and Wells, W. W. (1999) Thioltransferase overexpression increases resistance of MCF-7 cells to adriamycin, *Free Radic Biol Med 26*, 770-776.

126. Eom, Y. W., Kim, M. A., Park, S. S., Goo, M. J., Kwon, H. J., Sohn, S., Kim, W. H., Yoon, G., and Choi, K. S. (2005) Two distinct modes of cell death induced by doxorubicin: apoptosis and cell death through mitotic catastrophe accompanied by senescence-like phenotype, *Oncogene 24*, 4765-4777.

127. Bos, J. L., Rehmann, H., and Wittinghofer, A. (2007) GEFs and GAPs: critical elements in the control of small G proteins, *Cell 129*, 865-877.

128. Prior, I. A., Lewis, P. D., and Mattos, C. (2012) A comprehensive survey of Ras mutations in cancer, *Cancer Res 72*, 2457-2467.

129. Lowy, D. R., Zhang, K., DeClue, J. E., and Willumsen, B. M. (1991) Regulation of p21ras activity, *Trends Genet 7*, 346-351.

130. Fernandez-Medarde, A., and Santos, E. (2011) Ras in cancer and developmental diseases, *Genes Cancer 2*, 344-358.

131. Hobbs, G. A., Bonini, M. G., Gunawardena, H. P., Chen, X., and Campbell, S. L. (2013) Glutathiolated Ras: characterization and implications for Ras activation, *Free Radic Biol Med 57*, 221-229.

132. Gu, J., and Lewis, R. S. (2007) Effect of pH and metal ions on the decomposition rate of S-nitrosocysteine, *Ann Biomed Eng 35*, 1554-1560.

133. Shutes, A., and Der, C. J. (2005) Real-time in vitro measurement of GTP hydrolysis, *Methods 37*, 183-189.

134. Kelly, S. M., and Price, N. C. (2006) Circular dichroism to study protein interactions, *Curr Protoc Protein Sci Chapter 20*, Unit 20 10.

135. Franken, S. M., Scheidig, A. J., Krengel, U., Rensland, H., Lautwein, A., Geyer, M., Scheffzek, K., Goody, R. S., Kalbitzer, H. R., Pai, E. F., and et al. (1993) Three-dimensional structures and properties of a transforming and a nontransforming glycine-12 mutant of p21H-ras, *Biochemistry 32*, 8411-8420.

136. Krengel, U., Schlichting, I., Scherer, A., Schumann, R., Frech, M., John, J., Kabsch, W., Pai, E. F., and Wittinghofer, A. (1990) Three-dimensional structures of H-ras p21 mutants: molecular basis for their inability to function as signal switch molecules, *Cell 62*, 539-548.

137. Nava, C., Hanna, N., Michot, C., Pereira, S., Pouvreau, N., Niihori, T., Aoki, Y., Matsubara, Y., Arveiler, B., Lacombe, D., Pasmant, E., Parfait, B., Baumann, C., Heron, D., Sigaudy, S., Toutain, A., Rio, M., Goldenberg, A., Leheup, B., Verloes, A., and Cave, H. (2007) Cardio-facio-cutaneous and Noonan syndromes due to mutations in the RAS/MAPK signalling pathway: genotype-phenotype relationships and overlap with Costello syndrome, *J Med Genet 44*, 763-771.

138. Dance-Barnes, S. T., Kock, N. D., Floyd, H. S., Moore, J. E., Mosley, L. J., D'Agostino, R. B., Jr., Pettenati, M. J., and Miller, M. S. (2008) Effects of mutant human Ki-ras(G12C) gene dosage on murine lung tumorigenesis and signaling to its downstream effectors, *Toxicol Appl Pharmacol*.

139. Jemal, A., Cokkinides, V. E., Shafey, O., and Thun, M. J. (2003) Lung cancer trends in young adults: an early indicator of progress in tobacco control (United States), *Cancer Causes Control 14*, 579-585.

140. Aoki, Y., Niihori, T., Kawame, H., Kurosawa, K., Ohashi, H., Tanaka, Y., Filocamo, M., Kato, K., Suzuki, Y., Kure, S., and Matsubara, Y. (2005) Germline mutations in HRAS proto-oncogene cause Costello syndrome, *Nat Genet 37*, 1038-1040.

141. Colby, W. W., Hayflick, J. S., Clark, S. G., and Levinson, A. D. (1986) Biochemical characterization of polypeptides encoded by mutated human Ha-ras1 genes, *Mol Cell Biol 6*, 730-734.

142. Gremer, L., Gilsbach, B., Ahmadian, M. R., and Wittinghofer, A. (2008) Fluoride complexes of oncogenic Ras mutants to study the Ras-RasGap interaction, *Biol Chem 389*, 1163-1171.

143. Leone-Kabler, S., Wessner, L. L., McEntee, M. F., D'Agostino, R. B., Jr., and Miller, M. S. (1997) Ki-ras mutations are an early event and correlate with tumor stage in transplacentally-induced murine lung tumors, *Carcinogenesis 18*, 1163-1168.

144. Rodenhuis, S., Slebos, R. J., Boot, A. J., Evers, S. G., Mooi, W. J., Wagenaar, S. S., van Bodegom, P. C., and Bos, J. L. (1988) Incidence and possible clinical significance of K-ras oncogene activation in adenocarcinoma of the human lung, *Cancer Res 48*, 5738-5741.

145. Campbell, S. L., Khosravi-Far, R., Rossman, K. L., Clark, G. J., and Der, C. J. (1998) Increasing complexity of Ras signaling, *Oncogene 17*, 1395-1413.

146. Malliri, A., and Collard, J. G. (2003) Role of Rho-family proteins in cell adhesion and cancer, *Curr Opin Cell Biol 15*, 583-589.

147. Shields, J. M., Pruitt, K., McFall, A., Shaub, A., and Der, C. J. (2000) Understanding Ras: 'it ain't over 'til it's over', *Trends Cell Biol 10*, 147-154.

148. Heo, J., and Campbell, S. L. (2005) Superoxide anion radical modulates the activity of Ras and Ras-related GTPases by a radical-based mechanism similar to that of nitric oxide, *J Biol Chem 280*, 12438-12445.

149. Del Villar, K., Dorin, D., Sattler, I., Urano, J., Poullet, P., Robinson, N., Mitsuzawa, H., and Tamanoi, F. (1996) C-terminal motifs found in Ras-superfamily G-proteins: CAAX and C-seven motifs, *Biochem Soc Trans 24*, 709-713.

150. Reuther, G. W., and Der, C. J. (2000) The Ras branch of small GTPases: Ras family members don't fall far from the tree, *Curr Opin Cell Biol 12*, 157-165.

151. Hirshberg, M., Stockley, R. W., Dodson, G., and Webb, M. R. (1997) The crystal structure of human rac1, a member of the rho-family complexed with a GTP analogue, *Nat Struct Biol 4*, 147-152.

152. Ihara, K., Muraguchi, S., Kato, M., Shimizu, T., Shirakawa, M., Kuroda, S., Kaibuchi, K., and Hakoshima, T. (1998) Crystal structure of human RhoA in a dominantly active form complexed with a GTP analogue, *J Biol Chem 273*, 9656-9666.

153. Feltham, J. L., Dotsch, V., Raza, S., Manor, D., Cerione, R. A., Sutcliffe, M. J., Wagner, G., and Oswald, R. E. (1997) Definition of the switch surface in the solution structure of Cdc42Hs, *Biochemistry 36*, 8755-8766.

154. Andreyev, H. J., Norman, A. R., Cunningham, D., Oates, J. R., and Clarke, P. A. (1998) Kirsten ras mutations in patients with colorectal cancer: the multicenter "RASCAL" study, *J Natl Cancer Inst 90*, 675-684.

155. Vega, F., Iniesta, P., Caldes, T., Sanchez, A., Lopez, J., Dejuan, C., Diazrubio, E., Torres, A., Balibrea, J., and Benito, M. (1996) Association of K-ras codon 12 transversions with short survival in non-small cell lung cancer, *Int J Oncol 9*, 1307-1311.

156. Al-Mulla, F., Milner-White, E. J., Going, J. J., and Birnie, G. D. (1999) Structural differences between valine-12 and aspartate-12 Ras proteins may modify carcinoma aggression, *J Pathol 187*, 433-438.

157. Shields, J. M., Pruitt, K., McFall, A., Shaub, A., and Der, C. J. (2000) Understanding Ras: 'it ain't over 'til it's over', *Trends in cell biology 10*, 147-154.

158. Burridge, K., and Wennerberg, K. (2004) Rho and Rac take center stage, *Cell 116*, 167-179.

159. Kaibuchi, K., Kuroda, S., and Amano, M. (1999) Regulation of the cytoskeleton and cell adhesion by the Rho family GTPases in mammalian cells, *Annual review of biochemistry 68*, 459-486.

160. Scita, G., Tenca, P., Frittoli, E., Tocchetti, A., Innocenti, M., Giardina, G., and Di Fiore, P. P. (2000) Signaling from Ras to Rac and beyond: not just a matter of GEFs, *The EMBO journal 19*, 2393-2398.

161. Bokoch, G. M. (2000) Regulation of cell function by Rho family GTPases, *Immunol Res 21*, 139-148.

162. Hall, A., and Nobes, C. D. (2000) Rho GTPases: molecular switches that control the organization and dynamics of the actin cytoskeleton, *Philosophical transactions of the Royal Society of London. Series B, Biological sciences 355*, 965-970.

163. Nobes, C. D., and Hall, A. (1995) Rho, rac and cdc42 GTPases: regulators of actin structures, cell adhesion and motility, *Biochemical Society transactions 23*, 456-459.

164. Mitchell, L., Hobbs, G. A., Aghajanian, A., and Campbell, S. L. (2013) Redox regulation of Ras and Rho GTPases: mechanism and function, *Antioxid Redox Signal 18*, 250-258.

165. Ihara, K., Muraguchi, S., Kato, M., Shimizu, T., Shirakawa, M., Kuroda, S., Kaibuchi, K., and Hakoshima, T. (1998) Crystal structure of human RhoA in a dominantly active form complexed with a GTP analogue, *J Biol Chem 273*, 9656-9666.

166. Zhang, B., Zhang, Y., Wang, Z., and Zheng, Y. (2000) The role of Mg2+ cofactor in the guanine nucleotide exchange and GTP hydrolysis reactions of Rho family GTP-binding proteins, *J Biol Chem 275*, 25299-25307.

167. Zuckerbraun, B. S., Stoyanovsky, D. A., Sengupta, R., Shapiro, R. A., Ozanich, B. A., Rao, J., Barbato, J. E., and Tzeng, E. (2007) Nitric oxide-induced inhibition of smooth muscle cell proliferation involves S-nitrosation and inactivation of RhoA, *Am J Physiol Cell Physiol 292*, C824-831.

168. Chang, Y., Ceacareanu, B., Dixit, M., Sreejayan, N., and Hassid, A. (2002) Nitric oxide-induced motility in aortic smooth muscle cells: role of protein tyrosine phosphatase SHP-2 and GTP-binding protein Rho, *Circ Res 91*, 390-397.

169. Chandra, S., Romero, M. J., Shatanawi, A., Alkilany, A. M., Caldwell, R. B., and Caldwell, R. W. (2012) Oxidative species increase arginase activity in endothelial cells through the RhoA/Rho kinase pathway, *Brit J Pharmacol 165*, 506-519.

170. Rossman, K. L., Worthylake, D. K., Snyder, J. T., Siderovski, D. P., Campbell, S. L., and Sondek, J. (2002) A crystallographic view of interactions between Dbs and Cdc42: PH domain-assisted guanine nucleotide exchange, *Embo J 21*, 1315-1326.

171. Kelly, S. M., Jess, T. J., and Price, N. C. (2005) How to study proteins by circular dichroism, *Biochim Biophys Acta 1751*, 119-139.

172. Gasmi-Seabrook, G. M., Marshall, C. B., Cheung, M., Kim, B., Wang, F., Jang, Y. J., Mak, T. W., Stambolic, V., and Ikura, M. (2010) Real-time NMR study of guanine nucleotide exchange and activation of RhoA by PDZ-RhoGEF, *J Biol Chem 285*, 5137-5145.

173. Heo, J., Thapar, R., and Campbell, S. L. (2005) Recognition and activation of Rho GTPases by Vav1 and Vav2 guanine nucleotide exchange factors, *Biochemistry 44*, 6573-6585.

174. Chitaley, K., and Webb, R. C. (2002) Nitric oxide induces dilation of rat aorta via inhibition of rho-kinase signaling, *Hypertension 39*, 438-442.

175. Sauzeau, V., Le Jeune, H., Cario-Toumaniantz, C., Smolenski, A., Lohmann, S. M., Bertoglio, J., Chardin, P., Pacaud, P., and Loirand, G. (2000) Cyclic GMP-dependent protein kinase signaling pathway inhibits RhoA-induced Ca2+ sensitization of contraction in vascular smooth muscle, *J Biol Chem 275*, 21722-21729.

176. Sawada, N., Itoh, H., Yamashita, J., Doi, K., Inoue, M., Masatsugu, K., Fukunaga, Y., Sakaguchi, S., Sone, M., Yamahara, K., Yurugi, T., and Nakao, K. (2001) cGMP-dependent protein kinase phosphorylates and inactivates RhoA, *Biochem Biophys Res Commun 280*, 798-805.

177. Poole, L. B., and Nelson, K. J. (2008) Discovering mechanisms of signaling-mediated cysteine oxidation, *Curr Opin Chem Biol 12*, 18-24.

178. Davis, M. F., Zhou, L., Ehrenshaft, M., Ranguelova, K., Gunawardena, H. P., Chen, X., Bonini, M. G., Mason, R. P., and Campbell, S. L. (2012) Detection of Ras GTPase protein radicals through immuno-spin trapping, *Free Radic Biol Med 53*, 1339-1345.

179. Young, A., Lou, D., and McCormick, F. (2013) Oncogenic and wild-type Ras play divergent roles in the regulation of mitogen-activated protein kinase signaling, *Cancer Discov 3*, 112-123.

180. Hicke, L. (2001) Protein regulation by monoubiquitin, *Nat Rev Mol Cell Biol 2*, 195-201.

181. Jura, N., Scotto-Lavino, E., Sobczyk, A., and Bar-Sagi, D. (2006) Differential modification of Ras proteins by ubiquitination, *Mol Cell 21*, 679-687.

182. Komander, D., Clague, M. J., and Urbe, S. (2009) Breaking the chains: structure and function of the deubiquitinases, *Nat Rev Mol Cell Biol 10*, 550-563.

183. Wennerberg, K., Rossman, K. L., and Der, C. J. (2005) The Ras superfamily at a glance, *J Cell Sci 118*, 843-846.

184. Feig, L. A., and Cooper, G. M. (1988) Relationship among guanine nucleotide exchange, GTP hydrolysis, and transforming potential of mutated ras proteins, *Mol Cell Biol 8*, 2472-2478.

185. Micel, L. N., Tentler, J. J., Smith, P. G., and Eckhardt, G. S. (2013) Role of ubiquitin ligases and the proteasome in oncogenesis: novel targets for anticancer therapies, *J Clin Oncol 31*, 1231-1238.

186. Gremer, L., Gilsbach, B., Ahmadian, M. R., and Wittinghofer, A. (2008) Fluoride complexes of oncogenic Ras mutants to study the Ras-RasGap interaction, *Biol Chem 389*, 1163-1171.

187. Gao, C., and Eriksson, L. A. (2013) Impact of Mutations on K-Ras-p120GAP Interaction, *Computational Molecular Bioscience*, 9-17.

188. Aitken, A., and Learmonth, M. (2002) Carboxymethylation of Cysteine using Iodoacetamide/iodoacetic acid, *The Protein Protocols Handbook 2nd Edition*, 455-456.

189. Smythe, C. V. (1936) The Reaction of Iodoacetate and of Iodoacetamide with various sulfhydryl groups, with urease, and with yeast preparations, *J Biol Chem*, 601-612.

190. Camps, J., Carrillo, O., Emperador, A., Orellana, L., Hospital, A., Rueda, M., Cicin-Sain, D., D'Abramo, M., Gelpi, J. L., and Orozco, M. (2009) FlexServ: an integrated tool for the analysis of protein flexibility, *Bioinformatics 25*, 1709-1710.

191. Kotting, C., Kallenbach, A., Suveyzdis, Y., Wittinghofer, A., and Gerwert, K. (2008) The GAP arginine finger movement into the catalytic site of Ras increases the activation entropy, *Proc Natl Acad Sci U S A 105*, 6260-6265.

192. Kotting, C., and Gerwert, K. (2013) The dynamics of the catalytic site in small GTPases, variations on a common motif, *Febs Lett*.

193. Rudack, T., Xia, F., Schlitter, J., Kotting, C., and Gerwert, K. (2012) Ras and GTPase-activating protein (GAP) drive GTP into a precatalytic state as revealed by combining FTIR and biomolecular simulations, *Proc Natl Acad Sci U S A 109*, 15295-15300.

194. Rudack, T., Xia, F., Schlitter, J., Kotting, C., and Gerwert, K. (2012) The role of magnesium for geometry and charge in GTP hydrolysis, revealed by quantum mechanics/molecular mechanics simulations, *Biophys J 103*, 293-302.

195. Grigorenko, B. L., Nemukhin, A. V., Shadrina, M. S., Topol, I. A., and Burt, S. K. (2007) Mechanisms of guanosine triphosphate hydrolysis by Ras and Ras-GAP proteins as rationalized by ab initio QM/MM simulations, *Proteins 66*, 456-466.

196. Netto, L. E., de Oliveira, M. A., Monteiro, G., Demasi, A. P., Cussiol, J. R., Discola, K. F., Demasi, M., Silva, G. M., Alves, S. V., Faria, V. G., and Horta, B. B. (2007) Reactive cysteine in proteins: protein folding, antioxidant defense, redox signaling and more, *Comp Biochem Physiol C Toxicol Pharmacol 146*, 180-193.

197. Martinez-Ruiz, A., and Lamas, S. (2007) Signalling by NO-induced protein S-nitrosylation and S-glutathionylation: convergences and divergences, *Cardiovasc Res 75*, 220-228.

198. Mieyal, J. J., and Chock, P. B. (2012) Posttranslational modification of cysteine in redox signaling and oxidative stress: Focus on s-glutathionylation, *Antioxid Redox Signal 16*, 471-475.

199. Wang, Y., Yang, J., and Yi, J. (2012) Redox sensing by proteins: oxidative modifications on cysteines and the consequent events, *Antioxid Redox Signal 16*, 649-657.

200. Adler, V., Yin, Z., Tew, K. D., and Ronai, Z. (1999) Role of redox potential and reactive oxygen species in stress signaling, *Oncogene 18*, 6104-6111.

201. Reddie, K. G., and Carroll, K. S. (2008) Expanding the functional diversity of proteins through cysteine oxidation, *Curr Opin Chem Biol 12*, 746-754.

202. Roos, G., Foloppe, N., and Messens, J. (2013) Understanding the pK(a) of Redox Cysteines: The Key Role of Hydrogen Bonding, *Antioxid Redox Signal 18*, 94-127.

203. Bulaj, G., Kortemme, T., and Goldenberg, D. P. (1998) Ionization-reactivity relationships for cysteine thiols in polypeptides, *Biochemistry 37*, 8965-8972.

204. Nelson, K. J., Parsonage, D., Hall, A., Karplus, P. A., and Poole, L. B. (2008) Cysteine pK(a) values for the bacterial peroxiredoxin AhpC, *Biochemistry 47*, 12860-12868.

205. Dyson, H. J., Jeng, M. F., Tennant, L. L., Slaby, I., Lindell, M., Cui, D. S., Kuprin, S., and Holmgren, A. (1997) Effects of buried charged groups on cysteine thiol ionization and reactivity in Escherichia coli thioredoxin: structural and functional characterization of mutants of Asp 26 and Lys 57, *Biochemistry 36*, 2622-2636.

206. Chivers, P. T., Prehoda, K. E., Volkman, B. F., Kim, B. M., Markley, J. L., and Raines, R. T. (1997) Microscopic pKa values of Escherichia coli thioredoxin, *Biochemistry 36*, 14985-14991.

207. Tosatto, S. C., Bosello, V., Fogolari, F., Mauri, P., Roveri, A., Toppo, S., Flohe, L., Ursini, F., and Maiorino, M. (2008) The catalytic site of glutathione peroxidases, *Antioxid Redox Signal 10*, 1515-1526.

208. Isom, D. G., Marguet, P. R., Oas, T. G., and Hellinga, H. W. (2011) A miniaturized technique for assessing protein thermodynamics and function using fast determination of quantitative cysteine reactivity, *Proteins 79*, 1034-1047.

209. Chait, B. T. (2006) Chemistry. Mass spectrometry: bottom-up or top-down?, *Science 314*, 65-66.

210. Yates, J. R., Ruse, C. I., and Nakorchevsky, A. (2009) Proteomics by mass spectrometry: approaches, advances, and applications, *Annu Rev Biomed Eng 11*, 49-79.

211. Grossi, L., and Montevecchi, P. C. (2002) S-nitrosocysteine and cystine from reaction of cysteine with nitrous acid. A kinetic investigation, *J Org Chem 67*, 8625-8630.

212. Moore, K. P., and Mani, A. R. (2002) Measurement of protein nitration and S-nitrosothiol formation in biology and medicine, *Methods Enzymol 359*, 256-268.

213. Jones, D. P. (2008) Radical-free biology of oxidative stress, *Am J Physiol Cell Physiol 295*, C849-868.

214. Sander, R. (1999) Compilation of Henry's Law Constants for Inorganic and Organic Species of Potential Importance in Environmental Chemistry.

215. Gygi, S. P., Rist, B., Gerber, S. A., Turecek, F., Gelb, M. H., and Aebersold, R. (1999) Quantitative analysis of complex protein mixtures using isotope-coded affinity tags, *Nat Biotechnol 17*, 994-999.

216. Chiappetta, G., Ndiaye, S., Igbaria, A., Kumar, C., Vinh, J., and Toledano, M. B. (2010) Proteome screens for Cys residues oxidation: the redoxome, *Methods Enzymol 473*, 199-216.

217. Marino, S. M., Li, Y., Fomenko, D. E., Agisheva, N., Cerny, R. L., and Gladyshev, V. N. (2010) Characterization of surface-exposed reactive cysteine residues in Saccharomyces cerevisiae, *Biochemistry 49*, 7709-7721.

218. Sethuraman, M., McComb, M. E., Huang, H., Huang, S., Heibeck, T., Costello, C. E., and Cohen, R. A. (2004) Isotope-coded affinity tag (ICAT) approach to redox proteomics: identification and quantitation of oxidant-sensitive cysteine thiols in complex protein mixtures, *J Proteome Res 3*, 1228-1233.

219. Leichert, L. I., Gehrke, F., Gudiseva, H. V., Blackwell, T., Ilbert, M., Walker, A. K., Strahler, J. R., Andrews, P. C., and Jakob, U. (2008) Quantifying changes in the thiol redox proteome upon oxidative stress in vivo, *Proc Natl Acad Sci U S A 105*, 8197-8202.

220. Chouchani, E. T., James, A. M., Fearnley, I. M., Lilley, K. S., and Murphy, M. P. (2011) Proteomic approaches to the characterization of protein thiol modification, *Curr Opin Chem Biol 15*, 120-128.

221. Wisniewski, J. R., Ostasiewicz, P., and Mann, M. (2011) High recovery FASP applied to the proteomic analysis of microdissected formalin fixed paraffin embedded cancer tissues retrieves known colon cancer markers, *J Proteome Res 10*, 3040-3049.

222. Wisniewski, J. R., Zielinska, D. F., and Mann, M. (2011) Comparison of ultrafiltration units for proteomic and N-glycoproteomic analysis by the filter-aided sample preparation method, *Anal Biochem 410*, 307-309.

223. Wisniewski, J. R., Zougman, A., and Mann, M. (2009) Combination of FASP and StageTip-based fractionation allows in-depth analysis of the hippocampal membrane proteome, *J Proteome Res 8*, 5674-5678.

224. Wisniewski, J. R., Zougman, A., Nagaraj, N., and Mann, M. (2009) Universal sample preparation method for proteome analysis, *Nat Methods 6*, 359-362.

225. Houk, J., Singh, R., and Whitesides, G. M. (1987) Measurement of thiol-disulfide interchange reactions and thiol pKa values, *Methods Enzymol 143*, 129-140.

226. Lukesh, J. C., 3rd, Palte, M. J., and Raines, R. T. (2012) A potent, versatile disulfide-reducing agent from aspartic acid, *J Am Chem Soc 134*, 4057-4059.

227. Saville, B. (1958) A Scheme for the Colorimetric Determination of Microgram Amounts of Thiols, *Analyst 83*, 670-672.

228. Keshive, M., Singh, S., Wishnok, J. S., Tannenbaum, S. R., and Deen, W. M. (1996) Kinetics of S-nitrosation of thiols in nitric oxide solutions, *Chem Res Toxicol 9*, 988-993.

229. Hobbs, G. A., Bonini, M. G., Gunawardena, H. P., Chen, X., and Campbell, S. L. (2012) Glutathiolated Ras: Characterization and Implications for Ras Activation, *Free Radic Biol Med*.

230. Yu, Y., Xie, L., Gunawardena, H. P., Khatun, J., Maier, C., Spitzer, W., Leerkes, M., Giddings, M. C., and Chen, X. (2012) GOFAST: an integrated approach for efficient and comprehensive membrane proteome analysis, *Anal Chem 84*, 9008-9014.

231. Bishop, A. L., and Hall, A. (2000) Rho GTPases and their effector proteins, *Biochem J 348 Pt 2*, 241-255.

232. Repasky, G. A., Chenette, E. J., and Der, C. J. (2004) Renewing the conspiracy theory debate: does Raf function alone to mediate Ras oncogenesis?, *Trends Cell Biol 14*, 639-647.

233. Kaibuchi, K., Kuroda, S., and Amano, M. (1999) Regulation of the cytoskeleton and cell adhesion by the Rho family GTPases in mammalian cells, *Annu Rev Biochem 68*, 459-486.

234. Scita, G., Tenca, P., Frittoli, E., Tocchetti, A., Innocenti, M., Giardina, G., and Di Fiore, P. P. (2000) Signaling from Ras to Rac and beyond: not just a matter of GEFs, *Embo J 19*, 2393-2398.

235. Wei, W., Das, B., Park, W., and Broek, D. (1994) Cloning and analysis of human cDNAs encoding a 140-kDa brain guanine nucleotide-exchange factor, Cdc25GEF, which regulates the function of Ras, *Gene 151*, 279-284.

236. Simon, I., Zerial, M., and Goody, R. S. (1996) Kinetics of interaction of Rab5 and Rab7 with nucleotides and magnesium ions, *J Biol Chem 271*, 20470-20478.

237. Jiang, W. G., Watkins, G., Lane, J., Cunnick, G. H., Douglas-Jones, A., Mokbel, K., and Mansel, R. E. (2003) Prognostic value of rho GTPases and rho guanine nucleotide dissociation inhibitors in human breast cancers, *Clin Cancer Res 9*, 6432-6440.

238. Ellenbroek, S. I., and Collard, J. G. (2007) Rho GTPases: functions and association with cancer, *Clin Exp Metastasis 24*, 657-672.

239. Touyz, R. M. (2006) Magnesium and hypertension, *Curr Opin Nephrol Hypertens 15*, 141-144.

240. Katoh, H., Hiramoto, K., and Negishi, M. (2006) Activation of Rac1 by RhoG regulates cell migration, *J Cell Sci 119*, 56-65.

241. Wennerberg, K., Ellerbroek, S. M., Liu, R. Y., Karnoub, A. E., Burridge, K., and Der, C. J. (2002) RhoG signals in parallel with Rac1 and Cdc42, *J Biol Chem 277*, 47810-47817.

242. Prieto-Sanchez, R. M., and Bustelo, X. R. (2003) Structural basis for the signaling specificity of RhoG and Rac1 GTPases, *J Biol Chem 278*, 37916-37925.

243. Thapar, R., Williams, J. G., and Campbell, S. L. (2004) NMR characterization of full-length farnesylated and non-farnesylated H-Ras and its implications for Raf activation, *J Mol Biol 343*, 1391-1408.

244. Abe, K., Rossman, K. L., Liu, B., Ritola, K. D., Chiang, D., Campbell, S. L., Burridge, K., and Der, C. J. (2000) Vav2 is an activator of Cdc42, Rac1, and RhoA, *J Biol Chem 275*, 10141-10149.

245. Hiramoto, K., Negishi, M., and Katoh, H. (2006) Dock4 is regulated by RhoG and promotes Rac-dependent cell migration, *Exp Cell Res 312*, 4205-4216.

246. Ellerbroek, S. M., Wennerberg, K., Arthur, W. T., Dunty, J. M., Bowman, D. R., DeMali, K. A., Der, C., and Burridge, K. (2004) SGEF, a RhoG guanine nucleotide exchange factor that stimulates macropinocytosis, *Mol Biol Cell 15*, 3309-3319.

247. Gentile, S., Darden, T., Erxleben, C., Romeo, C., Russo, A., Martin, N., Rossie, S., and Armstrong, D. L. (2006) Rac GTPase signaling through the PP5 protein phosphatase, *Proc Natl Acad Sci U S A 103*, 5202-5206.

248. Wennerberg, K., and Der, C. J. (2004) Rho-family GTPases: it's not only Rac and Rho (and I like it), *J Cell Sci 117*, 1301-1312.

249. Lapouge, K., Smith, S. J., Walker, P. A., Gamblin, S. J., Smerdon, S. J., and Rittinger, K. (2000) Structure of the TPR domain of p67phox in complex with Rac.GTP, *Mol Cell 6*, 899-907.

250. Schumacker, P. T. (2006) Reactive oxygen species in cancer cells: live by the sword, die by the sword, *Cancer Cell 10*, 175-176.

251. Katoh, H., Yasui, H., Yamaguchi, Y., Aoki, J., Fujita, H., Mori, K., and Negishi, M. (2000) Small GTPase RhoG is a key regulator for neurite outgrowth in PC12 cells, *Mol Cell Biol 20*, 7378-7387.

252. Bokoch, G. M. (1995) Regulation of the phagocyte respiratory burst by small GTP-binding proteins, *Trends Cell Biol 5*, 109-113.

253. Cheng, G., Diebold, B. A., Hughes, Y., and Lambeth, J. D. (2006) Nox1-dependent reactive oxygen generation is regulated by Rac1, *J Biol Chem 281*, 17718-17726.

254. Condliffe, A. M., Webb, L. M., Ferguson, G. J., Davidson, K., Turner, M., Vigorito, E., Manifava, M., Chilvers, E. R., Stephens, L. R., and Hawkins, P. T. (2006) RhoG regulates the neutrophil NADPH oxidase, *J Immunol 176*, 5314-5320.